ISTANBUL TECHNICAL UNIVERSITY ★ GRADUATE SCHOOL OF SCIENCE ENGINEERING AND TECHNOLOGY

DEVELOPMENT OF MESHLESS METHODS BASED ON DIFFERENTIAL TRANSFORM METHOD

Ph.D. THESIS

Armağan Fatih KARAMANLI

Department of Mechanical Engineering

Mechanical Engineering Programme

JUNE 2013

ISTANBUL TECHNICAL UNIVERSITY ★ GRADUATE SCHOOL OF SCIENCE ENGINEERING AND TECHNOLOGY

DEVELOPMENT OF MESHLESS METHODS BASED ON DIFFERENTIAL TRANSFORM METHOD

Ph.D. THESIS

Armağan Fatih Karamanlı
(503052013)

Department of Mechanical Engineering

Mechanical Engineering Programme

Thesis Advisor: Prof. Dr. Ata MUĞAN

JUNE 2013

İSTANBUL TEKNİK ÜNİVERSİTESİ ★ FEN BİLİMLERİ ENSTİTÜSÜ

DİFERANSİYEL TRANSFORMASYON YÖNTEMİNİ KULLANARAK AĞSIZ YÖNTEMLERİN GELİŞTİRİLMESİ

DOKTORA TEZİ

Armağan Fatih KARAMANLI
(503052013)

Makina Mühendisliği Anabilim Dalı

Makina Mühendisliği Programı

Tez Danışmanı: Prof. Dr. Ata MUĞAN

HAZİRAN 2013

Armağan Fatih Karamanlı, **a Ph.D.** student of ITU **Graduate School of Science Engineering and Technology** student ID 503052013, successfully defended the **thesis** entitled "**DEVELOPMENT OF MESHLESS METHODS BASED ON DIFFERENTIAL TRANSFORM METHOD**", which he prepared after fulfilling the requirements specified in the associated legislations, before the jury whose signatures are below.

Thesis Advisor : **Prof. Dr. Ata MUĞAN**
İstanbul Technical University

Jury Members : **Prof. Dr. C. Erdem İMRAK**
İstanbul Technical University

Assist. Prof. Dr. Hakan ERSOY
Akdeniz University

Prof. Dr. Uğur GÜVEN
Yildiz Technical University

Assoc. Prof. Dr. Celaletdin ERGUN
İstanbul Technical University

Date of Submission : 7 May 2013
Date of Defense : 25 June 2013

To my parents and my lovely wife,

FOREWORD

I wish to first and foremost acknowledge my advisor Prof.Dr. Ata Muğan. Without his guidance, advice and encouragement, this work would not have come to existence. I would like to express my deep gratitude to my parents (Gönül and Necdet) who have always supported me, believed in me and covered me with love during all my studies. Next, I would like to thanks Prof.Dr. C. Erdem İmrak, Yrd.Doç.Dr. Hakan Ersoy, my other committee members, Prof.Dr.Uğur Güven and Doç.Dr. Celaletdin Ergun. And finally, I would like to thank my lovely wife Beril for her endless support and help during those difficult years.

June 2013 Armağan Fatih KARAMANLI

TABLE OF CONTENTS

Page

ABBREVIATIONS

BDT : Bilgisayar Destekli Tasarım
BNM : Boundary Node Method
BPIM : Boundary Point Interpolation Method
BRPIM : Boundary Radial Point Interpolation Method
CAE : Computer Aided Engineering
CPU : Central Processing Unit
CSPM : Corrective Smoothed Particle Method
CSRBF : Compactly Supported Radial Basis Functions
DEM : Diffisu Element Method
DTM : Differential Transform Method
EFG : Element Free Galerkin
FDM : Finite Difference Method
FEM : Finite Element Method
FPM : Finite Point Method
MLPG : Meshless Local Petrov Galerkin
MLS : Moving Least Squares
MSPH : Modified Smoothed Particle Hydrodynamics
PIM : Point Interpolation Method
RBF : Radial Basis Functions
RKPM : Reproducing Kernel Particle Method
RPIM : Radial Point Interpolation Method
SPH : Smoothed Particle Hydrodynamics
SSPH : Symmetric Smoothed Particle Hydrodynamics
TSE : Taylor Series Expansion

LIST OF TABLES

Page

LIST OF FIGURES

Page

LIST OF SYMBOLS

L_2	: Global Error Norm
1D	: One Dimensional
2D	: Two Dimensional
h	: Smoothing Length
Δ	: Smallest Distance Between Two Adjacent Nodes
$u^{\boldsymbol{h}}(x)$	: Approximated Function
$\Phi^{T}(x)$	: Shape Function
U_s	: Vector for Nodal Values
d	: Dimension of the Support Domain
ρ	: Dimensionless Size of the Support Domain
Ω_s	: Compact Support Domain
Ω	: Entire Problem Domain
W	: Weight Function
δ	: Kronecker Delta
G	: Normalizing Constant
λ	: Dimensionality of the Space
Π	: Total Potential Energy
Π_s	: Strain Energy
W_f	: Work Done by External Forces
$\boldsymbol{\varepsilon}$	: Strain Vector
$\boldsymbol{\sigma}$	: Stress Vector
$\mathbf{u}$	: Displacement Vector
Γ_t	: Boundary on Where Traction Forces
$\mathbf{b}$	: External Forces Vector
$\bar{\mathbf{t}}$	: Prescribed Tractions
n_j	: Unit Outward Normal Vector
∇	: Spatial Derivative
m_j	: Particle Mass
ρ_j	: Particle Density
$C(x-\xi)$	: Correction Function
$\mathbf{P}$	: Polynomial Matrix
$m_k(x)$	: k^{th} Order Moment of the Original Kernel
$\mathbf{b}$	: A vector
$\mathbf{M}(x)$	: Moment Matrix
f_i	: A Function
f_{xi}	: First Derivative of a Function
f_{xxi}	: Second Derivative of a Function
$\mathbf{a}(\mathbf{x})$	: A vector
u_I	: Fictitious Value of the Function
$N(\mathbf{x})$	: The Number of Particles in the Compact Support
$\mathbf{A}(\mathbf{x})$	: A Matrix

$\mathbf{B}(\mathbf{x})$: A Matix
$\mathbf{P}_m$: A Polynomial Matrix
$R(\mathbf{x})$: Radial Basis Function
$\mathbf{G}$: A Matrix
! : Factorial
$\mathbf{Q}(\mathbf{x})$: A Vector
$\mathbf{H}(\boldsymbol{\xi}, \mathbf{x})$: A Matrix
$\mathbf{F}^{(x)}(\boldsymbol{\xi}, \mathbf{x})$: Nodal Values Vector
$\mathbf{C}(\boldsymbol{\xi}, \mathbf{x})$: A Matrix
$\mathbf{D}(\boldsymbol{\xi}, \mathbf{x})$: A Matrix
$\mathbf{K}^{(x)}(\boldsymbol{\xi}, \mathbf{x})$: A Matrix
K_{IJ} : I[th] Row of the Matrix K
$w(x)$: A Function
$W(k)$: Transformed Function
$T_i(x)$: A Function
$\boldsymbol{U}_i$: A Vector
N_g : Number of Particles in the Support Domain
v_{num}^{j} : Value of the Function v at the j^{th} Node Calculated by Numerical Solution
v_{exact}^{j} : Value of the Function v at the j^{th} Node Calculated by the Analytical Solution
$\mathbf{D}$: The Matrix of Elastic Constants
E : Modulus of Eleasticity
υ : Poisson Ratio
$\mathbf{L}$: Differential Operator Matrix

DEVELOPMENT OF MESHLESS METHODS BASED ON DIFFERENTIAL TRANSFORM METHOD

SUMMARY

Based on the differential transform method, meshless methods are developed to establish the algebraic equations for the whole problem domain. Meshless methods use a set of nodes scattered within the problem domain as well as sets of nodes scattered on the boundaries of the domain to represent the problem domain and its boundaries. In practice, many meshless methods have found applications, and are shown to have very good potential to become powerful numerical tools.

Meshless methods, as an alternative numerical approaches to eleminate the well-known drawbacks in the FEM, have attracted much attention in recent decades, due to their flexibility and, most importantly, due to their potential in negating the need for the human-labor intensive process of constructing geometric meshes in a domain. Such meshless methods are especially useful in those problems with discontinuities or moving boundaries. The main objective of the meshless methods is to get rid of, or at least alleviate the difficulty of, meshing and re-meshing the entire structure by only adding or deleting nodes in the entire structure. Meshless methods may also alleviate some other problems associated with the FEM such as locking, element distortions and others.

One of the methods discussed in this thesis is the symmetric smoothed particle hydrodynamics (SSPH) method which has been used for generating basis functions for a meshless method. The SSPH method admits a larger class of kernel functions than some other methods, including the smoothed particle hydrodynamics (SPH), the modified smoothed particle hydrodynamics (MSPH), the reproducing kernel particle method (RKPM) and the moving least squares (MLS) methods. For finding kernel estimates of derivatives of a function, the SSPH method does not use derivatives of the kernel function while other methods do. On the other hand, the SSPH method is more suitable for homogeneous boundary value problems, cannot be easily applicable to nonlinear problems, requires at least fourth order terms in basis functions for the buckling problems which increases the CPU time.

Motivated by the fact that the SSPH method may not yield accurate results for solving nonhomogeneous problems due to its underlying formulation, an alternative approach was investigated especially for nonhomegenous problems. To this end, based on the Taylor series expansion (TSE) and employing the technique of Differential Transform Method (DTM), three new meshless approaches called DTM based meshless method I, II and III are presented in this thesis. Although the SSPH method and DTM based meshless methods depend on TSEs, the main difference between these two approaches is as follows: the SSPH method calculates the value of the solution at a node by using the values of the solution at the other nodes and then substitute it into the governing differential equation; thus, nonhomogeneous terms in the governing differential equation are also evaluated pointwise at the nodes. This

approach results in approximation errors especially in the existence of nonsmooth nonhomogeneous terms. On the other hand, the proposed DTM based meshless methods substitute the TSEs of the solution and nonhomogeneous term into the governing differential equation and then utilize exact recursive relations between the coefficients of the expansions of the solution and nonhomogeneous term.

To compare the performance of the SSPH and DTM based meshless methods, 1D nonhomogeneous boundary value problem, 2D homogeneous Laplace equation, 2D nonhomogeneous Laplace equation and plane stress deformations of a plate in 2D were studied in this thesis. Different numbers of nodes were used in the problem domain and the convergence rate of the above mentioned methods were evaluated based on the global L_2 error norm by using revised super Gauss function. Especially for the studied nonhomogeneous boundary value problems, the DTM based meshless methods are shown to have significant advantage in terms of global L_2 error norm.

Regarding to the results obtained for the 1D nonhomogeneous boundary value problem, by using 5 terms in the TSE's, the DTM based meshless method II and method III gave the exact solution even with the 5 nodes in the problem domain.

The next problem studied in this thesis is the two dimensional homogeneous Laplace equation. All DTM based meshless methods have better convergence rates compared with the SSPH method. Especially the DTM based meshless method II consistently gave the lowest global L_2 error norm with increasing number of nodes in the problem domain. In this problem, the performance of the DTM based meshless methods was also compared with the FEM. It is observed that DTM based meshless methods always gave the lowest global L_2 error norm with increasing number of nodes in the problem domain.

The nonhomogeneous Laplace equation in 2D was also studied in this thesis. The performances of all four methods were evaluated regarding to the variation of the radius of the compact support domain and variation of the smoothing length by using different number of nodes in the problem domain. The DTM based meshless method II and III have better performance than the other two methods. It is also observed that the SSPH method is stable for $h=1.8\Delta$ (Δ is the smallest distance between the nodes and the other nodes in the compact support domain) and node distribution of 171 nodes; however, the DTM based meshless method I, II and III are stable even for $h=2\Delta$. The DTM based meshless method III always gave the lowest global L_2 error norm with increasing number of nodes in the problem domain.

The last problem studied to evaluate the performance of all four methods is the plane stress deformations of a plate in 2D. The DTM based meshless method II and III always gave the lowest global L_2 error norm with increasing the number of nodes in the problem domain. These methods also gave the less deviation than the SSPH method in terms of the dimensionless stress $\sigma_{xx}(L_2/F_0)$ along the top of the surface of the plate for different numbers of nodes in the problem domain. The DTM based meshless method I did not give satisfactory results for this problem. The CPU times of the DTM based meshless method II, III and the SSPH method were also evaluated for this problem. It is clear that CPU times required for the DTM based meshless method II and III are much higher than those of the SSPH method provided that the same number of terms are employed in the associated TSEs for both methods. However, the codes developed for all methods can be optimized to decrease the CPU time required for the computations. Optimization of the codes to reduce the CPU

times for the computations was not the focus of this thesis that will be pursued in future studies.

In the last chapter, by using compactly supported radial basis functions (CSRBFs), performance of the DTM based meshless method I was compared with the SSPH method. The basis functions were used to solve the numerical examples given in Sections 5.2 and 5.3. Comparisons were made with the analytical solutions and results of the SSPH method. Total nine CSRBFs were examined to evaluate the accuracy of the DTM based meshless method I and SSPH method by considering various particle distributions and nonhomogeneous terms. It is observed that the use of CSRBFs yield better accuracy for both methods than revised super Gauss function, and both methods have the conventional convergence properties. The DTM based meshless method I yields smaller L_2 error norms than the SSPH method, especially in the existence of nonsmooth nonhomogeneous terms.

DİFERANSİYEL TRANSFORMASYON YÖNTEMİNİ KULLANARAK AĞSIZ YÖNTEMLERİN GELİŞTİRİLMESİ

ÖZET

Bu tez kapsamında diferansiyel transformasyon yöntemi yardımı ile ağsız yöntemler geliştirilmiş ve bu yöntemlerin performansları simetrik düzgünleştirilmiş parçacık hidrodinamiği ile farklı tipteki mühendislik problemlerinin çözümünde karşılaştırılmıştır.

Ağsız yöntemler, sonlu elemanlar yönteminin çok iyi bilinen; ağ örme veya yeniden yapılandırma işleminin zorluğu ve maliyeti, kilitlenme, eleman çarpılması gibi zaafiyetlerinin elemine edilebilecek alternatif numerik yaklaşımlardır. Ağsız yöntemler pratikte uygulanma fırsatı bulmuş ve güçlü bir numerik araç olma yönünde büyük bir potansiyel göstermektedir.

Ağsız yöntem, tüm problem bölgesi için önceden tanımlamış ağlar kullanmadan, cebrik denklemler sistemi oluşturmak için kullanılan bir yöntemdir. Ağsız yöntemler problem bölgesini sunmak için sınırlar üzerinde ve problem bölgesi içinde oluşturulan nodları kullanır. Birçok ağsız yöntem efektif uygulama alanları bulmuş ve bir sayısal araç olarak iyi bir potansiyel göstermiştir.

İlk olarak, düzgünleştirilmiş parçacık hidrodinamiği (SPH) yöntemi 1977 yılında Lucy tarafından önerilmiş olup, süreksiz akışkan mekaniği ve katı cisim mekaniği problemlerine başarıyla uygulanmaktadır. Bununla birlikte, iki önemli kusura sahiptir, birincisi sınırlarda bulunan tanelerdeki kusur ve gerilme kararsızlığı. Birçok teknik, örneğin; düzeltilmiş düzgünleştirilmiş parçacık hidrodinamiği, yeniden oluşan kernel parçacık yöntemi ve modifiye edilmiş parçacık hidrodinamiği , bu kusurları ortadan kaldırmak için geliştirilmiştir. Modifiye edilmiş parçacık hidrodinamiği yöntemi, kısımlara ayrılmış lineer elastik bir çubukta dalga yayılımı, kırık ucu yakınında gerilme alanının yakalanması, lineer elastik bir gövde üzerinde çatlakların ilerlemesinin simülasyonu gibi çalışmalarda uygulanmıştır.

Bununla birlikte modifiye edilmiş parçacık hidrodinamiği yöntemi, deneme çözümü değerlerini yaratmak için kullanılan kernel (ağırlık) fonksiyonunun tüm türevlerine gereksinim duyar ve türevlerinin bir noktada sabit bir değer alamaması kernel fonksiyonu seçimini sınırlamaktadır. Buna ilave olarak, deneme çözümünün kernel fonksiyonlarının bulunması için tersi alınacak matris ve türevleri asimetriktir. Simetrik düzgünleştirilmiş parçacık hidrodinamiği yönteminde, bu matrisin simetrik olması sağlanmakla birlikte, işlem zamanında ve kapasite gereksiniminde azalma sağlamakta, kernel fonksiyonunun sabit olamama durumu bu yöntem ile birlikte elemine edilmekte ve daha önemlisi modifiye edilmiş parçacık hidrodinamiği yönteminde elde edilen sayısal çözüme göre daha düşük hata vermektedir.

Simetrik düzgünleştirilmiş parçacık hidrodinamiği homojen olan sınır değer problemleri için daha uygun bir yöntem olup, lineer olmayan problemlere, işlem zamanını arttıran temel fonksiyonlarda dördüncü mertebeden yüksek terimler içermesi gereken burkulma problemlerine kolayca uygulanmayabilir.

Simetrik düzgünleştirilmiş parçacık hidrodinamiği yönteminin formülasyonu sebebiyle homojen olmayan sınır değer problemlerinde yaklaşık sonuçlar üretememesinden hareketle özellikle homojen olmayan problemler için alternatif bir yaklaşım araştırılmıştır. Taylor seri açılımı tabanında diferansiyel transformayon metodu uygulanarak üç yeni ağsız yöntem; diferansiyel transformasyon tabanlı ağsız yöntem I, yöntem II ve yöntem III bu tezde sunulmuştur. Simetrik düzgünleştirilmiş parçacık hidrodinamiği yöntemi ve diferansiyel transformasyon tabanlı ağsız yöntemler Taylor seri açılımına bağlı olsalar da, bu yaklaşımlar arasında ana fark şu şekilde açıklanabilir; simetrik düzgünleştirilmiş parçacık hidrodinamiği bir noddaki çözüm değerini diğer nodlardaki çözüm değerlerini kullanarak ve daha sonra bunları ana denklemlere katarak hesaplar bununla birlikte ana denklemlerdeki homojen olmayan terimler nodlar yardımıyla noktasal olarak değerlendirilirler. Bu yaklaşım özellikle düzgün değişmeyen homojen olmayan terimlerin olması ile yaklaşım hataları oluşturmaktadır. Ancak, diferansiyel transformasyon tabanlı ağsız yöntemler, çözümün Taylor serisi açılımını ve homojen olmayan terimleri ana denklemlere koyar ve sonrasında çözüm açılımlarındaki katsayılar ile homojen olmayan terimler arasında tekrarlanan kesin ilişkilerden faydalanır.

Simetrik düzgünleştirilmiş parçacık hidrodinamiği ve diferansiyel transformasyon tabanlı ağsız yöntemlerin performanslarını karşılaştırabilmek için bir boyutlu homojen olmayan sınır değer problemi, iki boyutlu homojen Laplace denklemi, iki boyutlu homojen olmayan Laplace denklemi ve iki boyutlu plaka deformasyonlarının düzlem gerilme durumu altında incelenmesine yönelik problemler bu tez kapsamında ele alınmıştır. Problem bölgelerinde farklı nod sayıları kullanılmış olup bahsi geçen yöntemlerin yaklaşım değerleri L_2 genel hata normu ile değerlendirilmiştir. Özellikle çalışılan homojen olmayan sınır değer problemleri için, diferansiyel transformasyon tabanlı ağsız yöntemleri L_2 genel hata normu değerlerinde önemli farklılıklar göstermişlerdir.

Bir boyutlu homojen olmayan sınır değer problemi çözümünden elde edilen sonuçlar ele alındığında, Taylor seri açılımında 5 terim kullanarak, diferansiyel transformasyon tabanlı ağsız yöntem II ve yöntem III problem bölgesinde 5 adet nod kullanıldığı halde bile kesin çözümü vermişlerdir.

Çalışılan bir sonraki problem iki boyutlu homojen Laplace denklemidir. Tüm diferansiyel transformasyon tabanlı ağsız yöntemler, simetrik düzgünleştirilmiş parçacık hidrodinamiği ile yaklaşık çözümler bazında karşılaştırıldığında daha yakınsak çözümler getirmişlerdir. Özellikle diferansiyel transformasyon tabanlı ağsız yöntem II sürekli olarak en düşük L_2 genel hata normunu problem bölgesinde artan nod sayısı ile gerçekleştirilen çözümlerde vermiştir. Diferansiyel transformasyon tabanlı ağsız yöntemlerin performansı sonlu elemanlar yöntemi ile de karşılaştırılmış olup, diferansiyel transformasyon tabanlı ağsız yöntemlerin daha düşük L_2 genel hata normunu verdiği tespit edilmiştir.

Homojen olmayan iki boyutlu Laplace denklemi bu tez kapsamında çalışılan diğer bir problemdir. Tüm dört ağsız yöntemin performansları; kompakt destek bölgesi çapının değişimi ve düzgünleştirme boy değişimi bazında problem bölgesindeki farklı nod dağılımları için karşılaştırılmıştır. Diferansiyel transformasyon tabanlı ağsız yöntem II ve III daima diğer iki yönteme kıyasla daha yakınsak çözüm değerleri vermişlerdir. Bunun yanında, simetrik düzgünleştirilmiş parçacık hidrodinamiği problem bölgesinde 171 nod bulundurularak gerçekleştirilen çözümlerde düzgünleştirme boyu $h=1.8\Delta$'ya (Δ kompakt destek bölgesi içindeki

nodlar arası en yakın mesafe) kadar ile stabil sonuçlar verirken diferansiyel transformasyon tabanlı ağsız yöntem II ve III düzgünleştirme boyu h=2Δ'ya kadar stabil sonuçlar vermiştir. Diferansiyel transformasyon tabanlı ağsız yöntem III, daima problem bölgesinde artan nod sayısı ile birlikte en düşük L_2 genel hata normu değerini vermiştir.

Tüm bu yöntemler kullanılarak çalışılan en son problem, iki boyutlu plaka deformasyonlarının düzlem gerilme durumu altında incelenmesidir. Diferansiyel transformasyon tabanlı ağsız yöntem II ve III daima problem bölgesinde artan nod sayısı ile birlikte en düşük L_2 genel hata normu değerini vermiştir. Bu yöntemler ayrıca, problem bölgesinde artan nod sayısı ile birlikte, plaka üst kenarı boyunca boyutsuz gerilme değerinde $\sigma_{xx}(L_2/F_0)$ en az değişimi vermişlerdir. Diferansiyel transformasyon tabanlı ağsız yöntem I tatmin edici sonuçlar vermemiş olup çözümlerde sadece 64 adet nod dağılımı dikkate alınmıştır. İşlem zamanları, Diferansiyel transformasyon tabanlı ağsız yöntem II, III ve simetrik düzgünleştirilmiş parçacık hidrodinamiği yöntemleri için karşılaştırılmış olup, simetrik düzgünleştirilmiş parçacık hidrodinamiği yönteminin en düşük işlem zamanına sahip olduğu görülmüştür.

Son bölümde diferansiyel transformasyon tabanlı ağsız yöntem I ve simetrik düzgünleştirilmiş parçacık hidrodinamiği yöntemlerinin performansları kompakt destekli radyal temel fonksiyonlar kullanılarak karşılaştırılmıştır. Kısım 5.2 ve 5.3'te verilen problemler için numerik çözümler elde edilmesinde 9 farklı kompakt destekli radyal temel fonksiyon kullanılmıştır.

Diferansiyel transformasyon tabanlı ağsız yöntem I tüm analizlerde simetrik düzgünleştirilmiş parçacık hidrodinamiğibe göre daha düşük global L_2 hata normları vermiş bununla birlikte her iki yöntemle elde edilen global L_2 hata normlarının revize edilmiş süper Gauss fonksiyonu ile elde edilenlere kıyasla daha düşük oldukları tespit edilmiştir.

1. INTRODUCTION

Recently, considerable research in computational mechanics has been devoted to the development of meshless methods that lessen difficulty of meshing and remeshing the entire structure by only adding or deleting nodes at suitable locations. Meshless methods may also alleviate some other problems associated with the Finite Element Method (FEM), such as locking and element distortion. In many applications, they provide smooth and accurate approximate solutions with a reduced number of nodes [1-3].

1.1 Purpose of Thesis

The purpose of this thesis is to evaluate the performance of the Symmetric Smoothed Particle Hydrodynamics (SSPH) method for some engineering problems such as two dimensional heat conduction and elasticity problems and develop a new approach that may provide more accurate results than the SSPH method by using strong formulations.

1.2 Literature Review

During the last decades, several meshless methods for seeking approximate solutions of partial differential equations have been proposed; these include the smoothed particle hydrodynamics method (SPH) [4-5], the diffuse element method [6], the reproducing kernel particle method (RKPM) [7], the element-free Galerkin method (EFG) [8], h-p clouds method [9], finite point method [10], boundary node method [11], meshless local Petrov-Galerkin method (MLPG) [12], point interpolation method [13], corrective smoothed particle method (CSPM) [14], boundary point interpolation methods [15], method of finite spheres [16], point collocation method [17], boundary cloud method [18], modified smoothed particle hydrodynamics method (MSPH) [19] and symmetric smoothed particle hydrodynamics (SSPH) [20].

All of these methods except the MLPG, SPH, MSPH, SSPH and point collocation method are not truly meshless since the use of shadow elements is required for evaluating integrals appearing in the governing weak formulations.

The SSPH method has been successfully applied to several structural problems; stress concentration in a plate (near a circular hole is a semi-infine isotropic and homogenous linear elastic plate) [21], plane stress deformations of a plate [20], wave propagation in bar [21], deformations of a rectangular plate with a crack at the center, deformations of a plate with two horizontal cracks emanating from opposite vertical edges [22] and heat transfer problems [23]. The SSPH basis functions can be applied to solve the engineering problems by implementing both strong and weak formulations.

2. OVERVIEW OF MESHLESS METHODS

2.1 Why Meshless Methods

Recently, there is a growing interest in developing meshless methods in the general area of computatitonal mechanics as alternatives of finite element methods (FEM). In the FEM procedure, the continuum structure is divided into elements of which are connected together by mesh. With the light of the studies done by using FEM, it can be concluded that the FEM is a robust and thoroughly developed method.

On the other hand FEM has some well known inherent shortcomings such as high cost of creating mesh, low accuracy in stress, difficulty in adaptive analysis and limitation in the analysis of some problems.

The creation of the FEM mesh is the most time consuming activity of the FEM analysis and becomes the major part of the computational cost of the computer aided engineering (CAE) project. The stress could not be predicted accurately by many FEM packages. To recover accurate stress, special tecniques are required in the post processing stage.

For the three dimensional problems the computational cost of re-meshing at each step is very expensive, even if an adaptive scheme were available. In addition, an adaptive analysis requires “mappings” of the field variables between meshes in successive stages of the analysis. The additional computation and degradation of accuracy in the solution can be the output of the mapping process.

Because of the element distortions under large deformation, considerable loss in accuracy is observed in FEM analysis. The simulation of the crack growth with arbitrary and complex paths which do not coincide with the original element interfaces and the simulation of the breakage of material with large number fragments is difficult. In FEM, the elements cannot be broken because the FEM is based on continuum mechanics.

2.2 Solution Procedure of Meshless Methods

In this section, the solution procedure of meshless methods will be outlined. Figure 2.1 shows the procedures of FEM and meshless method. The methods depart at the stage of mesh creation and constructions of the shape functions.

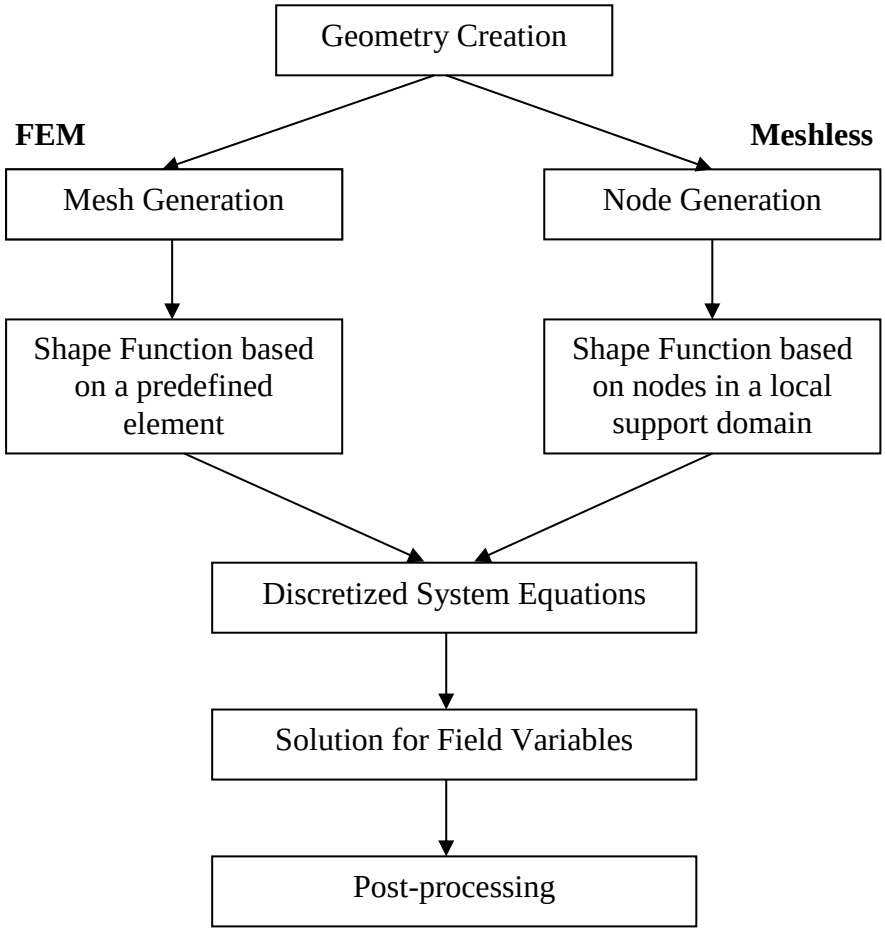

Figure 2.1 : Procedures of the FEM and meshless methods [25].

The problem domain and its boundary are created and represented by using sets of nodes scattered in the problem domain and on its boundary in meshless methods. The number of the nodes depends on the accuracy required and resources available. The nodal distribution is usually not uniform. Meshless methods should be able to work for an arbitrary node distribution.

In the FEM, this step is different. To discretize the geometry and create the elements, the meshing is needed. The geometry has to be meshed properly into elements of specific shapes such as triangles and quadrilaterals. The overlapping or gaps are not allowed. Mesh generation is a very important part of the pre-process of the FEM.

Figure 2.2 shows the differences of the domain representation in the meshless method and FEM [25].

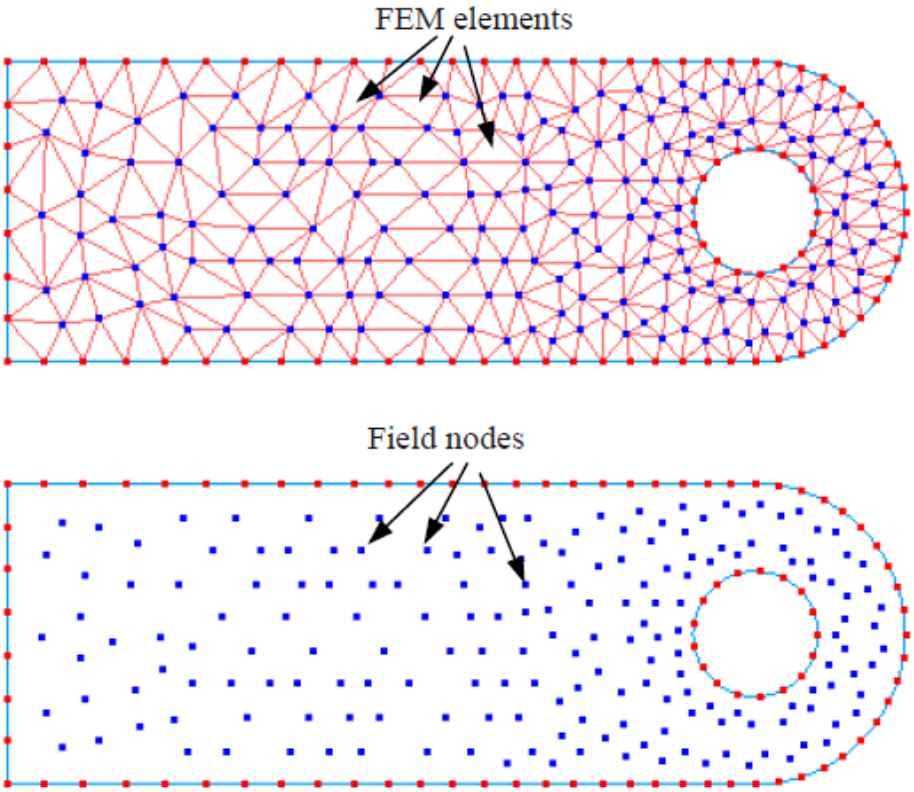

Figure 2.2 : Domain representation in FEM and meshless methods [24].

The approximated function can be written by a meshless method as follows;

$$\mathbf{u}^{h}(\mathbf{x}) = \sum_{\mathbf{i=1}}^{\mathbf{n}} \emptyset_{\mathbf{i}}(\mathbf{x})\mathbf{u}_{\mathbf{i}} = \mathbf{\Phi}^{\mathbf{T}}(\mathbf{x})\mathbf{U}_{\mathbf{s}} \qquad (\mathbf{2.1})$$

where n is the number of the nodes in the local support domain of the point at x, u_i is the nodal value at the ith node, U_s is the vector that collects all the nodal values at these n nodes, and $\emptyset_i(x)$ is the shape function of the i^{th} node determined by using these nodes included in the support domain of x.

The support domain can have different shapes, its dimension and shape can be different as shown in Figure 2.3, and they are usually circular or rectangular.

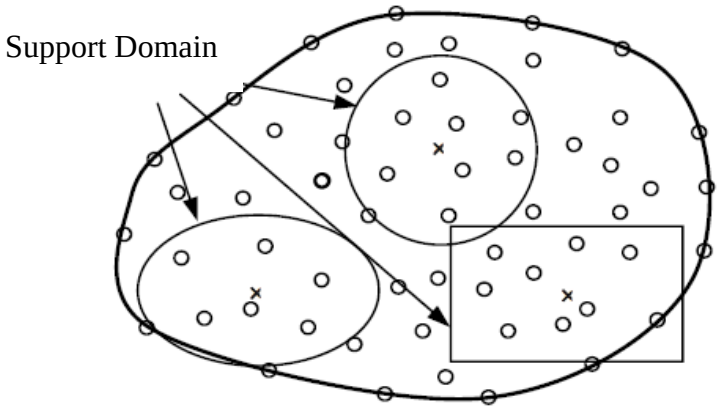

x: point of interest o: field node

Figure 2.3 : Support domains used in the meshless methods [24].

The discrete equations of a meshless method can be formulated using the shape functions and strong or weak form equation systems to be detailed in the next section [24]. Comparisons between the FEM and meshless method are listed in Table 2.1.

Table 2.1 : Differences between FEM and meshless method [24].

Items	FEM	Meshless Method
Mesh	Yes	No
Shape function	Based on predefined elements	Based on support domains
Discretized system stiffness matrix	Banded, symmetric	Banded, may or may not be symmetric depending on the method used
Imposition of essential boundary condition	Easy and standard	Special treatments may be required, depending on the method used
Computation speed	Fast	Slower compared to the FEM
Accuracy	Accurate compared to FDM	More accurate than FEM
Adaptive analysis	Difficult for 3D cases	Easier
Stage of develeopment	Well developed	Infant, with many challenging problems
Commercial software	Many	Few

2.3 Key Ingredients of Meshless Methods

The key ingredients of the meshless methods may be summarized as follows: support domain, smoothing length, weight function and weak and strong formulations. Details of them are provided below.

2.3.1 Support domain and smoothing length

The accuracy of the approximation depends on the nodes in the support domain as shown in Figure 2.4. Therefore, a suitable support domain should be chosen to ensure an efficient and accurate approximation. For a point of interest $\mathbf{x}_i$, the dimension of the support domain d is determined by

$$d = \rho h \qquad (\mathbf{2.2})$$

where ρ is the dimensionless size of support domain, and h is the smoothing length near the point at $\mathbf{x}_i$. If the nodes are uniformly distributed, h is simply the distance between two neighboring nodes. When nodes are non-uniformly distributed, h can be defined as the smallest distance between the node i and the other nodes in the compact support domain Ω_s. Ω is defined as the entire problem domain.

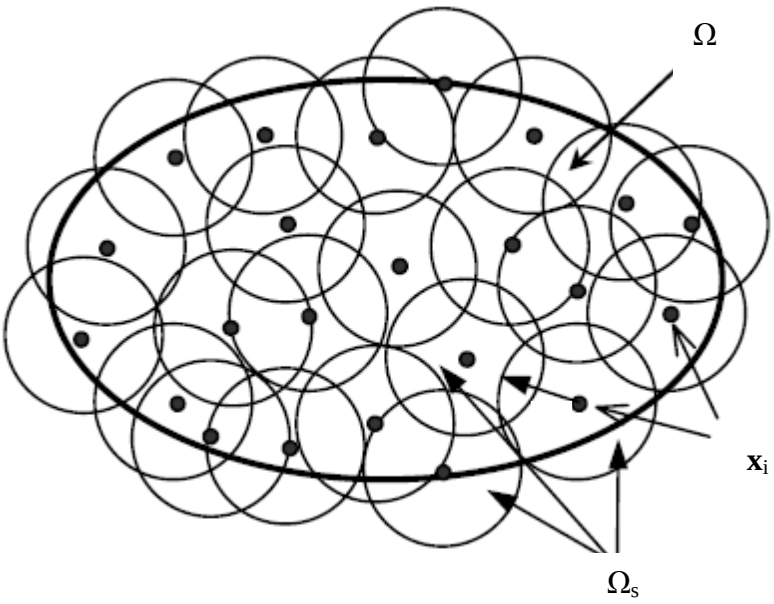

Figure 2.4 : Support domains of point of interest at $\mathbf{x}_i$ in meshless methods [24].

The dimensionless size of the compact support domain ρ controls the dimension of the support domain. For instance, ρ=3.5 means that a support domain whose radius is 3.5 times the smoothing length. The dimensionless size of the compact support

domain should be pre-determined by the analyst before the analysis, and it is usually determined by carrying out numerical experiments for a class of benchmark problems [24].

2.3.2 Weigth function

The weight function is the central and most important issue in meshless methods. The weight function should be constructed according to the conditions given below;

$$W(\mathbf{x}-\boldsymbol{\xi},\mathrm{h})>0 \text{ over } \Omega \qquad (\mathbf{2.3})$$

$$W(\mathbf{x}-\boldsymbol{\xi},\mathrm{h})=0 \; outside \; \Omega \qquad (\mathbf{2.4})$$

$$\int_{\Omega} W(\mathbf{x}-\boldsymbol{\xi},\mathrm{h})d\xi = 1 \qquad (\mathbf{2.5})$$

$$W(\mathrm{s},\mathrm{h}) \rightarrow \delta(s) \; as \; h \rightarrow 0 \qquad (\mathbf{2.6})$$

The first condition given in Equation (2.3) is the positivity, it is important to ensure a meaningful presentation of some physical phenomena.

The second condition given in Equation (2.4) is the compactness, it is important because it enables the approximation to be generated from a local representation of nodes.

The third condition given in Equation (2.5) is the unity, it assures the zeroth-order consistency (C°) of the integral form representation of the continuum function.

The forth condition given in Equation (2.6) is redundant; if a function satisfies the conditions given above, it would naturally satisfy the last condition. In addition, the smoothing length *h* never goes to zero in practical numerical analysis. Existence of this condition allows us to observe that the meshless method is converging to its exact solution. *W* is a monotonically decreasing function [24-25].

Most of the weight functions are bell shaped. The following is a list of commonly used weight functions.

The linear weight function:

$$W(d) = \frac{G}{h^{\lambda}} \begin{cases} \frac{2-d}{4} & 0 \le d \le 2 \\ 0 & 2 < d \end{cases} \tag{2.7}$$

The quadratic weight function:

$$W(d) = \frac{G}{h^{\lambda}} \begin{cases} 1 - d + d^2/4 & 0 \le d \le 2 \\ 0 & 2 < d \end{cases} \tag{2.8}$$

The quadratic spline weight function:

$$W(d) = \frac{G}{h^{\lambda}} \begin{cases} 1 - \frac{3}{2}d^2 + d^3 - \frac{3}{16}d^4 & 0 \le d \le 2 \\ 0 & 2 < d \end{cases} \tag{2.9}$$

The cubic B-spline weight function:

$$W(d) = \frac{G}{h^{\lambda}} \begin{cases} 1 - 1.5d^2 + 0.75d^3 & 0 \le d < 1 \\ (2 - d^3)/4 & 1 \le d \le 2 \\ 0 & 2 < d \end{cases} \tag{2.10}$$

The revised Gauss weight function:

$$W(d) = \frac{G}{h^{\lambda}} \begin{cases} (e^{-d^2} - e^{-4}) & 0 \le d \le 2 \\ 0 & 2 < d \end{cases} \tag{2.11}$$

The revised super Gauss weight function:

$$W(d) = \frac{G}{h^{\lambda}} \begin{cases} (4 - d^2)e^{-d^2} & 0 \le d \le 2 \\ 0 & 2 < d \end{cases} \tag{2.12}$$

Here $d = |\boldsymbol{x} - \boldsymbol{\xi}|/h$, λ equals the dimensionality of the space, *G* is the normalizing constant determined by the condition that the integral of the weight function over the domain equals 1.0. For $\lambda = 1$, *G* equals, respectively, 1, 0.75, 5/8, 2/3, 1.04823 and 2/7 for the linear, quadratic, quartic spline, cubic B-spline, revised Gauss and revised super Gauss functions [19].

2.4 Strong and Weak Formulations

Partial differential equations or governing equations are the strong forms of system equations. The ideal is to obtain the exact solution for a strong form of the equation system is, however it is very difficult for practical engineering problems that are usually complex in nature.

In a strong form formulation, the approximation function should have sufficient degree of consistency, so that it is differentiable up to the order of the partial differential equations. The weak form, in contrast to the strong form, requires a weaker consistency for the approximate function. This can be achieved by introducing an integral operation to the equation system based on a mathematical or physical principle. The weak form provides a variety of ways to formulate methods for approximate solutions of complex systems. Formulation based on weak forms can usually produce a very stable set of discretized equation systems that produces much more accurate results.

There are two major categories of principles used for constructing weak form formulations: variational and weighted residual methods. The Galerkin weak form and Petrov-Galerkin weak form formulations may be the most widely used approaches for establishing equation systems.

The minimum total potential energy principle is a convenient tool for deriving discrete equation systems for the FEM and many other types of meshless methods. The weighted residual method is a powerful mathematical tool that can be used for creating discretized equation systems for many types of engineering problems in general. Galerkin weak form (Global weak form) and Petrov-Galerkin weak form (Local weak form) formulations will be given below with details [24-25].

2.4.1 Galerkin weak form formulation

The Galerkin weak form can be derived directly from the minimum total potential energy principle. This principle states that at an equilibrium state, the total potential energy in the system is stationary for a given set of admissible displacements.

For solids and structures of elastic materials, the total potential energy can be written as

$$\Pi = \Pi_s - W_f \qquad (\mathbf{2.13})$$

where Π_s is the strain energy, and W_f is the work done by the external forces.

To create a set of discretized system equations the stationary conditions are used.

$$\frac{\partial \Pi}{\partial a} = \begin{Bmatrix} \frac{\partial \Pi}{\partial a_1} \\ \frac{\partial \Pi}{\partial a_2} \\ \cdot \\ \cdot \\ \cdot \end{Bmatrix} = 0 \qquad (\mathbf{2.14})$$

The number of equations created is equal to the total numbers of the nodal variables. The solution of this problem can be obtained by solving Equation (2.14).

The strain energy of the system for solids and structures of elastic materials can be expressed as

$$\Pi_s = \frac{1}{2}\int_{\Omega} \boldsymbol{\varepsilon}^T \boldsymbol{\sigma} d\Omega \qquad (\mathbf{2.15})$$

where $\boldsymbol{\varepsilon}$ is the strain vector and $\boldsymbol{\sigma}$ is the stress vector. The work done by the external forces is

$$W_f = \int_{\Omega} \mathbf{u}^T \mathbf{b} d\Omega + \int_{\Gamma_t} \mathbf{u}^T \bar{\mathbf{t}} d\Gamma \qquad (\mathbf{2.16})$$

where $\mathbf{u}$ is the displacement vector, Ω is the problem domain, Γ_t stands for the boundary of the solids on which traction forces are prescribed, the $\mathbf{b}$ is the vector of external forces and $\bar{\mathbf{t}}$ is the prescribed tractions.

Hence, the total potential energy can be expressed as

$$\Pi = \frac{1}{2}\int_{\Omega} \boldsymbol{\varepsilon}^T \boldsymbol{\sigma} d\Omega - \int_{\Omega} \mathbf{u}^T \mathbf{b} d\Omega - \int_{\Gamma_t} \mathbf{u}^T \bar{\mathbf{t}} d\Gamma \qquad (\mathbf{2.17})$$

The variation of potential energy can be written as

$$\delta\Pi = \frac{1}{2}\int_{\Omega} \delta(\boldsymbol{\varepsilon}^T \boldsymbol{\sigma}) d\Omega - \int_{\Omega} \delta\mathbf{u}^T \mathbf{b} d\Omega - \int_{\Gamma_t} \delta\mathbf{u}^T \bar{\mathbf{t}} d\Gamma \qquad (\mathbf{2.18})$$

The integrand in the first integral term can be written as follows using the chain rule of variation

$$\delta(\boldsymbol{\varepsilon}^T \boldsymbol{\sigma}) = \delta\boldsymbol{\varepsilon}^T \boldsymbol{\sigma} + \boldsymbol{\varepsilon}^T \delta\boldsymbol{\sigma} \qquad (\mathbf{2.19})$$

We note that

$$\boldsymbol{\varepsilon}^T \delta\boldsymbol{\sigma} = (\, \boldsymbol{\varepsilon}^T \delta\boldsymbol{\sigma} \,)^{\,T} = \delta\boldsymbol{\sigma}^T \boldsymbol{\varepsilon} \qquad (\mathbf{2.20})$$

By using the constitutive equation of solids and symmetry of the matrix of material constants **D**, we have

$$\delta\boldsymbol{\sigma}^T \boldsymbol{\varepsilon} = \delta(\boldsymbol{D}\boldsymbol{\varepsilon})^T \boldsymbol{\varepsilon} = \delta\boldsymbol{\varepsilon}^T \boldsymbol{D}^T \boldsymbol{\varepsilon} = \delta\boldsymbol{\varepsilon}^T \boldsymbol{D}\boldsymbol{\varepsilon} = \delta\boldsymbol{\varepsilon}^T \boldsymbol{\sigma} \qquad (\mathbf{2.21})$$

Therefore, Equation (2.19) becomes

$$\delta(\boldsymbol{\varepsilon}^T \boldsymbol{\sigma}) = 2\, \delta\boldsymbol{\varepsilon}^T \boldsymbol{\sigma} \qquad (\mathbf{2.22})$$

The minimum total potential energy principle requires $\delta\Pi = 0$. Then, the following Galerkin weak form can be obtained:

$$\int_{\Omega} \delta\boldsymbol{\varepsilon}^T \boldsymbol{\sigma} d\Omega - \int_{\Omega} \delta\mathbf{u}^T \mathbf{b} d\Omega - \int_{\Gamma_t} \delta\mathbf{u}^T \bar{\mathbf{t}} d\Gamma = 0 \qquad (\mathbf{2.23})$$

Equation (2.23) can also be seen as the principle of virtual work, which states that if a solid body is in its equilibrium state, the total virtual work performed by all stresses in the body and all external forces applied on the body vanishes, when the body is subjected to a virtual displacement. The first term in Equation (2.23) is the virtual work done by the internal stress in the problem domain; the second term is the virtual work done by the external body force and the third term is the virtual work done by the external tractions on the boundaries.

The Galerkin weak form is very handy in application to problems of solid mechanics, because the integration by parts is not needed to be performed any more. The discretized equation system can be derived very easily using approximated displacements of which are satisfying the admissible conditions [24-25].

2.4.2 Local Petrov-Galerkin weak form formulation

In deriving local weak forms, the Petrov-Galerkin procedure has to be used. The Petrov-Galerkin procedure is often used in the FEM formulation for convection dominated systems to obtain a stabilized solution. The local Petrov-Galerkin weak forms have been used to formulate the MLPG method.

In a problem domain Ω, the governing equation of 2D solids at a point $\mathbf{x}_I$ is approximately satisfied by a subdomain weighted residual method. A local weak

form of the governing equation over a subdomain Ω_q bounded by Γ_q can be obtained by using the weighted residual method locally

$$\int_{\Omega_q} W_I\left(\sigma_{ij,j} + b_i\right)\mathrm{d}\Omega = 0 \qquad (\mathbf{2.24})$$

where $W_I$is the weight function or the test function centered at the point $\mathbf{x}_I$. The first term on the left side of the Equation (2.24) can be integrated by parts to obtain

$$\int_{\Omega_q} W_I\sigma_{ij,j}\mathrm{d}\Omega = \int_{\Gamma_q} W_I n_j\sigma_{ij}\mathrm{d}\Gamma - \int_{\Omega_q} W_{I,j}\sigma_{ij}\,\mathrm{d}\Omega \qquad (\mathbf{2.25})$$

where n_j is the *j*th component of the unit outward normal vector on the boundary. By substituting Equation (2.25) into Equation (2.24), the following local weak form is obtained.

$$\int_{\Gamma_q} W_I n_j\sigma_{ij}\mathrm{d}\Gamma - \int_{\Omega_q} [W_{I,j}\sigma_{ij} - W_I b_i]\mathrm{d}\Omega = 0 \qquad (\mathbf{2.26})$$

Equation (2.26) is the local Petrov-Galerkin weak form for 2D solids. This equation suggests that instead of solving the strong form of the equation system, a relaxed weak form with integration over a small local quadrature domain is emploed. This integration operation can smear out the numerical error, and therefore make the discrete equation system much more accurate compared to the numerical procedures that operate directly on the strong forms of governing equations.

Because the local weak form is obtained by the weighted residual method, the weight function plays an important role. Any weight function is acceptable as long as the condition of continuity is satisfied and all the weight (test/trial) functions defined for all the nodes in the problem domain are linearly independent [24-25].

2.5 Smoothed Particle Hydrodynamics

The smoothed particle hydrodynamics method is one of the earliest meshless methods employing Lagrangian description of motion. It was proposed by Lucy [4] and Gingold and Monaghan [5] to analyze astrophysical problems in a three dimensional space. Libersky and Petschek [26] extended it to study the dynamic

response of materials. The method has been applied to several classes of problems, such as free surface flows [27], explosion phenomenon [28-31], impact and penetration [32-33], computational solid dynamics in problems such as: development of fracture and elastic behavior of solids with large deformation [34-38].

In the SPH method, the approximate value $f(\boldsymbol{x})$ of a function *f* at a point **x** in domain Ω is given by

$$f(\boldsymbol{x}) = \int_{\Omega} f(\boldsymbol{\xi}) W(\boldsymbol{x} - \boldsymbol{\xi}, h) \mathrm{d}\xi \qquad (\mathbf{2.27})$$

where $W(\boldsymbol{x} - \boldsymbol{\xi})$ is a kernel or a weight function. The approximate value of *f* depends on two parameters; the kernel *W* and smoothing length *h* which determines the compact support domain of *W*. The kernel function *W* is required to have the properties given in Section 2.3.2.

The spatial derivative ∇f at the point **x** is approximated by

$$\nabla f(\boldsymbol{x}) = \int_{\Omega} \nabla f(\boldsymbol{\xi}) W(\boldsymbol{x} - \boldsymbol{\xi}, h)\, \mathrm{d}\boldsymbol{\xi} = -\int_{\Omega} f(\boldsymbol{\xi}) \nabla W(\boldsymbol{x} - \boldsymbol{\xi}, h)\, \mathrm{d}\boldsymbol{\xi} \qquad (\mathbf{2.28})$$

For numerical study, the integral given in Equation (2.27) is approximated by imagining that the mass in Ω is divided into *N* particles of masses $m_1, m_2, m_3, \dots, m_N$ and densities $\rho_1, \rho_2, \rho_3, \dots, \rho_N$ respectively. The value of f_i of the integral given in Equation **(2.27)** for the *i*th particle is approximated by

$$f_i = \sum_{j=1}^{N} \frac{m_j f_j W_{ij}}{\rho_j}; \qquad W_{ij} = W\left(\boldsymbol{x}^{(i)} - \boldsymbol{\xi}^{(j)}\right) \qquad (\mathbf{2.29})$$

Because of the compact support of the kernel function *W*, the number of particles used in the summation given in Equation (2.29) is smaller than *N*. Similiarly, Equation (2.28) is approximated by

$$f_{\alpha i} \equiv \frac{\partial f}{\partial \boldsymbol{x}_{\alpha i}^{(i)}} = -\sum_{j=1}^{N} \frac{m_j f_j W_{ij}}{\rho_j}$$

$$W_{ij,\alpha} = -\frac{\partial W}{\partial \boldsymbol{x}_{\alpha}}\Big|_{\boldsymbol{x}=\boldsymbol{x}^{(i)}, \boldsymbol{\xi}=\boldsymbol{\xi}^{(j)}}, \alpha = 1,2,3. \qquad (\mathbf{2.30})$$

The range of index α equals to the spatial dimension of the domain Ω. For a constant function $f(\boldsymbol{x}) = f_i$, Equation (2.30) gives

$$\sum_{j=1}^{N} \frac{m_j f_j W_{ij}}{\rho_j} = 0 \qquad (\mathbf{2.31})$$

Addition of Equations (2.30) and (2.31) gives

$$f_{\alpha i} = \sum_{j=1}^{N} \frac{m_j (f_j - f_i) W_{ij,\alpha}}{\rho_j} \qquad (\mathbf{2.32})$$

Similiarly, one can deduce the following approximation for the second order derivatives;

$$f_{\alpha\beta i} = \sum_{j=1}^{N} \frac{m_j (f_j - f_i) W_{ij,\beta\alpha}}{\rho_j} \qquad (\mathbf{2.33})$$

where

$$f_{\alpha\beta i} = \left.\frac{\partial^2 f}{\partial x_\alpha \partial x_\beta}\right|_{\boldsymbol{x}=\boldsymbol{x}^{(i)}}$$

$$W_{ij,\alpha\beta} = \left.\frac{\partial^2 W}{\partial x_\alpha \partial x_\beta}\right|_{\boldsymbol{x}=\boldsymbol{x}^{(i)},\boldsymbol{\xi}=\boldsymbol{\xi}^{(j)}} \qquad (\mathbf{2.34})$$

2.6 Diffuse Element Method

The diffuse element method (DEM) was proposed by Nayroles, Touzot and Villon [6]. In this method, only a mesh of nodes and a boundary description are needed to develop the Galerkin equations. The interpolants are polynomials which are fit to the nodal values by a least squares approximation. This method was generalized and improved by Belytschko [8] and the mentioned method has been called as the element free Galerkin method. The details were given in Section 2.8.

2.7 Reproducing Kernel Particle Method

The RKPM was developed on the basis of the SPH method. For the finite field problems, the SPH method leads to low computational accuracy and instability because the compatibility conditions on the boundary cannot be satisfied. To

overcome the disadvantages of the SPH method for solving a finite domain problem, Liu proposed the RKPM [7] by introducing a corrected function to integral transformation in the SPH method to satisfy the boundary compatibility, and the instability of the SPH method can be eleminated.

The application of the RKPM to various mechanical problems has been given rise to remarkable results [39-50]. In comparison to the traditional finite element method, the RKPM commonly uses higher order weight functions which leads to shape functions with higher order of continuity. This fact proposes the RKPM as an efficient technique for studying various phenomena, particularly those suffering from mesh distortion, shootings and steep gradients.

The traditional SPH method does not have the zeroth order consistency on the boundaries. In the RKPM, it is remedied by modifying the kernel function for 1D problem to $\bar{W}(x-\xi)$ defined by

$$\bar{W}(x-\xi) = W(x-\xi)C(x-\xi) \qquad (\mathbf{2.38})$$

where $C(x-\xi)$ is a correction to the kernel function. Expanding the function $f(\xi)$ in terms of Taylor series around the point *x* and setting

$$m_k(x) = \int_{\Omega} (x-\xi)^k W(x-\xi)d\xi \qquad k = 0,1,2,\dots,n, \qquad (\mathbf{2.39})$$

Equation (2.27) can be written as

$$f(x) = m_0(x)f(x) - m_1(x)f'(x) + \cdots + \frac{(-1)^n}{n!}m_n(x)f^{(n)}(x) + \cdots \qquad (\mathbf{2.40})$$

In order to reproduce the orginal function, the correction kernel is chosen by setting coefficients of the first and higher order derivatives to zero and the coefficient of the constant term to one. That is,

$$\frac{(-1)^n}{n!}m_n(x) = \delta_{n0} \qquad (\mathbf{2.41})$$

where δ_{ij} is the Kronecker delta function. In general, $C(x-\xi)$ in the corrected kernel is chosen to be the polynomial function.

$$C(x-\xi) \approx \mathbf{Pb} \qquad (\mathbf{2.42})$$

where the matrix **P** is as follows

$$\mathbf{P}(\boldsymbol{\xi}-\mathbf{x}) = [1, (\xi_1 - x_1), (\xi_2 - x_2), (\xi_3 - x_3), (\xi_1 - x_1)^2, (\xi_2 - x_2)^2, (\xi_3 - x_3)^2,$$
$$(\xi_1 - x_1)(\xi_2 - x_2), (\xi_2 - x_2)(\xi_3 - x_3), (\xi_1 - x_1)(\xi_3 - x_3)] \qquad (\mathbf{2.43})$$

and $\mathbf{b} = [b_0(x), b_1(x), \dots, b_n(x)\ ]^T$. The k^{th} order moment of the corrected kernel function can be written as

$$m_k(x) = \int_{\Omega} (x-\xi)^k C(x-\xi) W(x-\xi) d\xi$$

$$= \int_{\Omega} (x-\xi)^k \mathbf{P}\mathbf{b} W(x-\xi) d\xi$$

$$= b_0(x)m_k(x) + b_1(x)m_{k+1}(x) + \cdots + b_n(x)m_{k+n}(x) \qquad (\mathbf{2.44})$$

where $m_k(x)$ is the k^{th} order moment of the original kernel $W(x-\xi)$.

From Equations (2.42) and (2.44), we get

$$\mathbf{M}(x)\mathbf{b}(x) = \{1,0,0\}^T = \mathbf{P}^T(0) \qquad (\mathbf{2.45})$$

where

$$\mathbf{M}(x) = \begin{bmatrix} m_0(x) & \cdots & m_n(x) \\ \vdots & \ddots & \vdots \\ m_n(x) & \cdots & m_{2n}(x) \end{bmatrix} \qquad (\mathbf{2.46})$$

And then we can write Equation (2.45) as

$$\mathbf{b}(x) = \mathbf{M}^{-1}(x)\mathbf{P}^T(0) \qquad (\mathbf{2.47})$$

By subsittuting **b** in Equation (2.42) and result in Equation (2.38), we get

$$f(x) = \int_{\Omega} \mathbf{P}\mathbf{b} W(x-\xi) f(\xi) d\xi \qquad (\mathbf{2.48})$$

Similiarly, we obtain the following for the first and second derivatives of the function $f(x)$

$$f'(x) = \int_{\Omega} f(\xi) \frac{d}{dx} [\mathbf{P}\mathbf{b} W(x-\xi)] d\xi,$$

$$f''(x) = \int_{\Omega} f(\xi) \frac{d^2}{dx^2} [\mathbf{P}\mathbf{b} W(x-\xi)] d\xi \qquad (\mathbf{2.49})$$

For the RKPM, we rewrite kernel estimates of the function $f(x)$ and of its first and second derivatives together in the matrix form as

$$\begin{Bmatrix} f_i \\ f_{xi} \\ f_{xxi} \end{Bmatrix} = \begin{Bmatrix} \int_\Omega \mathbf{Pb} W\left(x^{(i)} - \xi\right) f(\xi) d\xi \\ \int_\Omega \frac{d}{dx} [\mathbf{Pb} W\left(x^{(i)} - \xi\right)] f(\xi) d\xi \\ \int_\Omega \frac{d^2}{dx^2} [\mathbf{Pb} W\left(x^{(i)} - \xi\right)] f(\xi) d\xi \end{Bmatrix} \qquad (\mathbf{2.50})$$

2.8 Element Free Galerkin Method

Element free Galerkin (EFG) method was proposed by Belytschko [8] for modeling of the crack growth in static and dynamics problems [51-53]. Defined by Lancaster and Salkauskas [54], the moving least square (MLS) approximation which originated in scattered data fitting is chosen to construct element free Galerkin shape functions and their derivatives. In the element free Galerkin method, the value of an unknown field at a point is interpolated from nodal data at nodes in a prescribed vicinity of the point. This prescribed vicinity is known as the influnce zone of the point and it removes the need for elements. A background cell structure, which is independent of nodal points, is employed for the procedure to compute the integral expression. The Galerkin weak form is employed to develop the discretized sysem of equations.

The major differences between the diffuse element method and the element free Galerkin are as follows; element free Galerkin method includes certain terms in the derivatives of the interpolants which were omitted by Nayroles [6], the element free Galerkin method uses Lagrange multipliers to enforce essential boundary conditions and the element free Galerkin method uses a large number of quadrature points arranged in a cell structure that overlays the domain.

Fleming et al. [55] developed enriched element free Galerkin methods for simulating the crack tip fields. Xu and Saigal [56] further improved the formulation for stable crack growth in elastic solids. Tabbara and Stone [57] developed a computational element free Galerkin for quasi-static mixed-mode fracture problem. Fleming [58] developed and implemented the element free Galerkin method for fatique and quasi-static crack growth. Ventura [59] proposed a new level set method for the description of a propagating crack in the element free Galerkin method. Li ans Simonsen [60]

used the element free Galerkin method to simulate ductile crack growth and propagation under finite deformation and large scale yielding conditions.

Consider a function $u(\mathbf{x})$ of variable **x** defined in the domain Ω. The function $u(\mathbf{x})$ can be approximated by the function defined by

$$u^h(\mathbf{x}) = \mathbf{P}^T(\mathbf{x})\mathbf{a}(\mathbf{x}) \qquad (\mathbf{2.51})$$

where $\mathbf{P}^T(\mathbf{x})$ is a complete polynomial of order m and $\mathbf{a}(\mathbf{x})$ is a vector of undefined coefficients. An example of $\mathbf{P}^T(\mathbf{x})$ for a two dimensional problem with $\mathbf{x} = (\mathrm{x}, \mathrm{y})$ are; $\mathbf{P}^T(\mathbf{x}) = [1, x, y]$ where n=3, first order complete polynomial and $\mathbf{P}^T(\mathbf{x}) = [1, x, y, x^2, y^2, xy]$ where n=6, second order complete polynomial. The weighted discrete L^2 norm *J* can be defined by

$$J\big(\mathbf{a}(\mathbf{x})\big) = \sum_{I=1}^{N(\mathbf{x})} W^I(\mathbf{x})\,(\mathbf{P}^T(\mathbf{x}^I)\mathbf{a}(\mathbf{x}) - u_I)^2 \qquad (\mathbf{2.52})$$

where $W^I(\mathbf{x}) = W^I(\mathbf{x} - \mathbf{x}^I)$ is the weigth function of compact support associated with particle I having coordinates $\mathbf{x}^I$, u_I is the fictitious value of the function $u(\mathbf{x})$ at the point $\mathbf{x}^I$ and $N(\mathbf{x})$ is the number of particles in the compact support of $W^I(\mathbf{x})$. Values of coefficients $\mathbf{a}(\mathbf{x})$ are determined by minimizing $J\big(\mathbf{a}(\mathbf{x})\big)$ with respect to $\mathbf{a}(\mathbf{x})$. That is,

$$\frac{\partial J\big(\mathbf{a}(\mathbf{x})\big)}{\partial \mathbf{a}} = \mathbf{0} \Rightarrow \mathbf{A}(\mathbf{x})\mathbf{a}(\mathbf{x}) = \mathbf{B}(\mathbf{x})\mathbf{u} \qquad (\mathbf{2.53})$$

where

$$\mathbf{A}(\mathbf{x}) = \sum_{I=1}^{N(x)} \mathrm{W}^I(\mathbf{x})\mathbf{P}(\mathbf{x}^I)\,\mathbf{P}^T(\mathbf{x}^I),$$

$$\mathbf{B}(\mathbf{x}) = [\mathrm{W}^1(\mathbf{x})\mathbf{P}(\mathbf{x}^1), \mathrm{W}^2(\mathbf{x})\mathbf{P}(\mathbf{x}^2), \dots, \mathrm{W}^{N(x)}(\mathbf{x})\mathbf{P}\big(\mathbf{x}^{N(x)}\big)],$$

$$\mathbf{u}^T = \big[u_1, u_2, \dots, u_{N(x)}\big] \qquad (\mathbf{2.54})$$

Equation (2.53) gives

$$\mathbf{a}(\mathbf{x}) = \mathbf{A}^{-1}(\mathbf{x})\mathbf{B}(\mathbf{x})\mathbf{u} \qquad (\mathbf{2.55})$$

By substituting the term $\mathbf{a}(\mathbf{x})$ from Equation (2.55) into Equation (2.51), we get

$$u^h(\mathbf{x}) = \sum_{I=1}^{N(x)} \Phi^I(\mathbf{x})\, u_I \qquad (\mathbf{2.56})$$

where

$$\Phi^I(\mathbf{x}) = \sum_{J=1}^{n} \mathbf{P}_J [\mathbf{A}^{-1}(\mathbf{x})\mathbf{B}(\mathbf{x})]_{IJ} \qquad (\mathbf{2.57})$$

and $\Phi^I(\mathbf{x})$ is the moving least squares (MLS) basis function. In the MLS basis functions, the approximation of derivatives requires that the MLS basis functions be differentiable. The spatial derivatives of basis function $\Phi^I(\mathbf{x})$ are given by

$$\Phi^I_{,k}(\mathbf{x}) = \sum_{J=1}^{n} \left\{ \mathbf{P}_{J,k} [\mathbf{A}^{-1}(\mathbf{x})\mathbf{B}(\mathbf{x})]_{IJ} + \mathbf{P}_J [\mathbf{A}^{-1}(\mathbf{x})\mathbf{B}_{,k}(\mathbf{x}) + (\mathbf{A}^{-1}(\mathbf{x}))_{,k}\mathbf{B}(\mathbf{x})]_{IJ} \right\} \quad (\mathbf{2.58})$$

2.9 h-p Clouds Method

A generalization of the DEM, EFG and RKPM is the h-p cloud method proposed by Duarte and Oden [9]. In this technique, there is no matrix inversion during the computation of the trial/test functions because the Shepard functions [61] are used for inexpensively building a partition of unity and the associated lowest order trial/test functions.

In order to improve the quality of the results, h-p enrichment schemes were developed, where h now means an increase in nodal density and p means the increase of nodal parameters corresponding to additional approximation functions. The great advantage of this scheme is the freedom for defining these additional functions. They are, for example, complete polynomials, Trefftz functions, orthotropic expansion, singular functions and so on. In addition, this enrichment is much easier to implement than in the conventional hp-FEM.

The DEM, EFG and h-p clouds share difficulties in applying boundary conditions since the trial/test functions usually lack of Kronecker delta property. Therefore, a number of procedures have been applied like Lagrange multipliers [62] and modified functionals [63], among others. The other applications of h-p clouds method can be found in [64-66].

2.10 Finite Point Method

Finite point method (FPM) presented by Onate [10] is a conceptually simple discretization technique which was shown great capacity to solve convective-diffusive problems, incompressible and compressible fluid flow problems [67-69] and solid mechanics problems [70] with good accuracy.

The basis of the standard FPM is using a weighted least squares interpolation procedure for approximating the unknown function. The stable form found by the finite calculus procedure presented in [71] corrects the errors introduced by the point collocation procedure, mainly next to the boundary segments.

2.11 Boundary Node Method

The boundary node method (BNM) was proposed by Mukherjee and Mukherjee [11]. They applied the MLS approach to the boundary integration equations, and therefore one has to discretize only the boundary. Although this method does not require an element mesh for the interpolation of the boundary solution variables, a background mesh is still necessary for integration. The BNM has been applied successfully to elasticity problems [72-73], simulation of piezoelectric composites [74] and potential problems [75-76].

2.12 Meshless Local Petrov-Galerkin Method

The meshless local Petrov-Galerkin (MLPG) method was developed by Atluri [12]. The MLPG is a truly meshless method, which involves not only a mesh interpolation for the trial functions (such as the MLS, partition of unity, Shepard function or radial basis functions), but also a meshless integration of the weak form. In the EFG method, the trial and test functions are chosen from the same function space.

In the MLPG, the trial and test function may correspond to any one of the MLS, partition of unity, Shepard function or radial basis function type interpolations; and the test function may be totally different, and may correspond to any one of MLS, partition of unity, Shepard function, radial basis function, Heaviside step function, Dirac delta function, Gaussian weight function of the MLS, a special form of the fundamental solution to the differential equation, or any other convenient function in the compact support domain of the test function.

Furthermore, the physical sizes of the nodal trial and test functions may be different. These features make the MLPG method very flexible. The MLPG method, based on a local weak formulation, can include all other meshless methods based on the global formulation, as special cases.

Many of the so called meshless methods such as the EFG method are based on the global weak form over the entire domain Ω. In the MLPG, however, a local weak form over a local subdomain Ω_s, which is located entirely inside the global domain Ω is used. This is the most distinguishing feature of the MLPG. It is noted that local subdomain Ω_s can be of an arbitrary shape.

Even though a particular approximation of the local weak form will give the same resulting discretized equations as from the Galerkin approximation of the global weak form, the local weak form will provide a clear concept for a local meshless integration of the weak form, which does not need any background integration cells over the entire domain.

In addition, it will lead to a natural way to construct the global stiffness matrix: not through the integration over a contiguous mesh and by assembly of the stiffness matrices of the elements in the mesh, but through the integration over local subdomains.

The local subdomains do not form a contiguous mesh globally; but these disjointed local subdomains may overlap each other. In contrast to the conventional Galerkin finite element formulations, which are based the on global weak form, the MLPG method stems form a weak form over a subdomain Ω_s inside the global domain Ω as shown in Figure 2.5, where the domain of the test function Ω_{te}^{I} is synonymous with the subdomain Ω_s. Ω_{tr}^{I} is the subdomain of the trial function.

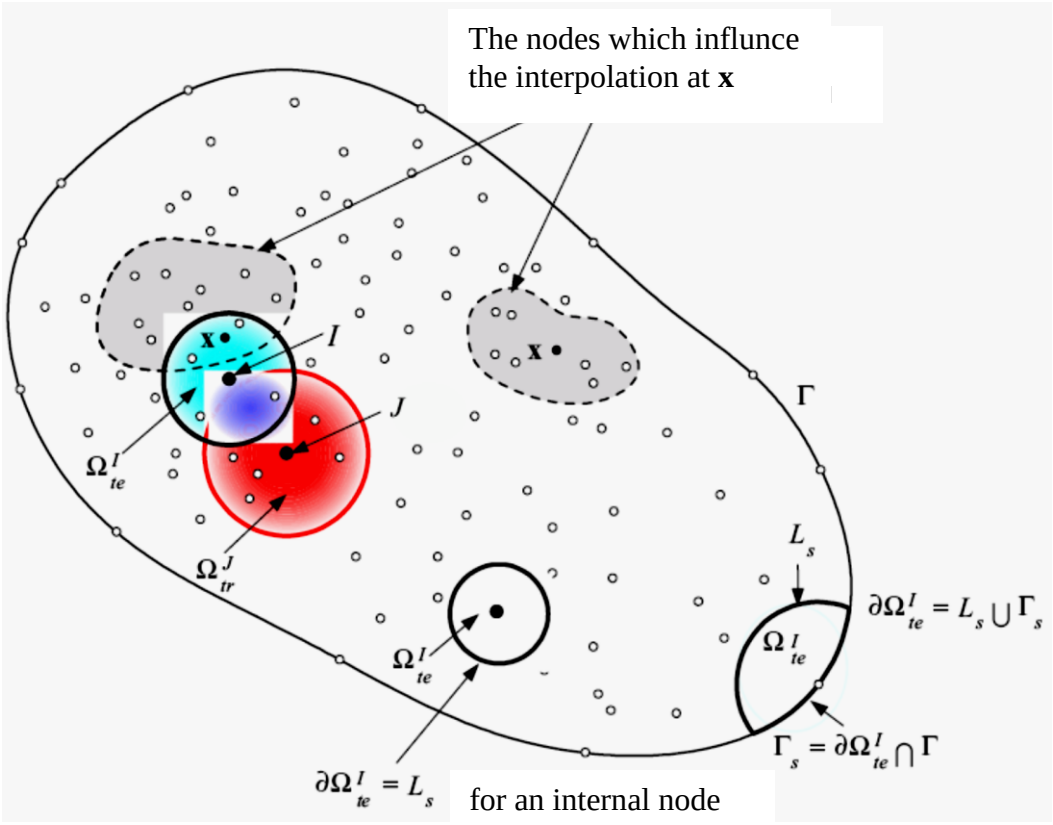

Figure 2.5 : Schematics of the MLPG method [12].

The MLPG has been successfully applied to solid mechanics problems such as 3D elastodynamics [77], free and forced vibration analysis of solids [78], bending problem of a thin plate [79], analysis of cylindrical bending thermoelastic deformations of functionally graded plates [80], analysis of elastodynamics deformations near a crack/notch tip [81], analysis of rubber-like materials [82], analysis of thick functionally graded plates [83], analysis of thin beams [84], problems with singularities and material discontinuities in 3D elasticity [85], nonlinear problems with large deformations and rotations [86], anisotropic elasticity [87], heat transfer problems such as analysis of transient heat conduction in 3D anisotropic functionally graded solids [88] and heat conduction problem in an anisotropic medium [89].

2.13 Point Interpolation Method

The point interpolation method (PIM) is one of the series representation methods for the function approximation and was developed by G.R. Liu [13]. Two types of PIM

shape functions have been developed so far using different forms of the basis functions: Polynomial basis functions [90] and radial basis functions (RBFs) [91].

Using polynomials as basis functions in the interpolation is one of the earliest interpolation schemes. Consider a continuous function $u(\mathbf{x})$ of variable **x** defined in the domain Ω. The function $u(\mathbf{x})$ can be approximated by the function defined by

$$u(\mathbf{x}) = \mathbf{P}^T(\mathbf{x})\mathbf{a} \qquad (\mathbf{2.59})$$

where $\mathbf{P}^T(\mathbf{x})$ is a given monomial in the polynomial basis function and **a** is the coefficient vector. The complete polynomial basis of order *p* for 1D and 2D can be written in the following general form.

$$\mathbf{P}^T(\mathbf{x}) = \{1 \;\; x \;\; x^2 \;\; \ldots \;\; x^{p-1} \;\; x^p\}$$

$$\mathbf{P}^T(\mathbf{x}) = \{1 \;\; x \;\; y \;\; x^2 \;\; xy \;\; y^2 \ldots x^p \;\; y^p\} \qquad (\mathbf{2.60})$$

Note that in the conventional PIM, the number of nodes *n* in the local support domain always equals to the number of basis functions of *m*. The coefficients **a** in Equation (2.59) can be determined by enforcing $u(\mathbf{x})$ to pass through the nodal values at these n nodes. This yields *n* equations for n nodes

$$u_1 = \sum_{i=1}^{n} a_i p(\mathbf{x}_1) = a_1 + a_2 x_1 + a_3 y_1 + \cdots + a_m p_m(\mathbf{x}_1)$$

$$u_2 = \sum_{i=1}^{n} a_i p(\mathbf{x}_2) = a_1 + a_2 x_2 + a_3 y_2 + \cdots + a_m p_m(\mathbf{x}_2)$$

$$u_n = \sum_{i=1}^{n} a_i p(\mathbf{x}_n) = a_1 + a_2 x_1 + a_3 y_1 + \cdots + a_m p_m(\mathbf{x}_n) \qquad (\mathbf{2.61})$$

which can be written in the following matrix form,

$$\mathbf{U}_s = \mathbf{P}_m \mathbf{a} \qquad (\mathbf{2.62})$$

Solving Equation (2.62) for **a**, we obtain

$$\mathbf{a} = \mathbf{P}_m^{-1}\mathbf{U}_s \qquad (\mathbf{2.63})$$

In obtaining the foregoing equations, it is assumed $\mathbf{P}_m^{-1}$ exists. It is noted that coefficients **a** are constants even if the point of interest at **x** changes, as long as the same set of *n* nodes are used in the interpolation, because $\mathbf{P}_m$ is a matrix of constants for this given set of nodes.

Substituting Equation (2.63) back into Equation (2.59) and considering *m*=*n* yield

$$u(\mathbf{x}) = \mathbf{P}^T(\mathbf{x})\mathbf{P}_m^{-1}\mathbf{U}_s = \mathbf{\Phi}^T(\mathbf{x})\mathbf{U}_s \qquad (\mathbf{2.64})$$

where $\mathbf{\Phi}(\mathbf{x})$ is a vector of shape functions defined by

$$\mathbf{\Phi}^T(\mathbf{x}) = \mathbf{P}^T(\mathbf{x})\mathbf{P}_m^{-1} = \{\phi_1(\mathbf{x}) \quad \phi_2(\mathbf{x}) \quad . \quad . \quad . \quad \phi_n(\mathbf{x})\} \qquad (\mathbf{2.65})$$

The derivatives of the shape functions can be easily obtained because the PIM shape function is of the polynomial form. The *l*th derivatives of PIM shape functions can be written as

$$\mathbf{\Phi}^{(l)}(\mathbf{x}) = \frac{\partial \mathbf{P}^T(\mathbf{x})}{\partial \mathbf{x}^l}\mathbf{P}_m^{-1} \qquad (\mathbf{2.66})$$

In order to avoid the singularity problem in the polynomial PIM, the RBF is used to develop the radial point interpolation method (RPIM) shape functions for meshless weak form methods [91]. The RPIM interpolation augmented with polynomials can be written as

$$u(\mathbf{x}) = \mathbf{R}^T(\mathbf{x})\mathbf{a} + \mathbf{P}^T(\mathbf{x})\mathbf{b} \qquad (\mathbf{2.67})$$

where $R(\mathbf{x})$ is a RBF, coefficients *a* and *b* are constants yet to be determined. In the radial basis function $R(\mathbf{x})$, the variable is only the distance between the point of interes $\mathbf{x}$ and a node at $\mathbf{x}_i$,

$$r = \sqrt{(x - x_i)^2 + (y - y_i)^2} \qquad (\mathbf{2.68})$$

There are a number of RBF types, and the characteristics of RBFs have been widely investigated [91-96]. Four often used RBFs are the multi-quadrics function, Gaussian function, thin plate spline function and Logarithmic radial basis function. In addition, the so-called compactly supported radial basis functions (CSRBFs) have also been developed [97-99]. The mentioned RBFs are listed in Table 2.2. In contrast to the CSRBFs, the RBFs can be called as classical RBFs.

Shape parameters are very important factors which determine the accuracy of the problem. For example, the multi-quadrics RBF, there are two shape parameters; α_c and *q* to be determined by the analyst. The CSRBFs are strictly positive definite for all *r* less than or equal to some fixed value and can be constructed to have desired amount of smoothness. In a CSRBF, there is a shape parameter *d* that determines the dimension of the compact support domain.

Table 2.2 : Radial basis functions [24-25].

No	Name	Expression
1	Multi-quadrics	$R(x,y) = (r^2 + (\alpha_c h)^2)^q$
2	Gaussian	$R(x,y) = \exp[-\alpha_c \left(\frac{r}{h}\right)^2]$
3	Thin plate spline	$R(x,y) = r^n$
4	Logarithmic	$R(x,y) = r^n log r$
5	Wu-C2	$R(x,y) = \left(1-\frac{r}{d}\right)^5 \left(8 + 40\frac{r}{d} + 48\frac{r^2}{d^2} + 25\frac{r^3}{d^3} + 5\frac{r^4}{d^4}\right)$
6	Wu-C4	$R(x,y) = \left(1-\frac{r}{d}\right)^6 \left(6 + 36\frac{r}{d} + 82\frac{r^2}{d^2} + 72\frac{r^3}{d^3} + 30\frac{r^4}{d^4} + 5\frac{r^5}{d^5}\right)$
7	Wendland-C2	$R(x,y) = \left(1-\frac{r}{d}\right)^4 \left(1 + 4\frac{r}{d}\right)$
8	Wendland-C4	$R(x,y) = \left(1-\frac{r}{d}\right)^6 \left(3 + 18\frac{r}{d} + 35\frac{r^2}{d^2}\right)$
9	Wendland-C6	$R(x,y) = \left(1-\frac{r}{d}\right)^8 \left(1 + 8\frac{r}{d} + 25\frac{r^2}{d^2} + 32\frac{r^3}{d^3}\right)$

Similar to the formulation procedure of the PIM, the following equation can be obtained

$$\mathbf{U}_s = \mathbf{R}_o \mathbf{a} + \mathbf{P}_m \mathbf{b} \qquad (\mathbf{2.69})$$

and then by using $\mathbf{P}_m^T \mathbf{b} = \mathbf{0}$

$$\widetilde{\mathbf{U}}_s = \begin{bmatrix} \mathbf{U}_s \\ \mathbf{0} \end{bmatrix} = \begin{bmatrix} \mathbf{R}_o & \mathbf{P}_m \\ \mathbf{P}_m & \mathbf{0} \end{bmatrix} \begin{bmatrix} \mathbf{a} \\ \mathbf{b} \end{bmatrix} = \mathbf{G}\mathbf{a}_o \qquad (\mathbf{2.70})$$

Because the matrix $\mathbf{R}_o$ is symmetric, the matrix **G** will also be symmetric. By solving Equation (2.70), we obtain

$$a_o = G^{-1} \widetilde{U}_s \qquad (\mathbf{2.71})$$

Inserting Equation (2.71) into Equation (2.67), we obtain

$$u(\mathbf{x}) = \{\mathbf{R}^T(\mathbf{x})\ \mathbf{P}^T(\mathbf{x})\}\mathbf{G}^{-1}\tilde{\mathbf{U}}_s = \boldsymbol{\Phi}^T(\mathbf{x})\tilde{\mathbf{U}}_s \qquad (\mathbf{2.72})$$

where the RPIM shape functions can be expressed as

$$\boldsymbol{\Phi}^T(\mathbf{x}) = \{\mathbf{R}^T(\mathbf{x})\ \mathbf{P}^T(\mathbf{x})\}\mathbf{G}^{-1} \qquad (\mathbf{2.73})$$

The derivaties of $u(\mathbf{x})$ are easily obtained as

$$u_{,l}(\mathbf{x}) = \boldsymbol{\Phi}_{,l}^T(\mathbf{x})\tilde{\mathbf{U}}_s \qquad (\mathbf{2.74})$$

2.14 Corrective Smoothed Particle Method

Based on the foundation of the conventional kernel approximation in the SPH, Chen et al. [14] extended the kernel estimate concept to the Taylor series expansion and developed a so-called corrective smoothed particle method (CSPM). The resulting corrective approximations for a function and derivatives not only are nodal complete, but the integrability problem can be avoided through a properly selected solution algorithm as well [100-101].

By invoking the Taylor series expansion, a corrective kernel estimate is given for 1D case here. Expanding the Taylor series for $f(x)$ about x_i, by multiplying both sides of the expansion by a kernel function and integrating over the entire domain Ω yields

$$\int_\Omega f(x)W_i(x)\mathrm{d}x = f_i\int_\Omega W_i(x)\mathrm{d}x + f_{xi}\int_\Omega (x-x_i)W_i(x)\mathrm{d}x$$

$$+\frac{f_{xxi}}{2}\int_\Omega (x-x_i)^2W_i(x)\mathrm{d}x + \cdots \qquad (\mathbf{2.75})$$

where $f_i = f(x_i)$, $f_{xi} = f_x(x_i) = \partial f_i/\partial x$, $f_{xxi} = f_{xx}(x_i) = \partial^2 f_i/\partial x^2$ and $W_i(x) = W_i(x_i - x, h)$. Equation (2.75) is the backbone for constructing the corrective 1D kernel estimate.

Neglecting all the derivative terms in Equation (2.75) gives the corrective kernel estimate for the function $f(x)$

$$f_i \cong \frac{\int_\Omega f(x)W_i(x)\mathrm{d}x}{\int_\Omega W_i(x)\mathrm{d}x} \qquad (\mathbf{2.76})$$

For those points x_i far away from a boundary, the integral of $W_i(x)$ is equal to one. Hence Equation (2.76) reduces to the conventional kernel estimate. Because the integral of $(x - x_i)W_i(x)$ is null due to the symmetry property of $W_i(x)$, the second term on the right hand side of Equation (2.75) vanishes. Consequently, the error of Equation (2.76) resulting from the truncated derivative terms is in the order of $(x - x_i)^2$ for the interior points. On the other hand, the truncation error is in the order of $(x - x_i)$ for those x_i near or on the boundary because the integral of $(x - x_i)W_i(x)$ is no longer equal to zero.

It is thus clear that ignoring the correction term, i.e., the integral of $W_i(x)$ in Equation (2.76), is the essential factor for the boundary deficiency in the conventional kernel estimate.

By replacing $W_i(x)$ in Equation (2.75) with $W_{i,x}(x)(= \partial W_i(x)/\partial x)$ and neglecting the second derivative term and higher order derivatives, a corrective kernel estimate for the first derivative $f_x(x)$ is generated

$$f_{xi} \cong \frac{\int_\Omega [f(x) - f(x_i)]W_{i,x}(x)\mathrm{d}x}{\int_\Omega (x - x_i)W_{i,x}(x)\mathrm{d}x} \qquad (\mathbf{2.77})$$

It should be pointed out that in order for Equation (2.77) to avoid becoming singular, the kernel function used for f_x must be anti-symmetric but is not necessarily to be $W_{,x}$. It can be seen that the truncation error for f_{xi} is again of order $(x - x_i)^2$ for the interior points and $(x - x_i)$ for the points near or on a boundary.

2.15 Boundary Point Interpolation Method

Boundary point interpolation method (BPIM) using polynomial basis in the construction of shape functions was proposed by Gu and Liu [15]. The PIM shape functions are constructed in a curvilinear coordinate system and possess the delta function property. The boundary conditions can be implemented with ease as in the conventional boundary element method. In addition, the rigid body movement can also be utilizied to avoid some singular integrals. For 2D problems, the BPIM with polynomial basis will have no singularity problem of interpolation as we have seen in the domain type of PIMs, as the boundaries are curved, and the interpolation is

basically one dimensional. Therefore, there is no reason to use the MLS approximation in this case [102].

For 3D problems for which 2D shape functions need to be constructed, there could be an issue of singular moment matrices. One effective way is to use the RPIM shape functions. This method was formulated and coded by Gu and Liu [104] and termed as the boundary radial point interpolation method (BRPIM). Although the BRPIM performs no better than the BPIM for 2D problems, its full advantages are expected to be seen for 3D problems. Formulation and applications of the BPIM and BRPIM methods can be found in [103-104].

2.16 Modified Smoothed Particle Hydrodynamics

Modified smoothed particle hydrodynamics method was developed by Zhang and Batra [19] and has been successfully applied to wave propagation in a functionally graded elastic plate [105], crack propagation in an elastic plate subjected to time-dependent loads [106], analysis of adiabatic shear bands in elasto-thermo-viscoplastic material [107], axisymmetric Taylor impact test, simulation of elastodynamic crack propagation [108], and stress concentration in a plate (near a circular hole is a semi-infine isotropic and homogenous linear elastic plate) [21].

For a function $f(\boldsymbol{x})$ having continuous derivatives up to the (n+1)th order, the value of the function at a point $\boldsymbol{\xi} = (\xi_1, \xi_2, \xi_3)$ located in the neighborhood of $\mathbf{x} = (x_1, x_2, x_3)$ can be approximated through the finite Taylor series expansion

$$f(\xi_1, \xi_2, \xi_3) = \sum_{m=0}^{n} \frac{1}{m!} [(\xi_1 - x_1) \frac{\partial}{\partial x_1} + (\xi_2 - x_2) \frac{\partial}{\partial x_2} + (\xi_3 - x_3) \frac{\partial}{\partial x_3}]^m f(x_1, x_2, x_3) \qquad (\mathbf{2.78})$$

where the symbol ! is the factorial with 0!=1. By neglecting the third and higher order terms and introducing two matices $\mathbf{P}(\boldsymbol{\xi}, \mathbf{x})$ and $\mathbf{Q}(\mathbf{x})$, we write Equation (2.78) as

$$f(\boldsymbol{\xi}) = \mathbf{P}(\boldsymbol{\xi}, \mathbf{x}) \boldsymbol{Q}(\mathbf{x}) \qquad (\mathbf{2.79})$$

where

$$\mathbf{Q}(\mathbf{x}) = [\, f(\mathbf{x}), \frac{\partial f(\mathbf{x})}{\partial x_1}, \frac{\partial f(\mathbf{x})}{\partial x_2}, \frac{\partial f(\mathbf{x})}{\partial x_3}, \frac{1}{2}\frac{\partial^2 f(\mathbf{x})}{\partial x_1^2}, \frac{1}{2}\frac{\partial^2 f(\mathbf{x})}{\partial x_2^2}, \frac{1}{2}\frac{\partial^2 f(\mathbf{x})}{\partial x_3^2},$$

$$\frac{\partial^2 f(\mathbf{x})}{\partial x_1 \partial x_2}, \frac{\partial^2 f(\mathbf{x})}{\partial x_2 \partial x_3}, \frac{\partial^2 f(\mathbf{x})}{\partial x_1 \partial x_3}]^T \qquad (\mathbf{2.80})$$

$$\mathbf{P}(\boldsymbol{\xi} - \mathbf{x}) = [1, (\xi_1 - x_1), (\xi_2 - x_2), (\xi_3 - x_3), (\xi_1 - x_1)^2, (\xi_2 - x_2)^2, (\xi_3 - x_3)^2,$$

$$(\xi_1 - x_1)(\xi_2 - x_2), (\xi_2 - x_2)(\xi_3 - x_3), (\xi_1 - x_1)(\xi_3 - x_3)] \qquad (\mathbf{2.81})$$

Elements of the matrix $\mathbf{Q}(\mathbf{x})$, the kernel estimate of the function, its first derivatives and its second derivatives at $\mathbf{x} = (x_1, x_2, x_3)$ are the unknown variables to be found from Equation (2.79).

Multiply both sides of the Equation (2.79) with a kernel function $W(\boldsymbol{\xi}, \mathbf{x})$, we obtain

$$f(\boldsymbol{\xi}) W(\boldsymbol{\xi}, \mathbf{x}) = \mathbf{P}(\boldsymbol{\xi}, \mathbf{x}) \mathbf{Q}(\mathbf{x}) W(\boldsymbol{\xi}, \mathbf{x}) \qquad (\mathbf{2.82})$$

In the compact support of the kernel function $W(\boldsymbol{\xi}, \mathbf{x})$ associated with the point $\mathbf{x} = (x_1, x_2, x_3)$, let there be $N(\mathbf{x})$ particles. In the global numbering system, let the particle number of the *j*th particle in the compact support of $W(\boldsymbol{\xi}, \mathbf{x})$ be *g*(*j*). Evaluate Equation (2.82) at every particle in the compact support of $W(\boldsymbol{\xi}, \mathbf{x})$ and sum each side over these particles to arrive at

$$\sum_{j=1}^{N(\mathbf{x})} f\left(\boldsymbol{\xi}^{g(j)}\right) W\left(\boldsymbol{\xi}^{g(j)}, \mathbf{x}\right) = \sum_{j=1}^{N(\mathbf{x})} \left[\mathbf{P}\left(\boldsymbol{\xi}^{g(j)}, \mathbf{x}\right)^T W\left(\boldsymbol{\xi}^{g(j)}, \mathbf{x}\right)\right] \mathbf{Q}(\mathbf{x}) \qquad (\mathbf{2.83})$$

where $\boldsymbol{\xi}^{g(j)}$ denotes the coordinates of the particle *g*(*j*).

In Equation (2.83), the matrix **P** is known, however the number of unknowns in the matrix **Q** exceeds the number of equations, which is one. Thus, additional equations are needed to solve for the unknown elements of the matrix **Q**. Multiplying both sides of Equation (2.79) with kernel function's first derivative $W_{\xi_\gamma} = \partial W / \partial \xi_\gamma$, and its second derivative $W_{\xi_\gamma \xi_\delta} = \partial^2 W / \partial \xi_\gamma \partial \xi_\delta$, we obtain

$$\sum_{j=1}^{N(\mathbf{x})} f\left(\boldsymbol{\xi}^{g(j)}\right) W_{\xi_\gamma}\left(\boldsymbol{\xi}^{g(j)}, \mathbf{x}\right) = \sum_{j=1}^{N(\mathbf{x})} \left[\mathbf{P}\left(\boldsymbol{\xi}^{g(j)}, \mathbf{x}\right)^T W_{\xi_\gamma}\left(\boldsymbol{\xi}^{g(j)}, \mathbf{x}\right)\right] \mathbf{Q}(\mathbf{x})$$

$$\sum_{j=1}^{N(\mathbf{x})} f\left(\boldsymbol{\xi}^{g(j)}\right) W_{\xi_\gamma \xi_\delta}\left(\boldsymbol{\xi}^{g(j)}, \mathbf{x}\right) = \sum_{j=1}^{N(\mathbf{x})} \left[\mathbf{P}\left(\boldsymbol{\xi}^{g(j)}, \mathbf{x}\right)^T W_{\xi_\gamma \xi_\delta}\left(\boldsymbol{\xi}^{g(j)}, \mathbf{x}\right)\right] \mathbf{Q}(\mathbf{x}) \quad (\mathbf{2.84})$$

Equations (2.83) and (2.84) can simultaneously be solved for the unknown element of the matrix **Q**. For the MSPH method, the kernel estimates of a function and its first and second order derivatives are respectively consistent up to the orders *m*, (*m*-1) and (*m*-2), if up to *m* terms are retained in the Taylor series expansion of the function [109].

3. THE MESHLESS SYMMETRIC SMOOTHED PARTICLE HYDRODYNAMICS METHOD

3.1 Introduction

The SSPH method was developed by Zhang and Batra [20] and has been successfully applied to elasticity problems such as stress concentration in a plate (near a circular hole is a semi-infine isotropic and homogenous linear elastic plate) [20-22], plane stress deformations of a plate [21], wave propagation in bar [20], deformations of a rectangular plate with a crack at the center, deformations of a plate with two horizontal cracks emanating from opposite vertical edges [22] and heat transfer problems [23].

The SSPH method constructs the basis functions for meshless methods that use only locations of nodes (particles). These basis functions are found similar to those in the FEM except that basis for the derivatives of a function need not to be obtained by differentiating those for the function. The basis for the derivatives of a function can be obtained by differentiating the basis function as in the FEM and meshless methods [21].

3.2 Symmetric Smoothed Particle Hydrodynamics Basis Functions

For a function $f(\boldsymbol{x})$ having continuous derivatives up to the (n+1)th order, the value of the function at a point $\boldsymbol{\xi} = (\xi_1, \xi_2, \xi_3)$ located in the neighborhood of $\mathbf{x} = (x_1, x_2, x_3)$ can be approximated through the finite Taylor series expansion.

$$f(\xi_1, \xi_2, \xi_3) = \sum_{m=0}^{n} \frac{1}{m!} [(\xi_1 - x_1) \frac{\partial}{\partial x_1} + (\xi_2 - x_2) \frac{\partial}{\partial x_2} + (\xi_3 - x_3) \frac{\partial}{\partial x_3}]^m f(x_1, x_2, x_3) \qquad (\mathbf{3.1})$$

Neglecting the third and higher order terms, and introducing two matrices $\mathbf{P}(\boldsymbol{\xi}, \mathbf{x})$ and $\mathbf{Q}(\mathbf{x})$, we write Equation (3.1) as

$$f(\boldsymbol{\xi}) = \mathbf{P}(\boldsymbol{\xi}, \mathbf{x})\boldsymbol{Q}(\mathbf{x}) \tag{3.2}$$

where

$$\mathbf{Q}(\mathbf{x}) = [\, f(\mathbf{x}), \frac{\partial f(\mathbf{x})}{\partial x_1}, \frac{\partial f(\mathbf{x})}{\partial x_2}, \frac{\partial f(\mathbf{x})}{\partial x_3}, \frac{1}{2}\frac{\partial^2 f(\mathbf{x})}{\partial x_1^2}, \frac{1}{2}\frac{\partial^2 f(\mathbf{x})}{\partial x_2^2}, \frac{1}{2}\frac{\partial^2 f(\mathbf{x})}{\partial x_3^2},$$

$$\frac{\partial^2 f(\mathbf{x})}{\partial x_1 \partial x_2}, \frac{\partial^2 f(\mathbf{x})}{\partial x_2 \partial x_3}, \frac{\partial^2 f(\mathbf{x})}{\partial x_1 \partial x_3}]^T \tag{3.3}$$

$$\mathbf{P}(\boldsymbol{\xi}, \mathbf{x}) = [1, (\xi_1 - x_1), (\xi_2 - x_2), (\xi_3 - x_3), (\xi_1 - x_1)^2, (\xi_2 - x_2)^2, (\xi_3 - x_3)^2,$$

$$(\xi_1 - x_1)(\xi_2 - x_2), (\xi_2 - x_2)(\xi_3 - x_3), (\xi_1 - x_1)(\xi_3 - x_3)] \tag{3.4}$$

Elements of the matrix $\mathbf{Q}(\mathbf{x})$, the kernel estimate of the function, its first derivatives and its second derivatives at $\mathbf{x} = (x_1, x_2, x_3)$ are the unknown variables to be found from Equation (3.2). Elements of the matrix $\mathbf{P}(\boldsymbol{\xi} - \mathbf{x})$ can be associated with the shape functions used in the FEM.

Multiply both sides of Equation (3.2) with $W(\boldsymbol{\xi}, \mathbf{x})\mathbf{P}(\boldsymbol{\xi}, \mathbf{x})^T$ and obtain

$$f(\boldsymbol{\xi})W(\boldsymbol{\xi}, \mathbf{x})\mathbf{P}(\boldsymbol{\xi}, \mathbf{x})^T = \mathbf{P}(\boldsymbol{\xi}, \mathbf{x})\mathbf{Q}(\mathbf{x})W(\boldsymbol{\xi}, \mathbf{x})\mathbf{P}(\boldsymbol{\xi}, \mathbf{x})^T,$$

$$= [\mathbf{P}(\boldsymbol{\xi}, \mathbf{x})^T W(\boldsymbol{\xi}, \mathbf{x})\mathbf{P}(\boldsymbol{\xi}, \mathbf{x})]\mathbf{Q}(\mathbf{x}) \tag{3.5}$$

In the compact support of the kernel function $W(\boldsymbol{\xi}, \mathbf{x})$ associated with the point $\mathbf{x} = (x_1, x_2, x_3)$ shown in Figure 3.1, let there be $N(\mathbf{x})$ particles. In the global numbering system, let the particle number of the *j*th particle in the compact support of $W(\boldsymbol{\xi}, \mathbf{x})$ be *g*(*j*). Evaluate Equation (3.5) at every particle in the compact support of $W(\boldsymbol{\xi}, \mathbf{x})$ and sum each side over these particles to arrive at

$$\sum_{j=1}^{N(\mathbf{x})} f\left(\boldsymbol{\xi}^{g(j)}\right) W\left(\boldsymbol{\xi}^{g(j)}, \mathbf{x}\right)\mathbf{P}\left(\boldsymbol{\xi}^{g(j)}, \mathbf{x}\right)^T$$

$$= \sum_{j=1}^{N(\mathbf{x})} [\mathbf{P}\left(\boldsymbol{\xi}^{g(j)}, \mathbf{x}\right)^T W\left(\boldsymbol{\xi}^{g(j)}, \mathbf{x}\right)\mathbf{P}\left(\boldsymbol{\xi}^{g(j)}, \mathbf{x}\right)]\, \mathbf{Q}(\mathbf{x}) \tag{3.6}$$

where $\boldsymbol{\xi}^{g(j)}$ denotes the coordinates of the particle *g*(*j*).

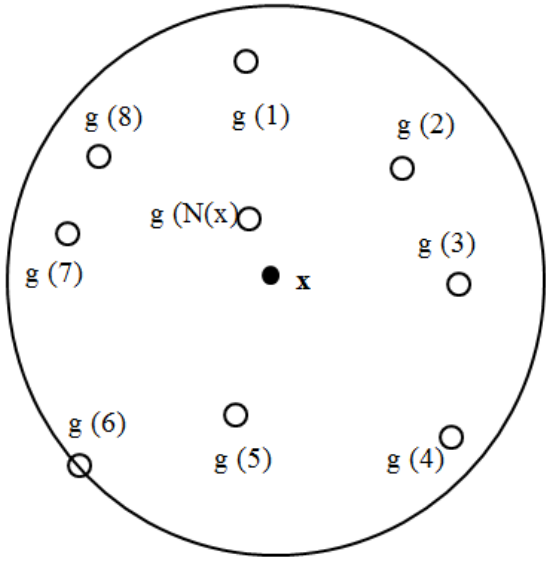

Figure 3.1 : Distribution of particles in the compact support of the kernel function.

With the definitions

$$\mathbf{H}(\boldsymbol{\xi},\mathbf{x}) = \left[\, \mathbf{P}^T\left(\boldsymbol{\xi}^{g(1)},\mathbf{x}\right), \mathbf{P}^T\left(\boldsymbol{\xi}^{g(2)},\mathbf{x}\right), \ldots, \mathbf{P}^T\left(\boldsymbol{\xi}^{g(N(\mathbf{x}))},\mathbf{x}\right)\right],$$

$$\mathbf{W}(\boldsymbol{\xi},\mathbf{x}) = \begin{bmatrix} W\left(\boldsymbol{\xi}^{g(1)},\mathbf{x}\right) & \cdots & 0 \\ \vdots & \ddots & \vdots \\ 0 & \cdots & W\left(\boldsymbol{\xi}^{g(N(\mathbf{x}))},\mathbf{x}\right) \end{bmatrix},$$

$$\mathbf{F}^{(x)T}(\boldsymbol{\xi},\mathbf{x}) = \left[f\left(\boldsymbol{\xi}^{g(1)}\right), f\left(\boldsymbol{\xi}^{g(2)}\right), \ldots\ldots, f\left(\boldsymbol{\xi}^{g(N(\mathbf{x}))}\right)\right] \qquad (\mathbf{3.7})$$

Equation **(3.6)** becomes

$$\mathbf{H}(\boldsymbol{\xi},\mathbf{x})\ \mathbf{W}(\boldsymbol{\xi},\mathbf{x})\mathbf{F}^{(x)}(\boldsymbol{\xi},\mathbf{x}) = \mathbf{H}(\boldsymbol{\xi},\mathbf{x})\ \mathbf{W}(\boldsymbol{\xi},\mathbf{x})\mathbf{H}(\boldsymbol{\xi},\mathbf{x})^T\mathbf{Q}(\mathbf{x}) \qquad (\mathbf{3.8})$$

Values of element matrices $\mathbf{H}(\boldsymbol{\xi},\mathbf{x}), \mathbf{W}(\boldsymbol{\xi},\mathbf{x})$ and $\mathbf{F}^{(x)}(\boldsymbol{\xi},\mathbf{x})$ depend upon the values of the matrix $\mathbf{P}(\boldsymbol{\xi},\mathbf{x})$, the kernel (weight) function $W(\boldsymbol{\xi},\mathbf{x})$ and the function f at all particles (nodes) located in the compact support of $W(\boldsymbol{\xi},\mathbf{x})$ associated with point $\mathbf{x}$. Equation (3.8) can be rewritten as

$$\mathbf{C}(\boldsymbol{\xi},\mathbf{x})\mathbf{Q}(\mathbf{x}) = \mathbf{D}(\boldsymbol{\xi},\mathbf{x})\mathbf{F}^{(x)}(\boldsymbol{\xi},\mathbf{x}) \qquad (\mathbf{3.9})$$

where $\mathbf{C}(\boldsymbol{\xi},\mathbf{x}) = \mathbf{H}(\boldsymbol{\xi},\mathbf{x})\ \mathbf{W}(\boldsymbol{\xi},\mathbf{x})\mathbf{H}(\boldsymbol{\xi},\mathbf{x})^T$ and $\mathbf{D}(\boldsymbol{\xi},\mathbf{x}) = \mathbf{H}(\boldsymbol{\xi},\mathbf{x})\ \mathbf{W}(\boldsymbol{\xi},\mathbf{x})$.

It is obvious that the matrix $\mathbf{C}(\boldsymbol{\xi},\mathbf{x})$ defined above is symmetric. That is why this technique is called the SSPH method. The set of simultaneous linear algebraic equations in Equation (3.9) can be solved for the unknown elements of the matrix

$\mathbf{Q}(\mathbf{x})$. The symmetry of the matrix $\mathbf{C}(\boldsymbol{\xi}, \mathbf{x})$ reduces the storage requirements and Central Processing Unit (CPU) time needed to solve Equation (3.9) for $\mathbf{Q}(\mathbf{x})$. It is interesting to note that none of the matrices in Equation (3.9) involves derivatives of the kernel function. So a much larger class of functions can be used as the kernel functions which improve the practicality and usefulness of the method. The $\mathbf{C}(\boldsymbol{\xi}, \mathbf{x})$ matrix is not singular. It can be found in [20].

For the non-singular matrix $\mathbf{C}(\boldsymbol{\xi}, \mathbf{x})$, the solution of Equation (3.9) is

$$\begin{aligned} \mathbf{Q}(\mathbf{x}) &= \mathbf{C}(\boldsymbol{\xi}, \mathbf{x})^{-1}\mathbf{D}(\boldsymbol{\xi}, \mathbf{x})\mathbf{F}^{(x)}(\boldsymbol{\xi}, \mathbf{x}) \\ &= \mathbf{K}^{(x)}(\boldsymbol{\xi}, \mathbf{x})\mathbf{F}^{(x)}(\boldsymbol{\xi}, \mathbf{x}) \end{aligned} \qquad (\mathbf{3.10})$$

and $\mathbf{K}^{(x)}(\boldsymbol{\xi}, \mathbf{x}) = \mathbf{C}(\boldsymbol{\xi}, \mathbf{x})^{-1}\mathbf{D}(\boldsymbol{\xi}, \mathbf{x})$. Equation (3.10) can be written as

$$\mathbf{Q}(\mathbf{x}) = \mathbf{K}(\boldsymbol{\xi}, \mathbf{x})\mathbf{F}(\boldsymbol{\xi}) \qquad (\mathbf{3.11})$$

and $\mathbf{F}(\boldsymbol{\xi}) = [\, f(\boldsymbol{\xi}^1), \ldots., f\left(\boldsymbol{\xi}^{g(1)}\right), \ldots, f\left(\boldsymbol{\xi}^{g(2)}\right), .., f\left(\boldsymbol{\xi}^{g(N(\mathbf{x}))}, \ldots.. f(\boldsymbol{\xi}^M)\right]^T$

where M is the total number of particles in the problem domain. Alternatively, Equation (3.11) can be written as

$$Q_I(\mathbf{x}) = \sum_{J=1}^{M} K_{IJ}F_J \ , \qquad I = 1,2, \ldots \ldots 10, \qquad (\mathbf{3.12})$$

where $F_J = f(\boldsymbol{\xi}^J)$. The value of the function and its derivatives at the point **x** are now expressed in terms of values of the function at all particles in the entire domain. Six components of Equation (3.12) for 2D case, when written explicitly, are given by

$$f(\mathbf{x}) = Q_1(\mathbf{x}) = \sum_{J=1}^{M} K_{1J}F_J$$

$$\frac{\partial f(\mathbf{x})}{\partial x_1} = Q_2(\mathbf{x}) = \sum_{J=1}^{M} K_{2J}F_J$$

$$\frac{\partial f(\mathbf{x})}{\partial x_2} = Q_3(\mathbf{x}) = \sum_{J=1}^{M} K_{3J}F_J$$

$$\frac{\partial^2 f(\mathbf{x})}{\partial x_1^2} = 2Q_4(\mathbf{x}) = \sum_{J=1}^{M} K_{4J} F_J$$

$$\frac{\partial^2 f(\mathbf{x})}{\partial x_2^2} = 2Q_5(\mathbf{x}) = \sum_{J=1}^{M} K_{5J} F_J$$

$$\frac{\partial^2 f(\mathbf{x})}{\partial x_1 \partial x_2} = Q_6(\mathbf{x}) = \sum_{J=1}^{M} K_{6J} F_J \qquad (\mathbf{3.13})$$

In the terminology of the FEM functions $K_{1J}, J = 1,2,\dots,M$ can be viewed as shape functions for the point **x**. Similarly, functions $K_{2J}, J = 1,2,\dots,M$, $K_{3J}, J = 1,2,\dots,M$, $K_{4J}, J = 1,2,\dots,M$, $K_{5J}, J = 1,2,\dots,M$ and $K_{6J}, J = 1,2,\dots,M$ can be regarded as shape functions for derivatives of $f(\mathbf{x})$. Thus shape functions for $f(\mathbf{x})$, its first derivative and second derivative at the position **x** are different. Recall that in the FEM

$$\frac{\partial^{\alpha+\beta+\gamma}}{\partial x_1^\alpha \partial x_2^\beta \partial x_3^\gamma} f(\mathbf{x}) = \sum_{J=1}^{M} \frac{\partial^{\alpha+\beta+\gamma}}{\partial x_1^\alpha \partial x_2^\beta \partial x_3^\gamma} N_J F_J \qquad (\mathbf{3.14})$$

For $\alpha = \beta = \gamma = 0$, Equation (3.14) giving the approximate value of the function in the FEM is exactly of the same as that in the SSPH method. However, expressions for approximate values of the first and second derivatives of the function at the point **x** in the SSPH method are different from those in the FEM. In order to compute approximate values of derivatives of the function in the SSPH method, it is needed to differentiate the basis functions. Instead, another set of basis functions are used.

Values of coefficients in Equation (3.13) for finding approximate values of the function $f(\mathbf{x})$, its first derivative and its second derivative at the point **x** are found simultaneously.

In the Moving Least Squares (MLS), RKPM and FEM, one can also use a different set of shape functions to approximate the trial solution and its derivatives, but it increases the number of unknowns at a node or a particle. Here the number of unknowns per particle remains the same but one does need to have more particles in the compact support domain of the kernel function associated with the point **x** to simultaneously find the basis for the function and its spatial derivatives in order for

the matrix $\mathbf{C}(\boldsymbol{\xi}, \mathbf{x})$ to be non-singular. This can be accomplished by enlarging either the radius of the compact support of the kernel function or the number of particles in the domain which generally reduces the error in approximating the trial solution.

As in the FEM, one can determine approximate values of the derivatives of the function f at the point $\mathbf{x}$ by differentiating with respect to x_i both sides of Equation (3.13). For the SSPH method, the estimates of a function, and its first and second order derivatives are respectively consistent up to orders m, (m-1) and (m-2), if up to m terms are retained in the Taylor series expansion of the function [21].

The SSPH basis functions have been derived without using any connectivity among particles. Therefore, like the MLS basis functions [22] they can be used as the basis to solve an initial boundary value problem. Like the MLS basis functions, the SSPH basis functions do not exhibit Kronecker delta property [21].

3.3 Comparison of SSPH and Finite Element Methods

The SSPH and the FEM are compared in Table 3.1.

Table 3.1 : Comparison of the SSPH and finite element methods [20].

Items	SSPH	Finite Element
Weak form	Not required	Global
Information needed about nodes	Locations only	Locations and connectivity
Subdomains	Circular/rectangular, not necessarily disjoint	Polygonal and disjoint
Basis functions	Polynomials, require more CPU time to find them	Polynomials, easy to find
Derivatives of trial solution	Easy to evaluate	Require more CPU time to evaluate them
Integration rule	Not needed in the strong form	Depends upon the degree of polynomials in basis functions
Mass/stiffness matrix	Asymmetric, large bandwith that cannot be determined a priori	Symmetric, banded, mass matrix positive definite, stiffness matrix positive definite after imposition of essential boundary conditions
Assembly of equation	Not required	Required
Stresses/strains	Smooth everywhere	Good at integration points
Addition of nodes	Easy	Difficult
Determination of time step size	Easy	Easy
Computation of total strain energy	Difficult (requires a background mesh)	Easy
Data preparation effort	Little	Extensive
Inposition of essential boundary condition	Easy	Easy

4. MESHLESS METHODS BASED ON DIFFERANTIAL TRANSFORM METHOD

4.1 Introduction

We proposed three new meshless approaches based on the Taylor series expansion and utilizing the formalism of the Differential Transform Method (DTM) called the DTM based meshless methods.

The formulations are derived by using the DTM expansions. Hence, the TSE is employed by utilizing the formalism and technique of the DTM in this thesis.

Unlike the traditional Taylor series method and DTM that is difficult to be applied to arbitrary boundary geometries, the DTM based meshless methods can be applied to arbitrary boundary geometries, nonlinear problems, and strong and weak formulations [109].

4.2 Differential Transform Method

One dimensional differential transform method (DTM) was first introduced by Zhou [110] for solving linear and non-linear initial boundary value problems in electrical circuit analysis. It has been also used in obtaining series solutions to a wide class of linear and non-linear ordinary differential equations [111-128].

DTM is based on Taylor series, on the other hand, further to a controversy on whether or not the DTM is the traditional Taylor series method, it is shown in the recent work of Bervillier [129] that when the DTM is applied to ordinary differential equations, it exactly coincides with the traditional Taylor series method; moreover, though often used trivially, the DTM is attainable and easily adaptable to different kinds of differentiation procedures that made it very attractive (e.g., see [129] for details).

4.2.1 One dimensional DTM

One dimensional differential transform of a function $w(x)$ can be defined as follows

$$W(k) = \frac{1}{k!}\left[\frac{d^k w(x)}{dx_k}\right]_{x=0} \quad (\mathbf{4.1})$$

where $w(x)$ is the original function and $W(k)$ is the transformed function. The differential inverse transform of $W(k)$ is also defined by

$$w(x) = \sum_{k=0}^{\infty} x^k W(k) \quad (\mathbf{4.2})$$

The transformation is called T-function and the lower case and upper case letters represent the original and transformed functions, respectively. From Equations (4.1) and (4.2), it is concluded that

$$w(x) = \sum_{k=0}^{\infty} \frac{1}{k!}\left[\frac{d^k w(x)}{dx^k}\right]_{x=0} x^k \quad (\mathbf{4.3})$$

which implies that the concept of differential transform is derived from Taylor series expansion, but the method does not evaluate the derivatives symbolically. However, relative derivatives are calculated by an iterative way which is described by transformed equations of the original functions [109].

4.2.2 Two dimensional DTM

For 2D DTM, the basic definitions and fundamental theorems are defined as follows

$$W(k,h) = \frac{1}{k!\,h!}\left[\frac{\partial^{k+h} w(x,y)}{\partial x^k y^h}\right]_{(0,0)} \quad (\mathbf{4.4})$$

where $w(x,y)$ is the original function and $W(k,h)$ is the transformed function. The differential inverse transform of $W(k,h)$ is also defined as

$$w(x,y) = \sum_{k=0}^{\infty}\sum_{h=0}^{\infty} W(k,h) x^k y^h \quad (\mathbf{4.5})$$

Then, it can be concluded from Equations (4.4) and (4.5) that

$$w(x,y) = \sum_{k=0}^{\infty}\sum_{h=0}^{\infty} \frac{1}{k!\,h!}\left[\frac{\partial^{k+h} w(x,y)}{\partial x^k y^h}\right]_{(0,0)} x^k y^h \quad (\mathbf{4.6})$$

4.2.3 Three dimensional DTM

By using the same theory as in 2D differential transform, the basic definitions of the 3D differential transform of $w(x, y, z)$ are defined as follows

$$W(k,h,m) = \frac{1}{k!\,h!\,m!}\left[\frac{\partial^{k+h+m} w(x,y,z)}{\partial x^k y^h z^m}\right]_{(0,0,0)} \qquad (\mathbf{4.7})$$

where $w(x,y,z)$ is the original function and $W(k,h,m)$ is the transformed function. The differential inverse transform of $W(k,h,m)$ is also defined as [109]

$$w(x,y,z) = \sum_{k=0}^{\infty}\sum_{h=0}^{\infty}\sum_{m=0}^{\infty} W(k,h,m)x^k y^h z^m \qquad (\mathbf{4.8})$$

From Equations (4.7) and (4.8), it can be obtained that

$$w(x,y,z) = \sum_{k=0}^{\infty}\sum_{h=0}^{\infty}\sum_{m=0}^{\infty} \frac{1}{k!\,h!\,m!}\left[\frac{\partial^{k+h+m} w(x,y,z)}{\partial x^k y^h z^m}\right]_{(0,0,0)} x^k y^h z^m \qquad (\mathbf{4.9})$$

4.2.4 Fundemental Theorems of DTM for One and Two Dimensional Cases

Some of the fundamental theorems of the DTM for one and two dimensional cases are as follows

Theorem 1

if $w(x) = u(x) \mp v(x),\ W(k) = U(k) \mp V(k)$

Theorem 2

if $w(x) = cu(x), W(k) = cU(k)$

where c is an arbitrary constant.

Theorem 3

if $w(x) = du/dx\,, W(k) = (k+1)U(k+1)$

Theorem 4

if $w(x) = du^j/dx^j, W(k) = (k+1)(k+2)\ldots(k+j)U(k+j)$

Theorem 5

if $w(x) = u(x)v(x)$,$W(k) = \sum_{r=0}^{k} U(r)V(k-r)$

Theorem 6

if $w(x) = x^j$, $W(k) = \delta(k-j) = \begin{cases} 1, & k = j \\ 0, & k \neq j \end{cases}$

Theorem 7

if $w(x,y) = u(x,y) \mp v(x,y)$, $W(k,h) = U(k,h) \mp V(k,h)$

Theorem 8

if $w(x,y) = cu(x,y)$, $W(k,h) = cU(k,h)$

Theorem 9

if $w(x,y) = \frac{\partial u(x,y)}{\partial x}$, $W(k,h) = (k+1)U(k+1,h)$

Theorem 10

if $w(x,y) = \frac{\partial u(x,y)}{\partial y}$, $W(k,h) = (h+1)U(k,h+1)$

Theorem 11

if $w(x,y) = \frac{\partial^{r+s} u(x,y)}{\partial x^r \partial y^s}$,

$W(k,h) = (k+1)(k+2)\dots(k+r)(h+1)(h+2)\dots(h+s)U(k+r,h+s)$

Theorem 12

if $w(x,y) = u(x,y)v(x,y)$, $W(k,h) = \sum_{r=0}^{k} \sum_{s=0}^{h} U(r,h-s)V(k-r,s)$

Theorem 13

if $w(x,y) = x^m y^n$, $W(k,h) = \delta(k-m,h-n) = \begin{cases} 1, & k = m \text{ and } h = n \\ 0, & otherwise \end{cases}$

Theorem 14

if $w(x,y) = \frac{\partial u(x,y)}{\partial x} \frac{\partial v(x,y)}{\partial x}$,

$$W(k,h) = \sum_{r=0}^{k}\sum_{s=0}^{h}(r+1)(k-r+1)U(r+1,h-s)V(k-r+1,s)$$

Theorem 15

if $w(x,y) = \frac{\partial u(x,y)}{\partial y}\frac{\partial v(x,y)}{\partial y}$,

$$W(k,h) = \sum_{r=0}^{k}\sum_{s=0}^{h}(s+1)(h-s+1)U(r,h-s+1)V(k-r,s+1)$$

Theorem 16

If $w(x,y) = \frac{\partial u(x,y)}{\partial x}\frac{\partial v(x,y)}{\partial y}$,

$$W(k,h) = \sum_{r=0}^{k}\sum_{s=0}^{h}(h-s+1)(k-r+1)U(k-r+1,s)V(r,h-s+1)$$

The proofs and further theorems on the DTM can be found in [121-129].

4.3 Formulations of Meshless Methods Based On Differential Transform Method

In this section, three different basis function formulations based on the DTM are given for 1D and 2D dimensional cases. These methods are named as followings;

1. DTM based meshless method I,
2. DTM based meshless method II and
3. DTM based meshless method III

4.3.1 DTM based meshless method I

One Dimensional Case:

For a function $T(x)$ which has continuous derivatives up to the (n+1)th order, the value of the function at a point $\xi = x$ located in the neighborhood of the point $x = x_i$ can be written through the DTM as follows

$$T_i(x) = \sum_{k=0}^{\infty} U_i(k)(x-x_i)^k \qquad (\mathbf{4.10})$$

By introducing the two matrices P(x) and U_i, Equation (4.10) can be cast into the following form

$$T_i(x) = \boldsymbol{P}(x,\xi)\boldsymbol{U}_i \qquad (\mathbf{4.11})$$

where

$$\boldsymbol{P}(x,\xi) = [(x-x_i)^0, (x-x_i)^1, \dots, (x-x_i)^k],$$

$$U_i = [U_i(0), U_i(1), U_i(2), \dots, U_i(k)]^T \qquad (\mathbf{4.12})$$

Elements of the matrix $\boldsymbol{U}_i$ are the unknown variables that can be defined as

$$U_i(k) = \frac{1}{k!}\left[\frac{d^k T_i(x)}{dx^k}\right]_{(x_i)} \qquad (\mathbf{4.13})$$

Depending on the number of unknowns of the matrix $\boldsymbol{U}_i$,the derivatives of the $T_i(x)$ (basis function) are obtained. By neglecting the sixth and higher order terms in the DTM expansions, the formulation of the DTM based meshless method I for a 1D problem can be written as follows

$$T_i(x) = \boldsymbol{P}(x,\xi)\boldsymbol{U}_i$$

$$\frac{dT_i(x)}{dx} = \frac{d\boldsymbol{P}(x,\xi)}{dx}\boldsymbol{U}_i$$

$$\frac{d^2T_i(x)}{dx^2} = \frac{d^2\boldsymbol{P}(x,\xi)}{dx^2}\boldsymbol{U}_i$$

$$\frac{d^3T_i(x)}{dx^3} = \frac{d^3\boldsymbol{P}(x,\xi)}{dx^3}\boldsymbol{U}_i$$

$$\frac{d^4T_i(x)}{dx^4} = \frac{d^4\boldsymbol{P}(x,\xi)}{dx^4}\boldsymbol{U}_i$$

$$\frac{d^5T_i(x)}{dx^5} = \frac{d^5\boldsymbol{P}(x,\xi)}{dx^5}\boldsymbol{U}_i \qquad (\mathbf{4.14})$$

Then multiply both sides of the basis function and its derivatives given above by $W(\xi,x)$

$$W(\xi,x)T_i(x) = W(\xi,x)\boldsymbol{P}(x,\xi)\boldsymbol{U}_i$$

$$W(\xi,x)\frac{dT_i(x)}{dx} = W(\xi,x)\frac{d\boldsymbol{P}(x,\xi)}{dx}\boldsymbol{U}_i$$

$$W(\xi,x)\frac{d^2T_i(x)}{dx^2} = W(\xi,x)\frac{d^2\boldsymbol{P}(x,\xi)}{dx^2}\,\boldsymbol{U}_i$$

$$W(\xi,x)\frac{d^3T_i(x)}{dx^3} = W(\xi,x)\frac{d^3\boldsymbol{P}(x,\xi)}{dx^3}\,\boldsymbol{U}_i$$

$$W(\xi,x)\frac{d^4T_i(x)}{dx^4} = W(\xi,x)\frac{d^4\boldsymbol{P}(x,\xi)}{dx^4}\,\boldsymbol{U}_i$$

$$W(\xi,x)\,\frac{d^5T_i(x)}{dx^5} = W(\xi,x)\frac{d^5\boldsymbol{P}(x,\xi)}{dx^5}\,\boldsymbol{U}_i \qquad (\mathbf{4.15})$$

In the compact support of the kernel function $W(\boldsymbol{\xi},\boldsymbol{x})$ associated with the point $\boldsymbol{x} = (x_i, y_i)$ shown in Figure 4.1, let there be N_g particles.

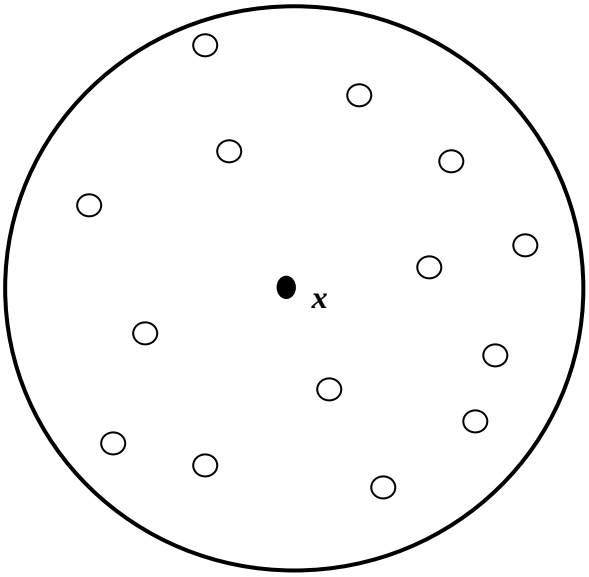

Figure 4.1 : Distribution of particles in the compact support of the weight function.

Lets rewrite Equation (4.15) with respect to the compact support domain shown in Figure 4.1, evaluate this equation at every particle in the compact support domain of $W(\boldsymbol{\xi},\boldsymbol{x})$ and sum each side over these particles, then

$$\sum_{g=1}^{N_g} W(x_g,x_i)\,T_i(x_g) = \sum_{g=1}^{N_g} W(x_g,x_i)\,\boldsymbol{P}(x_g,x_i)\boldsymbol{U}_i$$

$$\sum_{g=1}^{N_g} W(x_g,x_i)\,T_x(x_g) = \sum_{g=1}^{N_g} W(x_g,x_i)\,\boldsymbol{P}_x(x_g,x_i)\boldsymbol{U}_i$$

$$\sum_{g=1}^{N_g} W(x_g, x_i)\, T_{xx}(x_g) = \sum_{g=1}^{N_g} W(x_g, x_i)\, \boldsymbol{P}_{xx}(x_g, x_i)\boldsymbol{U}_i$$

$$\sum_{g=1}^{N_g} W(x_g, x_i)\, T_{xxx}(x_g) = \sum_{g=1}^{N_g} W(x_g, x_i)\, \boldsymbol{P}_{xxx}(x_g, x_i)\boldsymbol{U}_i$$

$$\sum_{g=1}^{N_g} W(x_g, x_i)\, T_{xxxx}(x_g) = \sum_{g=1}^{N_g} W(x_g, x_i)\, \boldsymbol{P}_{xxxx}(x_g, x_i)\, \boldsymbol{U}_i$$

$$\sum_{g=1}^{N_g} W(x_g, x_i)\, T_{xxxxx}(x_g) = \sum_{g=1}^{N_g} W(x_g, x_i)\, \boldsymbol{P}_{xxxxx}(x_g, x_i)\, \boldsymbol{U}_i \qquad (\mathbf{4.16})$$

Then, we can solve a set of simultaneous linear algebraic equations given by Equation (4.16) for the unknowns of $\boldsymbol{U}_i$ for all particles.

Two Dimensional Case:

For a function $T(x, y)$ which has continuous derivatives up to the (n+1)th order, the value of the function at a point $\boldsymbol{\xi} = (x, y)$ located in the neighborhood of the point $\boldsymbol{x} = (x_i, y_i)$ can be written through the DTM as follows

$$T_i(x, y) = \sum_{k=0}^{\infty} \sum_{h=0}^{\infty} U_i(k, h)(x - x_i)^k (y - y_i)^h \qquad (\mathbf{4.17})$$

With the same approach used for 1D case, the following equation can be written

$$T_i(x, y) = \boldsymbol{P}(\boldsymbol{x}, \boldsymbol{\xi})\boldsymbol{U}_i \qquad (\mathbf{4.18})$$

where

$$\boldsymbol{P}(\boldsymbol{x}, \boldsymbol{\xi}) = [(x - x_i)^0 (y - y_i)^0, (x - x_i)^1 (y - y_i)^0, (x - x_i)^0 (y - y_i)^1, \dots$$

$$\dots, (x - x_i)^k (y - y_i)^h\ ],$$

$$\boldsymbol{U}_i = [U_i(0,0), U_i(1,0), U_i(0,1), U_i(2,0), U_i(0,2), U_i(1,1), \dots, U_i(k, h)]^T \qquad (\mathbf{4.19})$$

Elements of the matrix $\boldsymbol{U}_i$ are unknown that can be defined as

$$U_i(k, h) = \frac{1}{k!\, h!} \left[\frac{\partial^{k+h} T_i(x, y)}{\partial x^k \partial y^h} \right]_{(x_i, y_i)} \qquad (\mathbf{4.20})$$

By applying the same procedures given for 1D case and neglecting the third and higher order terms in the DTM expansions, the formulation of the DTM based meshless method 1 for a 2D problem can be written as follows

$$\sum_{g=1}^{N_g} W(\boldsymbol{\xi_g}, \boldsymbol{x_i})\, T_i(\boldsymbol{x_g}) = \sum_{g=1}^{N_g} W(\boldsymbol{\xi_g}, \boldsymbol{x_i})\, \boldsymbol{P}(\boldsymbol{\xi_g}, \boldsymbol{x_i}) \boldsymbol{U}_i$$

$$\sum_{g=1}^{N_g} W(\boldsymbol{\xi_g}, \boldsymbol{x_i})\, T_x(\boldsymbol{x_g}) = \sum_{g=1}^{N_g} W(\boldsymbol{\xi_g}, \boldsymbol{x_i})\, \boldsymbol{P}_x(\boldsymbol{\xi_g}, \boldsymbol{x_i}) \boldsymbol{U}_i$$

$$\sum_{g=1}^{N_g} W(\boldsymbol{\xi_g}, \boldsymbol{x_i})\, T_y(\boldsymbol{x_g}) = \sum_{g=1}^{N_g} W(\boldsymbol{\xi_g}, \boldsymbol{x_i})\, \boldsymbol{P}_y(\boldsymbol{\xi_g}, \boldsymbol{x_i}) \boldsymbol{U}_i$$

$$\sum_{g=1}^{N_g} W(\boldsymbol{\xi_g}, \boldsymbol{x_i})\, T_{xx}(\boldsymbol{x_g}) = \sum_{g=1}^{N_g} W(\boldsymbol{\xi_g}, \boldsymbol{x_i})\, \boldsymbol{P}_{xx}(\boldsymbol{\xi_g}, \boldsymbol{x_i}) \boldsymbol{U}_i$$

$$\sum_{g=1}^{N_g} W(\boldsymbol{\xi_g}, \boldsymbol{x_i})\, T_{yy}(\boldsymbol{x_g}) = \sum_{g=1}^{N_g} W(\boldsymbol{\xi_g}, \boldsymbol{x_i})\, \boldsymbol{P}_{yy}(\boldsymbol{\xi_g}, \boldsymbol{x_i})\, \boldsymbol{U}_i$$

$$\sum_{g=1}^{N_g} W(\boldsymbol{\xi_g}, \boldsymbol{x_i})\, T_{xy}(\boldsymbol{x_g}) = \sum_{g=1}^{N_g} W(\boldsymbol{\xi_g}, \boldsymbol{x_i})\, \boldsymbol{P}_{xy}(\boldsymbol{\xi_g}, \boldsymbol{x_i})\, \boldsymbol{U}_i \qquad (\mathbf{4.21})$$

The set of simultaneous linear algebraic equations given in Equation (4.21) can be solved for the unknowns of $\boldsymbol{U}_i$ for all particles. The formulation for 3D problems can be obtained in a similar fashion as described above.

4.3.2 DTM based meshless method II

One Dimensional Case:

If we multiply both sides of Equation (4.11) by $W(\xi, x)$, we obtain

$$W(\xi, x)\, T_i(x) = W(\xi, x) \boldsymbol{P}(x) \boldsymbol{U}_i \qquad (\mathbf{4.22})$$

Depending on the number of unknowns of the matrix $\boldsymbol{U}_i$, the derivatives of Equation (4.22) are obtained. By neglecting the sixth and higher order terms in the DTM expansions, the formulation of the DTM based meshless method II for a 1D problem can be written by evaluating Equation (4.22) and its derivaties at every particle in the

compact support domain of $W(\xi, x)$ and sum each side over these particles as follows

$$\sum_{g=1}^{N_g} W(x_g, x_i)\, T_i(x_g) = \sum_{g=1}^{N_g} W(x_g, x_i)\, \boldsymbol{P}(x_g, x_i)\boldsymbol{U}_i \qquad (\mathbf{4.23})$$

$$\sum_{g=1}^{N_g} (W(x_g, x_i)\, T_x(x_g) + W_x(x_g, x_i)T(x_g)) =$$

$$\sum_{g=1}^{N_g} (W(x_g, x_i)\, \boldsymbol{P}_{\boldsymbol{x}}(x_g, x_i) + W_x(x_g, x_i)\boldsymbol{P}(x_g, x_i))\boldsymbol{U}_i \qquad (\mathbf{4.24})$$

$$\sum_{g=1}^{N_g} (W(x_g, x_i)\, T_{xx}(x_g) + 2W_x(x_g, x_i)T_x(x_g) + W_{xx}(x_g, x_i)T(x_g))$$

$$= \sum_{g=1}^{N_g} (W(x_g, x_i)\, \boldsymbol{P}_{xx}(x_g, x_i)$$

$$+ 2W_x(x_g, x_i)\boldsymbol{P}_x(x_g, x_i) + W_{xx}(x_g, x_i)\boldsymbol{P}(x_g, x_i))\boldsymbol{U}_i \qquad (\mathbf{4.25})$$

$$\sum_{g=1}^{N_g} (W(x_g, x_i)\, T_{xxx}(x_g) + 3W_x(x_g, x_i)T_{xx}(x_g) + 3W_{xx}(x_g, x_i)T_x(x_g)$$

$$+ W_{xxx}(x_g, x_i)T(x_g)) = \sum_{g=1}^{N_g} (W(x_g, x_i)\, \boldsymbol{P}_{xxx}(x_g, x_i)$$

$$+3W_x(x_g, x_i)\boldsymbol{P}_{xx}(x_g, x_i) + 3W_{xx}(x_g, x_i)\boldsymbol{P}_x(x_g, x_i)$$

$$+ W_{xxx}(x_g, x_i)\boldsymbol{P}(x_g, x_i))\boldsymbol{U}_i \qquad (\mathbf{4.26})$$

$$\sum_{g=1}^{N_g} (W(x_g, x_i)\, T_{xxxx}(x_g) + 4W_x(x_g, x_i)T_{xxx}(x_g) + 6W_{xx}(x_g, x_i)T_{xx}(x_g) +$$

$$4W_{xxx}(x_g, x_i)T_x(x_g) + W_{xxxx}(x_g, x_i)T(x_g)) =$$

$$\sum_{g=1}^{N_g} (W(x_g, x_i)\, \boldsymbol{P}_{xxxx}(x_g, x_i) + 4W_x(x_g, x_i)\boldsymbol{P}_{xxx}(x_g, x_i)$$

$$+6W_{xx}(x_g, x_i)\boldsymbol{P}_{xx}(x_g, x_i) + 4W_{xxx}(x_g, x_i)\boldsymbol{P}_x(x_g, x_i)$$

$$+ W_{xxxx}(x_g, x_i)\boldsymbol{P}(x_g, x_i))\boldsymbol{U}_i \qquad (\mathbf{4.27})$$

$$\sum_{g=1}^{N_g}(W(x_g,x_i)\,T_{xxxxx}(x_g)+5W_x(x_g,x_i)T_{xxxx}(x_g)+10W_{xx}(x_g,x_i)T_{xxx}(x_g)+10W_{xxx}(x_g,x_i)T_{xx}(x_g)+5W_{xxxx}(x_g,x_i)T_x(x_g))+W_{xxxxx}(x_g,x_i)T(x_g))=\sum_{g=1}^{N_g}(W(x_g,x_i)\,\boldsymbol{P}_{xxxxx}(x_g,x_i)+5W_x(x_g,x_i)\boldsymbol{P}_{xxxx}(x_g,x_i)+10W_{xx}(x_g,x_i)\boldsymbol{P}_{xxx}(x_g,x_i)+10W_{xxx}(x_g,x_i)\boldsymbol{P}_{xx}(x_g,x_i)+5W_{xxxx}(x_g,x_i)\boldsymbol{P}_x(x_g,x_i)+W_{xxxxx}(x_g,x_i)\boldsymbol{P}(x_g,x_i))\boldsymbol{U}_i \quad (\mathbf{4.28})$$

The set of simultaneous linear algebraic equations given by Equations **(4.23)** to **(4.28)** can be solved for the unknowns of $\boldsymbol{U}_i$ for all particles.

Two Dimensional Case:

If we multiply both sides of Equation (4.18) by $W(\boldsymbol{\xi},\boldsymbol{x})$, we obtain

$$W(\boldsymbol{\xi},\boldsymbol{x})\,T_i(x,y)=W(\boldsymbol{\xi},\boldsymbol{x})\boldsymbol{P}(\boldsymbol{x})\boldsymbol{U}_i \quad (\mathbf{4.29})$$

Depending on the number of unknowns of the matrix $\boldsymbol{U}_i$, the derivatives of the Equation (4.29) are obtained. By neglecting the third and higher order terms in the DTM expansions, the formulation of the DTM based meshless method II for a 2D problem can be written by evaluating Equation (4.29) and its derivaties at every particle in the compact support domain of $W(\boldsymbol{\xi},\boldsymbol{x})$ and sum each side over these particles as follows

$$\sum_{g=1}^{N_g} W(\boldsymbol{\xi_g},\boldsymbol{x_i})\,T_i(\boldsymbol{x_g})=\sum_{g=1}^{N_g} W(\boldsymbol{\xi_g},\boldsymbol{x_i})\,\boldsymbol{P}(\boldsymbol{\xi_g},\boldsymbol{x_i})\boldsymbol{U}_i \quad (\mathbf{4.30})$$

$$\sum_{g=1}^{N_g}(W(\boldsymbol{\xi_g},\boldsymbol{x_i})\,T_x(\boldsymbol{x_g})+W_x(\boldsymbol{\xi_g},\boldsymbol{x_i})T_i(\boldsymbol{x_g}))$$

$$=\sum_{g=1}^{N_g}(W(\boldsymbol{\xi_g},\boldsymbol{x_i})\,\boldsymbol{P}_x(\boldsymbol{\xi_g},\boldsymbol{x_i})+W_x(\boldsymbol{\xi_g},\boldsymbol{x_i})\boldsymbol{P}(\boldsymbol{\xi_g},\boldsymbol{x_i}))\boldsymbol{U}_i \quad (\mathbf{4.31})$$

$$\sum_{g=1}^{N_g}(W(\boldsymbol{\xi_g},\boldsymbol{x_i})\,T_y(\boldsymbol{x_g})+W_y(\boldsymbol{\xi_g},\boldsymbol{x_i})T_i(\boldsymbol{x_g}))$$

$$=\sum_{g=1}^{N_g}(W(\boldsymbol{\xi_g},\boldsymbol{x_i})\,\boldsymbol{P}_y(\boldsymbol{\xi_g},\boldsymbol{x_i})+W_y(\boldsymbol{\xi_g},\boldsymbol{x_i})\boldsymbol{P}(\boldsymbol{\xi_g},\boldsymbol{x_i}))\boldsymbol{U}_i \quad (\mathbf{4.32})$$

$$\sum_{g=1}^{N_g}(W(\boldsymbol{\xi_g},\boldsymbol{x_i})\,T_{xx}(\boldsymbol{x_g})+2W_x(\boldsymbol{\xi_g},\boldsymbol{x_i})T_x(\boldsymbol{x_g})+W_{xx}(\boldsymbol{\xi_g},\boldsymbol{x_i})T_i(\boldsymbol{x_g}))$$

$$=\sum_{g=1}^{N_g}(W(\boldsymbol{\xi_g},\boldsymbol{x_i})\,\boldsymbol{P}_{xx}(\boldsymbol{\xi_g},\boldsymbol{x_i})+2W_x(\boldsymbol{\xi_g},\boldsymbol{x_i})\boldsymbol{P}_x(\boldsymbol{\xi_g},\boldsymbol{x_i})$$

$$+W_{xx}(\boldsymbol{\xi_g},\boldsymbol{x_i})\boldsymbol{P}(\boldsymbol{\xi_g},\boldsymbol{x_i}))\boldsymbol{U}_i \qquad (\mathbf{4.33})$$

$$\sum_{g=1}^{N_g}(W(\boldsymbol{\xi_g},\boldsymbol{x_i})\,T_{yy}(\boldsymbol{x_g})+2W_y(\boldsymbol{\xi_g},\boldsymbol{x_i})T_y(\boldsymbol{x_g})+W_{yy}(\boldsymbol{\xi_g},\boldsymbol{x_i})T_i(\boldsymbol{x_g}))$$

$$=\sum_{g=1}^{N_g}(W(\boldsymbol{\xi_g},\boldsymbol{x_i})\,\boldsymbol{P}_{yy}(\boldsymbol{\xi_g},\boldsymbol{x_i})+2W_y(\boldsymbol{\xi_g},\boldsymbol{x_i})\boldsymbol{P}_y(\boldsymbol{\xi_g},\boldsymbol{x_i})$$

$$+W_{yy}(\boldsymbol{\xi_g},\boldsymbol{x_i})\boldsymbol{P}(\boldsymbol{\xi_g},\boldsymbol{x_i}))\boldsymbol{U}_i \qquad (\mathbf{4.34})$$

$$\sum_{g=1}^{N_g}(W(\boldsymbol{\xi_g},\boldsymbol{x_i})\,T_{xy}(\boldsymbol{x_g})+W_y(\boldsymbol{\xi_g},\boldsymbol{x_i})T_x(\boldsymbol{x_g})+W_x(\boldsymbol{\xi_g},\boldsymbol{x_i})T_y(\boldsymbol{x_g})$$

$$+W_{xy}(\boldsymbol{\xi_g},\boldsymbol{x_i})T_i(\boldsymbol{x_g}))$$

$$=\sum_{g=1}^{N_g}(W(\boldsymbol{\xi_g},\boldsymbol{x_i})\,\boldsymbol{P}_{xy}(\boldsymbol{\xi_g},\boldsymbol{x_i})+W_y(\boldsymbol{\xi_g},\boldsymbol{x_i})\boldsymbol{P}_x(\boldsymbol{\xi_g},\boldsymbol{x_i})$$

$$+W_x(\boldsymbol{\xi_g},\boldsymbol{x_i})\boldsymbol{P}_y(\boldsymbol{\xi_g},\boldsymbol{x_i})+W_{xy}(\boldsymbol{\xi_g},\boldsymbol{x_i})\boldsymbol{P}(\boldsymbol{\xi_g},\boldsymbol{x_i}))\boldsymbol{U}_i \qquad (\mathbf{4.35})$$

The set of simultaneous linear algebraic equations given by Equations (4.30) to (4.35) can be solved for the unknowns of $\boldsymbol{U}_i$ for all particles.

4.3.3 DTM based meshless method III

One Dimensional Case:

If we multiply both sides of Equation (4.11) by $W(\xi,x)$, we obtain

$$W(\xi,x)\,T_i(x)=W(\xi,x)\boldsymbol{P}(x)\boldsymbol{U}_i \qquad (\mathbf{4.36})$$

Lets rewrite Equation **(4.36)** with respect to the compact support domain shown in Figure 4.1, evaluate this equation at every particle in the compact support domain of $W(\xi,x)$ and sum each side over these particles, then

$$\sum_{g=1}^{N_g} W(x_g, x_i) T_i(x_g) = \sum_{g=1}^{N_g} W(x_g, x_i)\, \boldsymbol{P}(x_g, x_i) \boldsymbol{U}_i \qquad (\mathbf{4.37})$$

Repeating the above procedure regarding the number of terms included in $\boldsymbol{U}_i$ in Equation (4.12) by replacing W with the following

$$W_x = \partial W / \partial x,$$

$$W_{xx} = \frac{\partial^2 W}{\partial x^2},$$

$$W_{xxx} = \frac{\partial^3 W}{\partial x^3},$$

$$W_{xxxx} = \frac{\partial^4 W}{\partial x^4},$$

$$W_{xxxxx} = \frac{\partial^5 W}{\partial x^5} \qquad (\mathbf{4.38})$$

and so on. Then, we can solve a set of simultaneous linear algebraic equations for the unknowns of $\boldsymbol{U}_i$ for all particles.

By neglecting the sixth and higher order terms in the DTM expansions, the formulation of the DTM based meshless method III for a 1D problem can be written as follows

$$\sum_{g=1}^{N_g} W(x_g, x_i) T_i(x_g) = \sum_{g=1}^{N_g} W(x_g, x_i)\, \boldsymbol{P}(x_g, x_i) \boldsymbol{U}_i$$

$$\sum_{g=1}^{N_g} W_x(x_g, x_i) T_i(x_g) = \sum_{g=1}^{N_g} W_x(x_g, x_i)\, \boldsymbol{P}(x_g, x_i) \boldsymbol{U}_i$$

$$\sum_{g=1}^{N_g} W_{xx}(x_g, x_i) T_i(x_g) = \sum_{g=1}^{N_g} W_{xx}(x_g, x_i)\, \boldsymbol{P}(x_g, x_i) \boldsymbol{U}_i$$

$$\sum_{g=1}^{N_g} W_{xxx}(x_g, x_i) T_i(x_g) = \sum_{g=1}^{N_g} W_{xxx}(x_g, x_i)\, \boldsymbol{P}(x_g, x_i) \boldsymbol{U}_i$$

$$\sum_{g=1}^{N_g} W_{xxxx}(x_g, x_i) T_i(x_g) = \sum_{g=1}^{N_g} W_{xxxx}(x_g, x_i)\, \boldsymbol{P}(x_g, x_i) \boldsymbol{U}_i$$

$$\sum_{g=1}^{N_g} W_{xxxxx}(x_g, x_i) T_i(x_g) = \sum_{g=1}^{N_g} W_{xxxxx}(x_g, x_i)\, \boldsymbol{P}(x_g, x_i) \boldsymbol{U}_i \qquad \mathbf{4.39})$$

where

$$\boldsymbol{P}(x) = [1\,, (x - x_i)^1\,, (x - x_i)^2, (x - x_i)^3\,, (x - x_i)^4\ \,, (x - x_i)^5]$$
$$\boldsymbol{U}_i = [U_i(0), U_i(1), U_i(2), U_i(3), U_i(4), U_i(5)]^{\,T} \qquad (\mathbf{4.40})$$

The set of simultaneous linear algebraic equations given by Equation (4.39) can be solved for the unknowns of $\boldsymbol{U}_i$ for all particles.

Two Dimensional Case:

If we multiply both sides of Equation (4.18) by $W(\boldsymbol{\xi}, \boldsymbol{x})$, we obtain

$$W(\boldsymbol{\xi}, \boldsymbol{x})\, T_i(x, y) = W(\boldsymbol{\xi}, \boldsymbol{x}) \boldsymbol{P}(\boldsymbol{x}) \boldsymbol{U}_i \qquad (\mathbf{4.41})$$

Lets rewrite Equation (4.41) with respect to the compact support domain shown in Figure 4.1, evaluate this equation at every particle in the compact support domain of $W(\boldsymbol{\xi}, \boldsymbol{x})$ and sum each side over these particles, then

$$\sum_{g=1}^{N_g} W(\boldsymbol{\xi_g}, \boldsymbol{x_i}) T_i(\boldsymbol{\xi_g}) = \sum_{g=1}^{N_g} W(\boldsymbol{\xi_g}, \boldsymbol{x_i})\, \boldsymbol{P}(\boldsymbol{\xi_g}, \boldsymbol{x_i}) \boldsymbol{U}_i \qquad (\mathbf{4.42})$$

Repeating the above procedure regarding the number of terms included in U_i in Equation (4.18) by replacing W with the following

$$W_x = \partial W / \partial x,$$

$$W_y = \partial W / \partial y,$$

$$W_{xx} = \frac{\partial^2 W}{\partial x^2},$$

$$W_{yy} = \partial^2 W / \partial y^2,$$

$$W_{xy} = \frac{\partial^2 W}{\partial x \partial y} \tag{4.43}$$

and so on. By neglecting the third and higher order terms in the DTM expansions, the formulation of the DTM based meshless method III for a 2D problem can be written as follows

$$\sum_{g=1}^{N_g} W(\boldsymbol{\xi_g}, \boldsymbol{x_i}) T_i(\boldsymbol{\xi_g}) = \sum_{g=1}^{N_g} W(\boldsymbol{\xi_g}, \boldsymbol{x_i})\, \boldsymbol{P}(\boldsymbol{\xi_g}, \boldsymbol{x_i}) \boldsymbol{U}_i$$

$$\sum_{g=1}^{N_g} W_x(\boldsymbol{\xi_g}, \boldsymbol{x_i}) T_i(\boldsymbol{\xi_g}) = \sum_{g=1}^{N_g} W_x(\boldsymbol{\xi_g}, \boldsymbol{x_i})\, \boldsymbol{P}(\boldsymbol{\xi_g}, \boldsymbol{x_i}) \boldsymbol{U}_i$$

$$\sum_{g=1}^{N_g} W_y(\boldsymbol{\xi_g}, \boldsymbol{x_i}) T_i(\boldsymbol{\xi_g}) = \sum_{g=1}^{N_g} W_y(\boldsymbol{\xi_g}, \boldsymbol{x_i})\, \boldsymbol{P}(\boldsymbol{\xi_g}, \boldsymbol{x_i}) \boldsymbol{U}_i$$

$$\sum_{g=1}^{N_g} W_{xx}(\boldsymbol{\xi_g}, \boldsymbol{x_i}) T_i(\boldsymbol{\xi_g}) = \sum_{g=1}^{N_g} W_{xx}(\boldsymbol{\xi_g}, \boldsymbol{x_i})\, \boldsymbol{P}(\boldsymbol{\xi_g}, \boldsymbol{x_i}) \boldsymbol{U}_i$$

$$\sum_{g=1}^{N_g} W_{yy}(\boldsymbol{\xi_g}, \boldsymbol{x_i}) T_i(\boldsymbol{\xi_g}) = \sum_{g=1}^{N_g} W_{yy}(\boldsymbol{\xi_g}, \boldsymbol{x_i})\, \boldsymbol{P}(\boldsymbol{\xi_g}, \boldsymbol{x_i}) \boldsymbol{U}_i$$

$$\sum_{g=1}^{N_g} W_{xy}(\boldsymbol{\xi_g}, \boldsymbol{x_i}) T_i(\boldsymbol{\xi_g}) = \sum_{g=1}^{N_g} W_{xy}(\boldsymbol{\xi_g}, \boldsymbol{x_i})\, \boldsymbol{P}(\boldsymbol{\xi_g}, \boldsymbol{x_i}) \boldsymbol{U}_i \tag{4.44}$$

where

$$\boldsymbol{P}(x, y) = [1, (x - x_i)^1, (y - y_i)^1, (x - x_i)^2, (y - y_i)^2, (x - x_i)^1 (y - y_i)^1]$$

$$\boldsymbol{U}_i = [U_i(0,0), U_i(1,0), U_i(0,1), U_i(2,0), U_i(0,2), U_i(1,1)]^T \tag{4.45}$$

The set of simultaneous linear algebraic equations given by Equation (4.44) can be solved for the unknowns of $\boldsymbol{U}_i$ for all particles. The formulation for 3D problems can be obtained in a similar fashions as described above.

The SSPH formulation can be also used for the representation of the formulation of the fourth approach because the unknown elements of the matrix Q(x) are exactly the same with the unknown elements of the matrix U_i. However, it is not studied in this thesis.

5. NUMERICAL EXAMPLES

In this section, the DTM based meshless methods and SSPH method were used to solve 1D nonhomogeneous boundary value problem, 2D homogeneous Laplace equation, 2D nonhomogeneous Laplace equation and plane stress deformations of a plate in 2D. Numerical solutions obtained by each method are compared with the analytical solutions for each problem. All methods are also compared with each other by using global L_2 error norm for different number of nodes. Finally, the CPU times are also considered for comparisons.

5.1 1D Nonhomogeneous Boundary Value Problem

Consider the following 1D nonhomogeneous ordinary differential equation

$$\frac{d^2v}{dx^2} = f(x), \qquad f(x) = x^3 \qquad 0 \le x \le 2 \tag{5.1}$$

The boundary conditions are given by $v(0) = 1$ and $v(2) = 6.6$. The analytical solution of this ordinary differential equation can be expressed

$$v(x) = \frac{1}{20}x^5 + 2x + 1 \tag{5.2}$$

The above boundary value problem is solved by the DTM based mehsless methods I, II, and III and SSPH method for the particle distributions of 5 (Δ=0.4), 20 (Δ=0.1) and 100 (Δ=0.02) equally spaced particles in the domain $x \in [0,2]$. It is chosen that the smoothing length h equals to the minimum distance between two adjacent particles.

The following Revised Super Gauss Function is used for the kernel function since it yielded the least L_2 error norms in numerical solutions

$$W(x,\xi) = \frac{G}{(h\sqrt{\pi})^{\lambda}} \begin{cases} (4-d^2)\, e^{-d^2} & 0 \le d \le 2 \\ 0 & d > 2 \end{cases} \tag{5.3}$$

where $d = |\boldsymbol{x} - \boldsymbol{\xi}|/h$ is the radius of the support domain which is set to 2, λ is equal to the dimensionality of the space and G is the normalization parameter having the

values 1.04823, 1.10081 and 1.18516 for λ = 1, 2 and 3, respectively [21]. But all four methods discussed here do not require the normalization parameter *G* in the formulation. The revised super Gauss function is recommended as a weight (kernel) function for the SSPH method [21]. The linear and the quadratic weight function cannot be used fot the DTM based meshless method I and II if the first and the second order derivatives of the weight function are to be found. The derivatives of the Revised Super Gauss Function are needed in DTM based methods II and III formulations.

The numerical results obtained by using the DTM based meshless methods I, II, and III and SSPH method are compared with the analytical solutions, and their convergence and accuracy properties are evaluated by using the following global L_2 error norm given in [109]

$$L_2 = \frac{\left[\sum_{j=1}^{m}(v_{num}^{j} - v_{exact}^{j})^2\right]^{1/2}}{\left[\sum_{j=1}^{m}(v_{exact}^{j})^2\right]^{1/2}} x\%100 \qquad (\mathbf{5.4})$$

In Equation (5.4), v_{num}^{j} is the value of the function v at the j^{th} node calculated by the numerical solution and v_{exact}^{j} is the value of the function v at the j^{th} node calculated by the analytical solution. Considering Equation (5.1), we can obtain the following equation by using the formalism of DTM

$$(k+1)(k+2)V(k+2) = F(k)$$

$$F(k) = \frac{1}{k!}\left[\frac{d^k x^3}{dx^k}\right]_{x=x_j} \qquad (\mathbf{5.5})$$

By using Equation (5.5), we get the following relations between the elements of the matrix $\boldsymbol{U}_i$ for all particles defined by Equation (4.13)

For k=0, $V(2) = F(0)/2$

For k=1, $V(3) = F(1)/6$

For k=2, $V(4) = F(2)/12$

For k=3, $V(5) = F(3)/20$ $\qquad (\mathbf{5.6})$

By using these equations, the coefficients $V(2), V(3), V(4)$ and $V(5)$ can be found in terms of $F(0), F(1), F(2)$ and $F(3)$ for all particles located in the compact support domain. The sixth and higher order terms are neglected which are found to be zero for this problem.

Firstly, $V(2), V(3), V(4)$ and $V(5)$ for all particles are obtained, the next step is to find the rest of the unknowns for all particles. $V(0)$ and $V(1)$ are already defined by boundary conditions for particle number 1; thus, there is no unknown for particle number 1 located at x=0.

The global L_2 error norms of the solutions of the DTM based meshless methods I, II, and III and SSPH method are given in Table 5.1 to 5.4 where different numbers of particles and terms in expansions are considered. The results in Table 5.1 to 5.4 are obtained for the parameter values of d and h giving the best accuracy for each method.

In Table 5.1, it is observed that the DTM based meshless methods II, and III and SSPH method give the lowest error for the numerical solution obtained by using 3 terms. The DTM based meshless method I always gives the highest error norm when it is compared to other methods.

The DTM based meshless method I cannot provide satisfactory result for the compact support domain radius of 2 by using 5 nodes.

Table 5.1 : Global L_2 error norm for different number of nodes – 3 term.

Meshless Method	Number of Nodes		
	5 Nodes	20 Nodes	100 Nodes
DTM - I	*	1.4129277	0.15680171
DTM - II	1.0455434	0.0542322	0.0020706
DTM - III	1.0455434	0.0542322	0.0020706
SSPH	1.0454434	0.0542322	0.0020706

* There is no solution for the compact support domain radius d=2.

In Table 5.2, it is found that there is no difference between the methods in terms of global L_2 error norm for different number of nodes by using 4 term in the TSE expansion and all methods show convergence as the number of nodes is increased. The DTM based meshless method I cannot provide satisfactory results for the compact support domain radius of 2 by using 5 nodes.

Table 5.2 : Global L_2 error norm for different number of nodes – 4 term.

Meshless Method	Number of Nodes		
	5 Nodes	20 Nodes	100 Nodes
DTM - I	*	0.05299339	0.0020771
DTM - II	1.0455434	0.0542322	0.0020706
DTM - III	1.0455434	0.0542322	0.0020706
SSPH	1.0455434	0.0542322	0.0020706

* There is no solution for the compact support domain radius *d*=2.

It is observed in Table 5.3 that the DTM based meshless methods I and II always give the lowest global L_2 error norm for different number of nodes by using 5 term in the TSE expansion. The DTM based meshless method I cannot provide satisfactory results for the compact support domain radius of 2 by using 5 nodes.

Table 5.3 : Global L_2 error norm for different number of nodes – 5 term.

Meshless Method	Number of Nodes		
	5 Nodes	20 Nodes	100 Nodes
DTM - I	*	0.0019065	$1.6\text{x}10^{-6}$
DTM - II	$4.5\text{x}10^{-14}$	$1.2\text{x}10^{-11}$	$2.3\text{x}10^{-9}$
DTM - III	$3.1\text{x}10^{-14}$	$4.9\text{x}10^{-13}$	$3.6\text{x}10^{-12}$
SSPH	0.1258686 **	0.0001205 **	$3.6\text{x}10^{-8}$

* There is no solution for the compact support domain radius d=2

** The compact support domain radius d is chosen as 4, because d=2 results in large L_2 error norms or no solution with the current smoothing length assumption.

It is clear that, even with the same number of terms, solutions of the DTM based meshless methods II and III agree very well with the analytical solution; however, those obtained by using the SSPH method and DTM based meshless method I differ noticeably from the analytical solution especially for 5 nodes and 5 terms in the TSEs.

It is observed in Table 5.4 that the DTM based meshless methods II and III agree very well with the analytical solution. The SSPH method cannot provide solution by using 5 nodes in the problem domain when it uses 6 terms in TSE. The DTM based meshless method I cannot provide satisfactory result for the compact support domain radius of 2 by using 5 nodes.

Table 5.4 : Global L_2 error norm for different number of nodes – 6 term.

Meshless Method	Number of Nodes		
	5 Nodes	20 Nodes	100 Nodes
DTM - I	*	$2.4\text{x}10^{-13}$	$3.9\text{x}10^{-12}$
DTM - II	$7.9\text{x}10^{-14}$	$1.4\text{x}10^{-11}$	$3.6\text{x}10^{-9}$
DTM - III	$7.8\text{x}10^{-14}$	$3.3\text{x}10^{-13}$	$3.6\text{x}10^{-12}$
SSPH	**	$1.3\text{x}10^{-9}$ ***	$2.6\text{x}10^{-9}$ ***

* There is no solution for the compact support domain radius d=2

** At least 6 nodes are needed to solve the problem.

*** The compact support domain radius d is used as 5 because d=2, 3 and 4 result in large L_2 error norms with the current smoothing length assumption.

Regarding to the results obtained by using 6 terms in the TSEs, the DTM based meshless methods give the lowest L_2 error norms.

5.2 Homogeneous Laplace Equation in 2D

The Laplace equation in 2D is solved by using the DTM based meshless methods I, II and III and SSPH method in the domain shown in Figure 5.1. The governing differential equation and essential boundary conditions are given by

$$\frac{\partial^2 T}{\partial x^2}+\frac{\partial^2 T}{\partial y^2}=0, \quad T_1=T_3=T_4=0\ ℃, \quad T_2=100\ ℃ \tag{5.7}$$

where T is the temperature and T_i denote boundary temperatures.

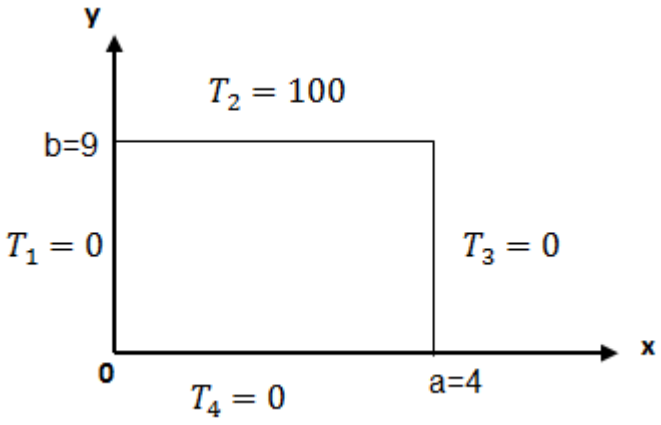

Figure 5.1 : Problem domain and boundary conditions.

The analytical solution of the above boundary value problem is given by

$$\frac{T(x,y)}{T_2}=\sum_{n=1}^{\infty}\frac{2[1-(-1)^n]}{n\pi}\sin\left(\frac{n\pi x}{a}\right)\frac{\sinh\left(\frac{n\pi y}{a}\right)}{\sinh\left(\frac{n\pi b}{a}\right)} \tag{5.8}$$

When solving this problem, equally spaced 50 (Δ=1), 171 (Δ=0.5) and 629 (Δ=0.25) particles are considered in the domain. The smoothing length h is equal to the minimum distance between two adjacent particles. The following Revised Super Gauss Function is used as the kernel function

$$W(d)=\frac{G}{(h\sqrt{\pi})^{\lambda}}\begin{cases}(16-d^2)\,e^{-d^2} & 0\le d\le 4\\ 0 & d>4\end{cases} \tag{5.9}$$

where $d=|\boldsymbol{x}-\boldsymbol{\xi}|/h$ is the radius of the support domain which is set to 4, λ is equal to the dimensionality of the space, and G is the normalization parameter having the values of 1.04823, 1.10081 and 1.18516 for λ = 1, 2 and 3, respectively [21].

The convergence and accuracy of the DTM based meshless methods I, II and III and SSPH method are calculated by using the following global L_2 error norm given in [109]

$$L_2 = \frac{\left[\sum_{j=1}^{m}\{(u_{num}^{j} - u_{exact}^{j})^2 + (v_{num}^{j} - v_{exact}^{j})^2\}\right]^{1/2}}{\left[\sum_{j=1}^{m}\{(u_{exact}^{j})^2 + (v_{exact}^{j})^2\}\right]^{1/2}} \text{ x } 100\ \% \qquad (\mathbf{5.10})$$

In Equation (5.10), u_{num}^{j} and v_{num}^{j} are respectively the values of functions u and v at the j^{th} node calculated by the numerical solution, and u_{exact}^{j} and v_{exact}^{j} are respectively the values of functions u and v at the j^{th} node calculated by the analytical solution.

From the governing Equation (5.7), we can obtain the following equation by using the notation of DTM

$$(k+1)(k+2)T(k+2,m) + (m+1)(m+2)T(k,m+2) = 0$$

For k=0 and m=0: $\quad -T(2,0) = T(0,2)$

For k=1 and m=0: $\quad -3\,T(3,0) = T(1,2) \qquad (\mathbf{5.11})$

The number of equations derived from Equation (5.11) can be increased depending on the required number of terms in the matrix $\boldsymbol{U_i}$. The matrices $\boldsymbol{P}$ and $\boldsymbol{U_i}$ defined by Equation (4.18) can be rearranged by using Equation (5.11) as follows

$$\boldsymbol{P}(\boldsymbol{x},\boldsymbol{\xi}) = \ [1, (x-x_i)^1, (y-y_i)^1, (x-x_i)^2 - \ (y-y_i)^2\ , (x-x_i)^1(y-y_i)^1,$$
$$(x-x_i)^3 - 3.(x-x_i)^1(y-y_i)^2]$$
$$\boldsymbol{U}_i = [U_i(0,0), U_i(1,0), U_i(0,1), U_i(2,0), U_i(1,1), U_i(3,0)\ ]^T \qquad (\mathbf{5.12})$$

Following, above nodal equations are assembled to obtain the global equations; then, boundary conditions are imposed by using the direct method and the resulting equation system is solved. Note that there are 6 terms in the vector $\boldsymbol{U}_i$.

To evaluate the performance, numerical solutions are obtained for 6 terms for the DTM based meshless methods I, II and III and SSPH method. Numerical solutions obtained by using 6 terms in the associated expansions and 50, 171 and 629 nodes are presented in Figures 5.2, 5.3 and 5.4, respectively.

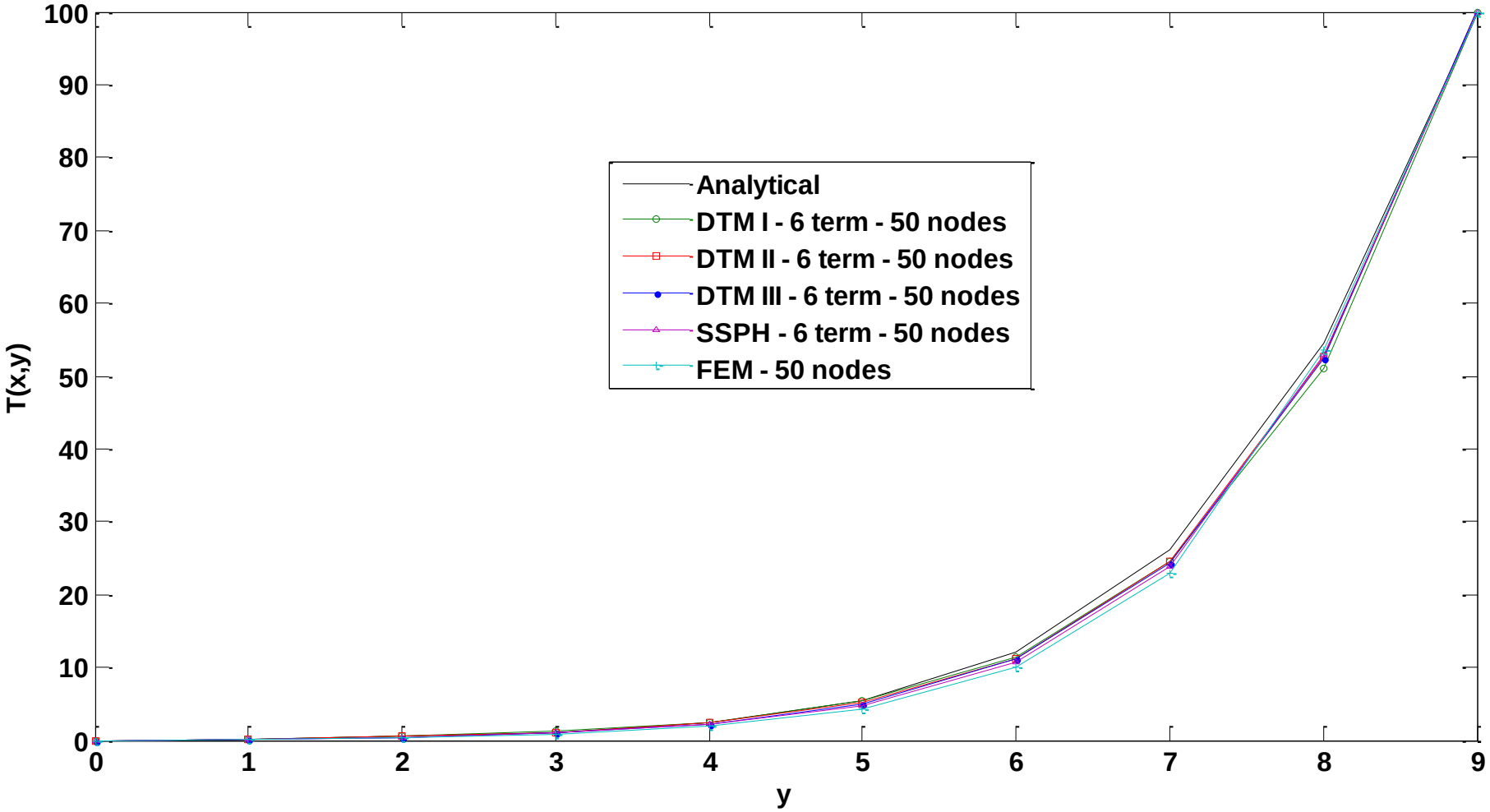

Figure 5.2 : Temperatures along the *y*-axis (*x*=2) computed by all four methods and analytical solution where equally spaced 50 nodes are used.

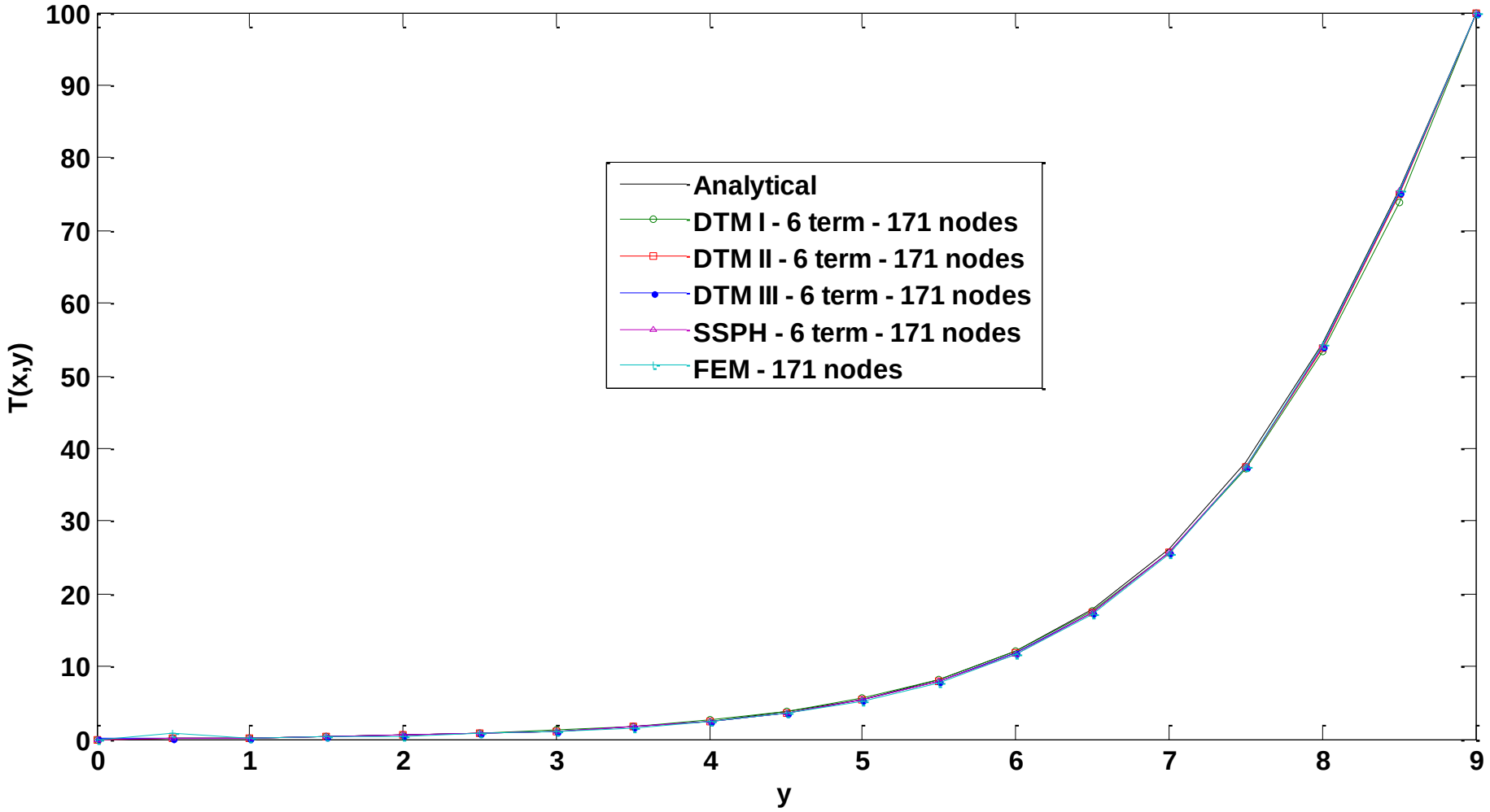

Figure 5.3 : Temperatures along the *y*-axis (*x*=2) computed by all four methods and analytical solution where equally spaced 171 nodes are used.

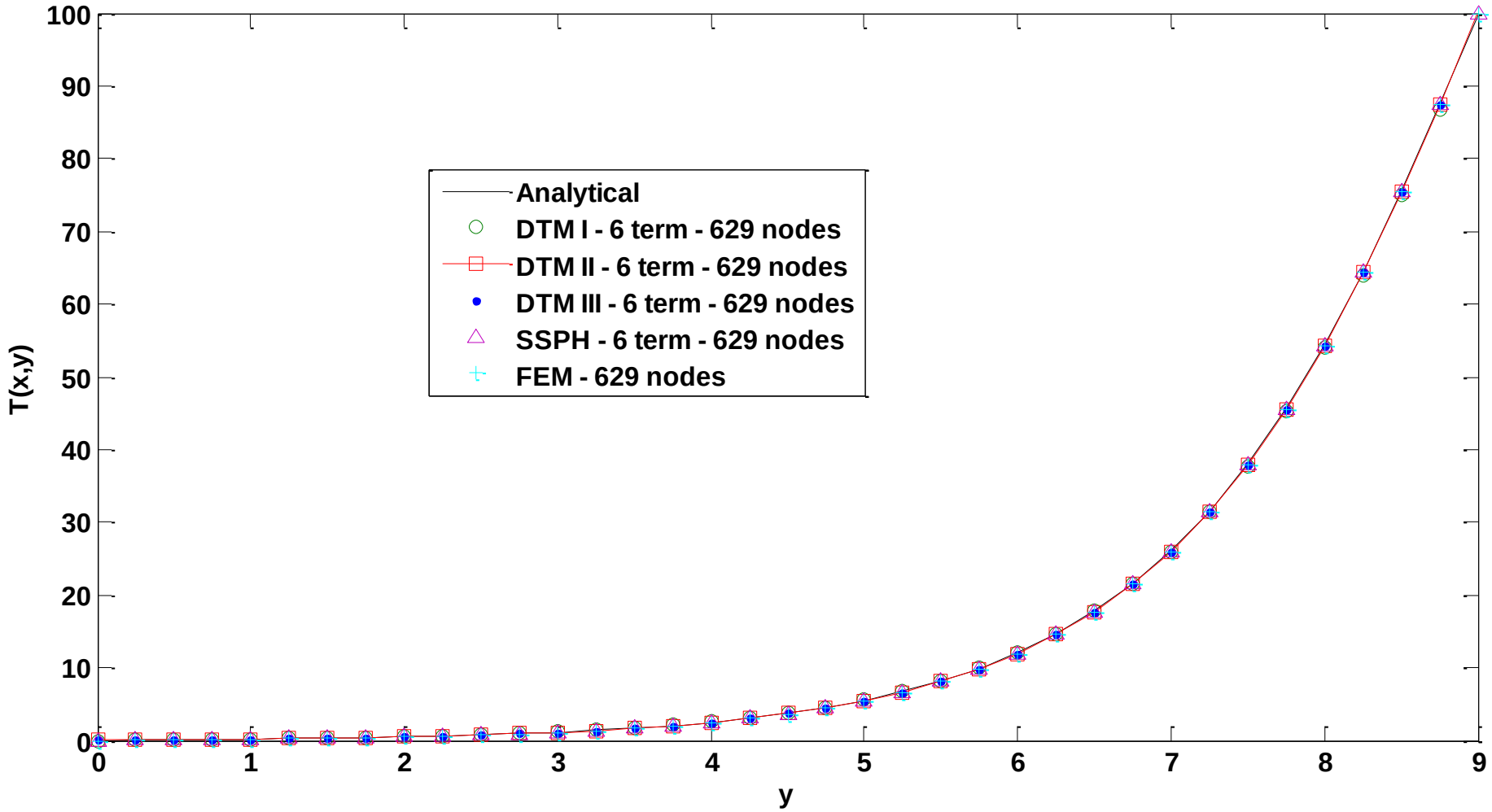

Figure 5.4 : Temperatures along the *y*-axis (*x*=2) computed by all four methods and analytical solution where equally spaced 629 nodes are used.

It is observed in Figures 5.2, 5.3 and 5.4 that accuracy of the DTM based meshless methods are better than that of the SSPH method and FEM and all studied methods show convergence as the number of nodes is increased.

The global L_2 error norms obtained by the DTM based meshless method, SSPH and FEM methods are given in Table 5.5.

It is clear that the L_2 error norms of the results of the DTM based meshless methods are much lower than those of the SSPH and FEM methods provided that the same number of terms in the associated expansions are employed for the DTM based meshless methods and the SSPH method.

By using the same number of terms, the DTM based meshless method II always gives the lowest global L_2 error norm when comparing with the other methods. The SSPH method always gives the highest L_2 error norms for different number of nodes in the problem domain.

Numerical results also show that lower L_2 error norms can be obtained for all methods as the number of particles distributed in the problem domain is increased.

Table 5.5 : Global L_2 error norm for different number of nodes.

Meshless Method	Number of Nodes		
	50 Nodes	171 Nodes	629 Nodes
DTM - I	3.7853	2.1886	1.2718
DTM - II	3.2134	1.6750	0.9927
DTM - III	3.7313	1.9813	1.0541
SSPH	8.4205	4.3004	2.3956
FEM	5.7661	3.3604	1.9451

The DTM based meshless methods I,II,III, SSPH and FEM methods are compared in terms of CPU times required for the analysis. The measured values are given in Table 5.6. It is clear that CPU times required for the DTM based meshless methods I,II and III and FEM method are much higher than those of the SSPH method.

Table 5.6 : Comparison of CPU time in second.

Meshless Method	Number of Nodes		
	50 Nodes	171 Nodes	629 Nodes
DTM - I	0.11	1.12	15.3
DTM - II	0.18	1.54	20.8
DTM - III	0.12	1.15	15
SSPH	0.02	0.07	1.68
FEM	2	3	4

5.3 Nonhomogeneous Laplace Equation in 2D

The nonhomogeneous Laplace equation in 2D is solved by using the DTM based meshless m and SSPH method in the domain shown in Figure 5.5. The governing differential equation and essential boundary conditions are given by

$$\frac{\partial^2 T}{\partial x^2} + \frac{\partial^2 T}{\partial y^2} = -2SinxCosy$$

$$T_1 = 0\ ℃, T_2 = \overline{T_2}\ ℃, T_3 = \overline{T_3}\ ℃ \quad T_4(x,0) = Sinx \qquad (\mathbf{5.13})$$

where T is the temperature and T_i denote the boundary temperatures.

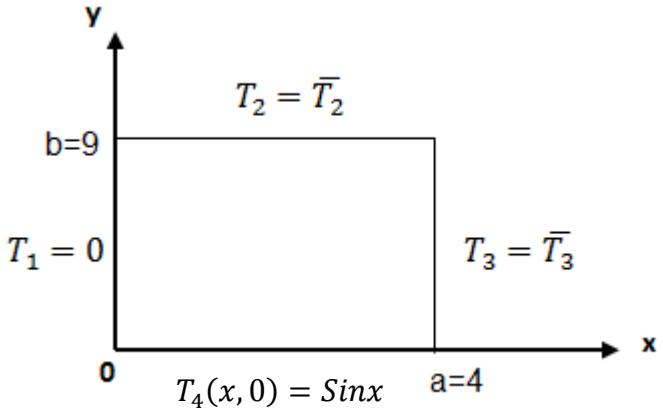

Figure 5.5 : Problem domain and boundary conditions.

The analytical solution of the above boundary value problem is given by

$$T(x,y) = SinxCosy \qquad (\mathbf{5.14})$$

The solution of the problem is obtained by using the same node distributions, the same weight function and the same weight function parameters given in Section 5.2. The convergence and accuracy properties of the DTM based meshless methods and SSPH method are examined by using the global L_2 error norm given by Equation (5.10).

From the governing equation and boundary condition given by Equation (5.13), we can obtain the following equation by using the notation of DTM

$$(k+1)(k+2)T(k+2,m) + (m+1)(m+2)T(k,m+2) = -2SinxCosy \qquad (\mathbf{5.15})$$

that yields

For k=0 and m=0: $T(2,0) + T(0,2) = -SinxCosy$ $\qquad (\mathbf{5.16})$

And for the particles located on boundary 4, we can obtain

$T_4(0,0) = Sinx$

$T_4(1,0) = Cosx$

$T_4(2,0) = -0.5Sinx$

$$T(0,2) = 0.5Sinx - SinxCosy \qquad (\mathbf{5.17})$$

The matrices $\boldsymbol{P}$ and $\boldsymbol{U_i}$ given by Equation **(4.18)** can be written as follows

$$\boldsymbol{P}(x,y) = [1, (x-x_i)^1, (y-y_i)^1, (x-x_i)^2, (y-y_i)^2, (x-x_i)^1(y-y_i)^1]$$
$$\boldsymbol{U}_i = [U_i(0,0), U_i(i,1,0), U_i(0,1), U_i(2,0), U_i(0,2), U_i(1,1)]^T \qquad (\mathbf{5.18})$$

The numerical solutions obtained by using 6 terms in the associated expansions and 50, 171 and 629 nodes are presented in Figures 5.6 to Figure 5.11.

In Figures 5.6 to 5.8, it is observed that the L_2 error norms of the DTM based meshless methods II and III with the variation of the radius of the support domain (where h=Δ) are much lower than those the DTM based meshless method I and the SSPH method provided that the same number of terms are employed in the associated TSEs for both methods.

It is observed in Figures 5.9 to 5.11 that accuracy of the DTM based meshless methods II and III is better than that of the DTM based meshless method I and SSPH

method as the smoothing length parameter varies provided that the same number of terms are employed in the associated TSEs for both methods.

Numerical results imply that the global L_2 error norm of numerical solutions increase as smoothing length parameter increases for all methods. It is observed that the SSPH method is stable for $h=1.8\Delta$ and node distribution of 171 nodes; however, the DTM based meshless methods I, II and III are stable even for $h=2\Delta$ as can be seen in Figure 5.10.

It is also observed that the SSPH method is stable for $h=2\Delta$ and node distribution of 629 nodes; however, the DTM based meshless methods II and III are stable even for $h=2.2\Delta$ as can be seen in Figure 5.11. Except for 629 nodes in the problem domain, the SSPH method always gives the highest global L_2 error norm; on the other hand, for 629 nodes, the DTM based meshless method I gives the highest global L_2 error norm.

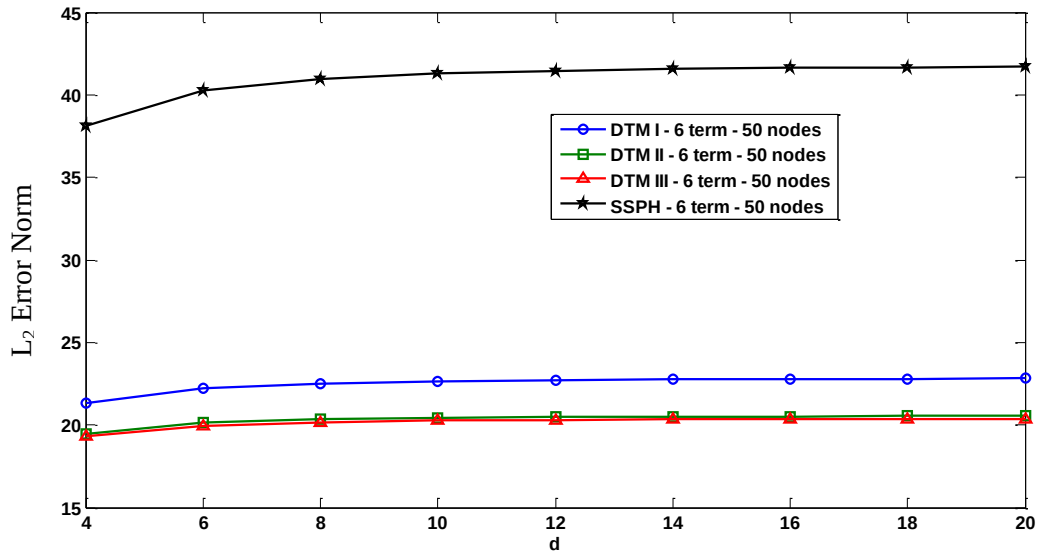

Figure 5. 6 : The global L_2 error norms as the radius of the support domain ($h=\Delta$) varies, where equally spaced 50 nodes are used.

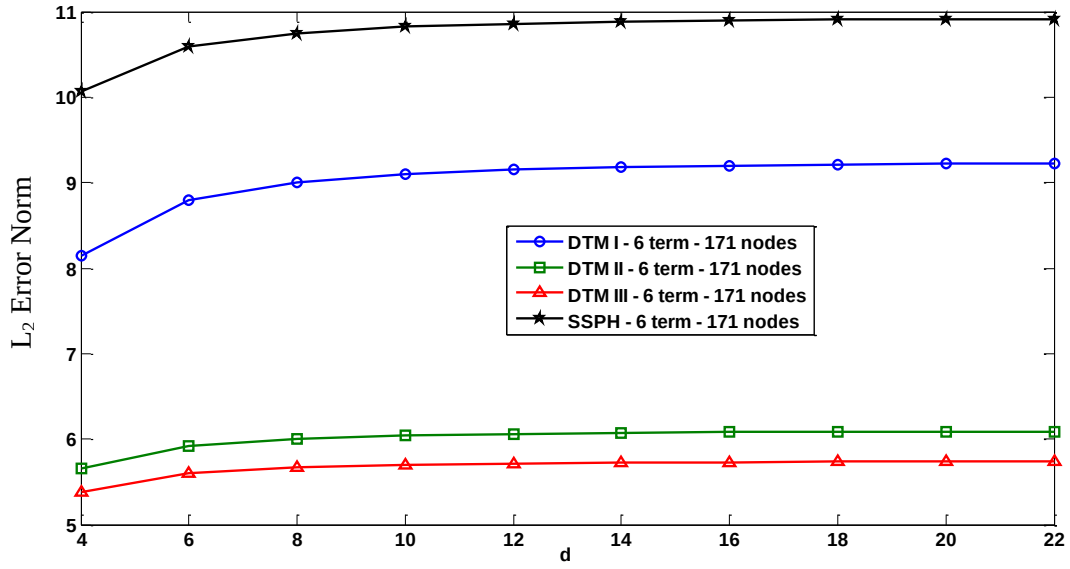

Figure 5. 7 : The global L_2 error norms as the radius of the support domain (h=Δ) varies, where equally spaced 171 nodes are used.

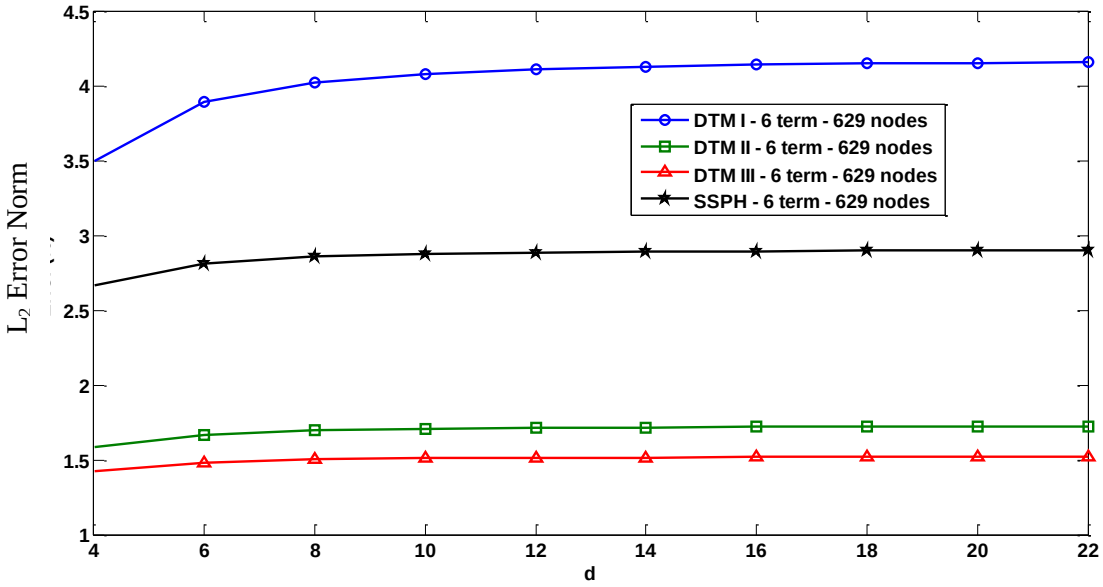

Figure 5. 8 : The global L_2 error norms as the radius of the support domain (h=Δ) varies, where equally spaced 629 nodes are used.

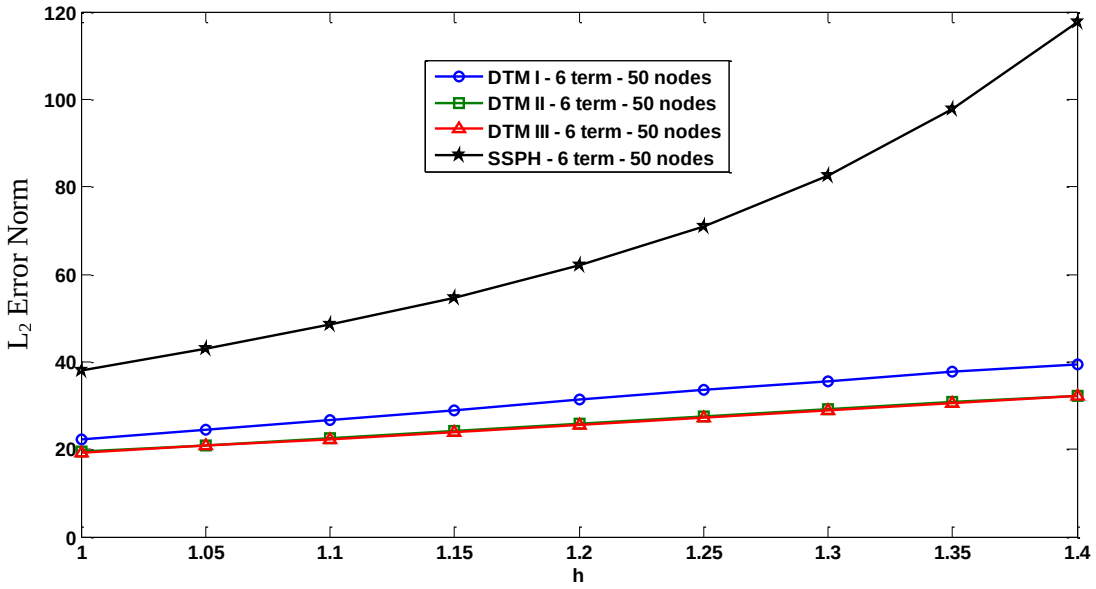

Figure 5. 9 : The global L_2 error norms as the smoothing length varies, where equally spaced 50 nodes are used.

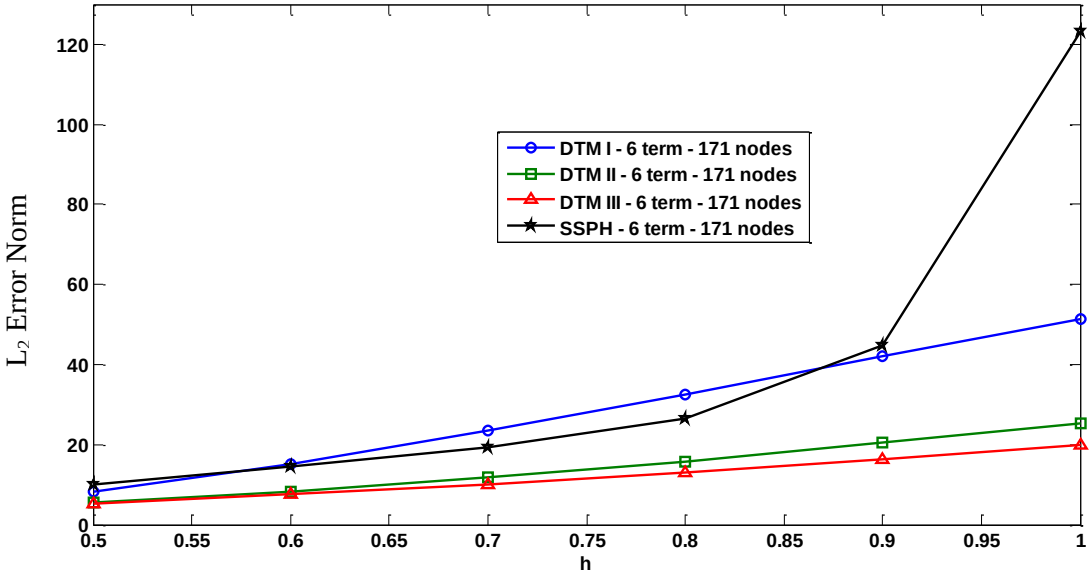

Figure 5. 10 : The global L_2 error norms as the smoothing length varies, where equally spaced 171 nodes are used.

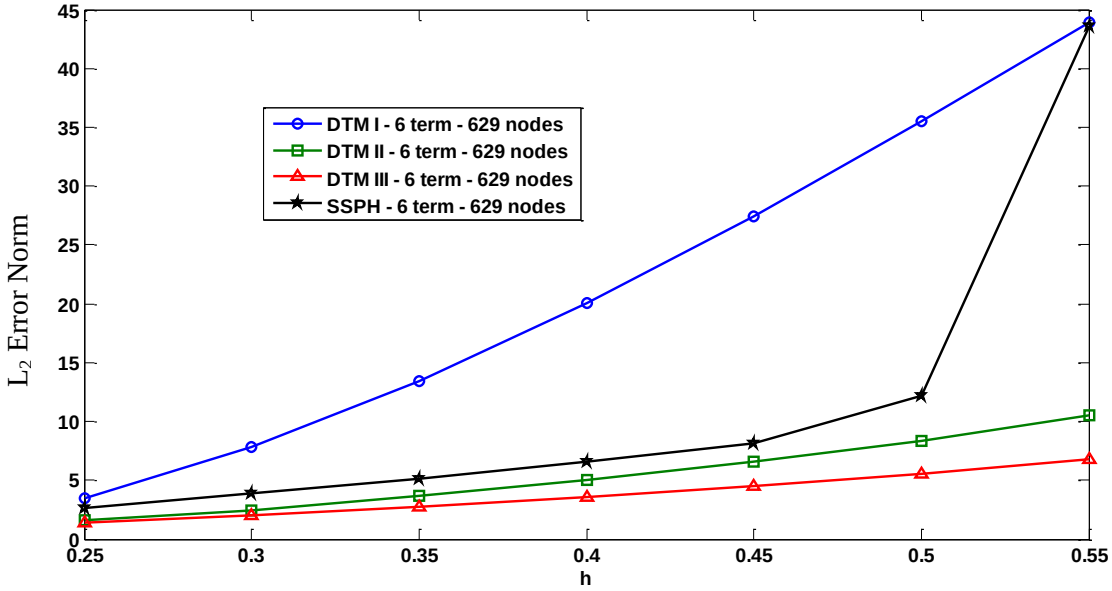

Figure 5. 11 : The global L_2 error norms as the smoothing length varies, where equally spaced 629 nodes are used.

5.4 Plane Stress Deformations of a Plate

The plane stress deformations of a plate in 2D is solved by using the DTM based meshless methods II and III and SSPH method in the domain shown in Figure 5.12.

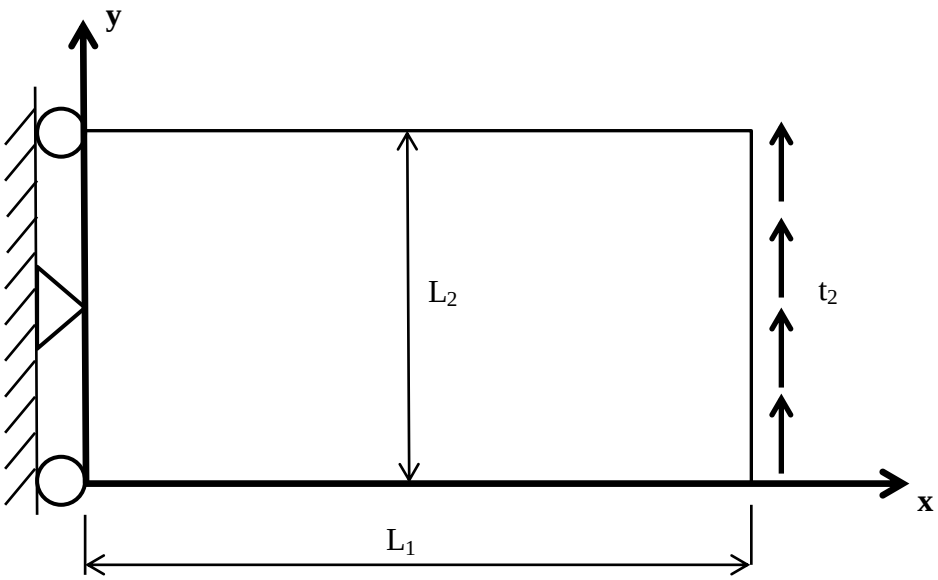

Figure 5.12 : Plane stress deformations of a plate in 2D.

Beforehand, the formulation of 2D elastostatic problems are given below.

In Cartesian coordinates, equations of equilibrium for 2D deformations of a linear elastic body occupying the domain Ω are

$$\sigma_{ij,j} + b_i = 0 \qquad \text{in } \Omega, \quad i = 1,2 \tag{5.19}$$

where a repeated index implies summation over the range of the index, b_i is the body force per unit volume which we take to be zero, $\sigma_{ij,j}$ is the Cauchy stress, and a comma followed by the index j denotes partial differentiation with respect to x_j (x and y). The boundary conditions may be written as

$$u_i = \overline{u_i} \text{ on } \Gamma_u$$

$$t_i \equiv \sigma_{ij} n_j = \overline{t_i} \text{ on } \Gamma_t \tag{5.20}$$

$\overline{u_i}$ is the prescribed displacement on Γ_u, and $\overline{t_i}$ is the prescribed surface traction on Γ_t, $\mathbf{n}=[n_x,n_y]^T$ is the unit outward normal to the boundary Γ_t. These two boundary conditions are the well known essential and natural boundary conditions, respectively.

The constitutive relation for a linear elastic isotropic homogeneous material is

$$\sigma = \mathbf{D}\boldsymbol{\varepsilon} \tag{5.21}$$

where $\boldsymbol{\varepsilon} = [\varepsilon_{xx}, \varepsilon_{yy}, 2\varepsilon_{xy}]^T$ is the strain tensor, $\boldsymbol{\sigma} = [\sigma_{xx}, \sigma_{yy}, \sigma_{xy}]^T$ is the stress tensor, and the matrix **D** is given by

$$\mathbf{D} = \frac{E_0}{1-\upsilon_0^2}\begin{bmatrix} 1 & \upsilon_0 & 0 \\ \upsilon_0 & 1 & 0 \\ 0 & 0 & \dfrac{1-\upsilon_0}{2} \end{bmatrix} \tag{5.22}$$

which is the matrix of elastic constants and

$$E_0 = \frac{E}{1-\upsilon^2}, \quad \upsilon_0 = \frac{\upsilon}{1-\upsilon} \quad \text{for plane strain}$$

$$E_0 = E, \quad \upsilon_0 = \upsilon \text{ for plane stress} \tag{5.23}$$

where E is the Young's modulus and υ is the Poisson's ratio. The strain tensor $\boldsymbol{\varepsilon}$ is defined by

$$\boldsymbol{\varepsilon} = \mathbf{L}\mathbf{u} \tag{5.24}$$

where the differential operator matrix **L** and the displacement vector **u** are given by

$$\mathbf{L} = \begin{bmatrix} \frac{\partial}{\partial x} & 0 \\ 0 & \frac{\partial}{\partial y} \\ \frac{\partial}{\partial y} & \frac{\partial}{\partial x} \end{bmatrix}, \qquad \mathbf{u} = \begin{bmatrix} u \\ v \end{bmatrix} \tag{5.25}$$

Equation (5.19), Equation (5.21) and Equation (5.24) constitute a set of two partial differential equations for the two unknown components of displacements *u* and *v* as given below

$$\left(\frac{\partial^2}{\partial x^2} + \frac{1-\upsilon_0}{2}\frac{\partial^2}{\partial y^2}\right)u + \frac{1+\upsilon_0}{2}\frac{\partial^2}{\partial x \partial y}v = 0,$$

$$\frac{1+\upsilon_0}{2}\frac{\partial^2}{\partial x \partial y}u + \left(\frac{1-\upsilon_0}{2}\frac{\partial^2}{\partial x^2} + \frac{\partial^2}{\partial y^2}\right)v = 0 \tag{5.26}$$

and the natural boundary conditions can be given as follows

$$\frac{E_0}{1-\upsilon_0^2}\begin{bmatrix} n_x\frac{du}{dx} + \frac{1-\upsilon_0}{2}n_y\frac{du}{dy} + \frac{1-\upsilon_0}{2}n_y\frac{dv}{dx} + \upsilon_0 n_x\frac{dv}{dy} \\ \upsilon_0 n_y\frac{du}{dx} + \frac{1-\upsilon_0}{2}n_x\frac{du}{dy} + \frac{1-\upsilon_0}{2}n_x\frac{dv}{dx} + n_y\frac{dv}{dy} \end{bmatrix} = \begin{bmatrix} \bar{t_x} \\ \bar{t_y} \end{bmatrix} \tag{5.27}$$

For the problem to be solved, following parameters and boundary conditions are used

$L_1 = 1\ \mathrm{m}, L_2 = 0.2\ m$

$u = \bar{u},\ \ v = \bar{v}$ on the left surface

$t_x = 0, \quad t_y = 0$ on the bottom and top surfaces

$t_x = \bar{t}_x, \quad t_y = \bar{t}_y$ on the right surface (5.28)

The predescribed displacements on the left edge, and the surface tractions on the right edge are calculated from the following analytical solution that satisfies the equations of equilibrium with zero body force

$$\begin{bmatrix} u \\ v \end{bmatrix} = \begin{bmatrix} -\frac{2F_0}{E_0}\left(\frac{y}{L_2} - 0.5\right)\left[3\frac{x}{L_2}\left(2\frac{L_1}{L_2} - \frac{x}{L_2}\right) + (2+\upsilon_0)\frac{y}{L_2}\left(\frac{y}{L_2} - 1\right)\right] \\ \frac{2F_0}{E_0}\left[\left(\frac{x}{L_2}\right)^2\left(3\frac{L_1}{L_2} - \frac{x}{L_2}\right) + 3\upsilon_0\left(\frac{L_1}{L_2} - \frac{x}{L_2}\right)\left(\frac{y}{L_2} - 0.5\right)^2 + \frac{4+5\upsilon_0}{4}\frac{x}{L_2}\right] \end{bmatrix} \tag{5.29}$$

$$\begin{bmatrix}\sigma_{xx}\\ \sigma_{yy}\\ \sigma_{xy}\end{bmatrix}=\begin{bmatrix}-12\dfrac{F_0}{L_2}\left(\dfrac{L_1}{L_2}-\dfrac{x}{L_2}\right)\left(\dfrac{y}{L_2}-0.5\right)\\ 0\\ -6\dfrac{F_0}{L_2}\dfrac{y}{L_2}\left(\dfrac{y}{L_2}-1\right)\end{bmatrix} \qquad (\mathbf{5.30})$$

Surface tractions are determined from $\bar{t}_x=\sigma_{xx}n_x+\sigma_{xy}n_y, \bar{t}_y=\sigma_{xy}n_x+\sigma_{yy}n_y$.

Material parameters of the plate are assumed as

$E=226.9$ GPa, $\upsilon=0.33$ and $F_0=10^6N$.

When solving this problem, equally spaced 64 (Δ=1/15), 217 (Δ=1/30) and 793 ((Δ=1/90) particles are considered in the domain. The smoothing length *h* is equal to the minimum distance between two adjacent particles. The following Revised Super Gauss Function is used as the kernel function

$$W(d)=\frac{G}{(h\sqrt{\pi})^{\lambda}}\begin{cases}(\rho^2-d^2)\,e^{-d^2} & 0\le d\le\rho\\ 0 & d>\rho\end{cases} \qquad (\mathbf{5.31})$$

where $d=|\boldsymbol{x}-\boldsymbol{\xi}|/h$ is the radius of the support domain, ρ is the dimensionless size of support domain (or scaling factor), λ is equal to the dimensionality of the space, and *G* is the normalization parameter having the values of 1.04823, 1.10081 and 1.18516 for λ = 1, 2 and 3, respectively. The dimensionless size of support domain is choosen as 4 for the analysis.

The convergence and accuracy of the DTM based meshless methods and SSPH method are calculated by using the following global L_2 error norm

$$L_2=\frac{\left[\sum_{j=1}^{m}\left\{(u_{num}^{j}-u_{exact}^{j})^2+(v_{num}^{j}-v_{exact}^{j})^2\right\}\right]^{1/2}}{\left[\sum_{j=1}^{m}\left\{(u_{exact}^{j})^2+(v_{exact}^{j})^2\right\}\right]^{1/2}}\text{ x }100\ \% \qquad (\mathbf{5.32})$$

In Equation (5.32), u_{num}^{j} and v_{num}^{j} are respectively the values of functions u and v at the j^{th} node calculated by the numerical solution, and u_{exact}^{j} and v_{exact}^{j} are respectively the values of functions u and v at the j^{th} node calculated by the analytical solution.

SSPH Formulation:

It is assumed that there are *M* scattered particles in the domain Ω. For the strong form formulation, Equation (5.26) is satisfied at every one of the *M* particles. The partial differential equations given by Equation (5.26) are transformed to algebraic

equations by using the SSPH basis functions. Replacing the function $f(\mathbf{x})$ by $u(\boldsymbol{x})$and $v(\boldsymbol{x})$. It is evaluated second order derivatives of $u(\boldsymbol{x})$and $v(\boldsymbol{x})$ in terms of values of $u(\boldsymbol{x})$and $v(\boldsymbol{x})$ at the M particles in the domain Ω. Substituting expressions for the second order derivatives of the displacement vector in Equation (5.26), we get the following system of algebraic equations

$$\sum_{J=1}^{M}\left[2K_{4J}+(1-\upsilon_0)K_{5J}\right]u_J+\frac{1+\upsilon_0}{2}\sum_{J=1}^{M}K_{6J}v_J=0,$$

$$\frac{1+\upsilon_0}{2}\sum_{J=1}^{M}K_{6J}u_J+\sum_{J=1}^{M}[(1-\upsilon_0)K_{4J}+2K_{5J}]v_J=0 \qquad (\mathbf{5.33})$$

Equations (5.33) can be written in the matrix form as follows

$$\sum_{J=1}^{M}\mathbf{K}_{IJ}\mathbf{u}_J=0$$

$$\mathbf{K}_{IJ}=\begin{bmatrix}2K_{4J}+(1-\upsilon_0)K_{5J} & \frac{1+\upsilon_0}{2}K_{6J}\\ \frac{1+\upsilon_0}{2}K_{6J} & (1-\upsilon_0)K_{4J}+2K_{5J}\end{bmatrix} \qquad (\mathbf{5.34})$$

The matrix $\mathbf{K}_{IJ}$ is symmetric but global matrix is not symmetric. For a particle on the boundary Γ_u where the essential boundary condition Equation (3.2) is prescribed

$$\sum_{J=1}^{M}\mathbf{K}_{IJ}\mathbf{u}_J=\bar{\mathbf{u}}_I$$

$$\mathbf{K}_{IJ}=\begin{bmatrix}\mathbf{K}_{1J} & \mathbf{0}\\ \mathbf{0} & \mathbf{K}_{1J}\end{bmatrix},\qquad \bar{\mathbf{u}}_I=\begin{bmatrix}\bar{u}_I\\ \bar{v}_I\end{bmatrix} \qquad (\mathbf{5.35})$$

Similiarly, for particles with the assigned natural boundary condition on the boundary Γ_t, we have

$$\sum_{J=1}^{M}\mathbf{K}_{IJ}\mathbf{u}_J=\bar{\mathbf{t}}_I$$

$$\mathbf{K}_{IJ}=\frac{E_0}{1-\upsilon_0^2}\begin{bmatrix}n_xK_{2J}+\frac{1-\upsilon_0}{2}n_yK_{3J}+\frac{1-\upsilon_0}{2}n_yK_{2J}+\upsilon_0n_xK_{3J}\\ \upsilon_0n_yK_{3J}+\frac{1-\upsilon_0}{2}n_xK_{2J}+\frac{1-\upsilon_0}{2}n_xK_{2J}+n_yK_{3J}\end{bmatrix},\ \bar{\mathbf{t}}_I=\begin{bmatrix}\bar{t_x}\\ \bar{t_y}\end{bmatrix} \qquad (\mathbf{5.36})$$

Equation (5.34), Equation (5.35) and Equation (5.36) are a set of simultaneous linear algebraic equations that can be solved for displacements of all *M* particles.

DTM Based Meshless Method II Formulation:

By neglecting the third and higher order terms in the DTM expansions, the formulation of the DTM based meshless method II for a 2D elasticity problem can be written as follows

$$\sum_{g=1}^{N_g} W(\boldsymbol{\xi_g}, \boldsymbol{x_i})\, u(\boldsymbol{x_i}) = \sum_{g=1}^{N_g} W(\boldsymbol{\xi_g}, \boldsymbol{x_i})\, \boldsymbol{P}(\boldsymbol{\xi_g}, \boldsymbol{x_i}) \boldsymbol{U}_g \qquad (\mathbf{5.37})$$

$$\sum_{g=1}^{N_g} (W(\boldsymbol{\xi_g}, \boldsymbol{x_i})\, u_x(\boldsymbol{x_i}) + W_x(\boldsymbol{\xi_g}, \boldsymbol{x_i}) u(\boldsymbol{x_i}))$$

$$= \sum_{g=1}^{N_g} (W(\boldsymbol{\xi_g}, \boldsymbol{x_i})\, \boldsymbol{P}_x(\boldsymbol{\xi_g}, \boldsymbol{x_i}) + W_x(\boldsymbol{\xi_g}, \boldsymbol{x_i}) \boldsymbol{P}(\boldsymbol{\xi_g}, \boldsymbol{x_i})) \boldsymbol{U}_g \qquad (\mathbf{5.38})$$

$$\sum_{g=1}^{N_g} (W(\boldsymbol{\xi_g}, \boldsymbol{x_i})\, u_y(\boldsymbol{x_i}) + W_y(\boldsymbol{\xi_g}, \boldsymbol{x_i}) u(\boldsymbol{x_i}))$$

$$= \sum_{g=1}^{N_g} (W(\boldsymbol{\xi_g}, \boldsymbol{x_i})\, \boldsymbol{P}_y(\boldsymbol{\xi_g}, \boldsymbol{x_i}) + W_y(\boldsymbol{\xi_g}, \boldsymbol{x_i}) \boldsymbol{P}(\boldsymbol{\xi_g}, \boldsymbol{x_i})) \boldsymbol{U}_g \qquad (\mathbf{5.39})$$

$$\sum_{g=1}^{N_g} (W(\boldsymbol{\xi_g}, \boldsymbol{x_i})\, u_{xx}(\boldsymbol{x_i}) + 2W_x(\boldsymbol{\xi_g}, \boldsymbol{x_i}) u_x(\boldsymbol{x_i}) + W_{xx}(\boldsymbol{\xi_g}, \boldsymbol{x_i}) u(\boldsymbol{x_i}))$$

$$= \sum_{g=1}^{N_g} (W(\boldsymbol{\xi_g}, \boldsymbol{x_i})\, \boldsymbol{P}_{xx}(\boldsymbol{\xi_g}, \boldsymbol{x_i}) + 2W_x(\boldsymbol{\xi_g}, \boldsymbol{x_i}) \boldsymbol{P}_x(\boldsymbol{\xi_g}, \boldsymbol{x_i}) + W_{xx}(\boldsymbol{\xi_g}, \boldsymbol{x_i}) \boldsymbol{P}(\boldsymbol{\xi_g}, \boldsymbol{x_i})) \boldsymbol{U}_g \qquad (\mathbf{5.40})$$

$$\sum_{g=1}^{N_g} (W(\boldsymbol{\xi_g}, \boldsymbol{x_i})\, u_{yy}(\boldsymbol{x_i}) + 2W_y(\boldsymbol{\xi_g}, \boldsymbol{x_i}) u_y(\boldsymbol{x_i}) + W_{yy}(\boldsymbol{\xi_g}, \boldsymbol{x_i}) u(\boldsymbol{x_i}))$$

$$= \sum_{g=1}^{N_g} (W(\boldsymbol{\xi_g}, \boldsymbol{x_i})\, \boldsymbol{P}_{yy}(\boldsymbol{\xi_g}, \boldsymbol{x_i}) + 2W_y(\boldsymbol{\xi_g}, \boldsymbol{x_i}) \boldsymbol{P}_y(\boldsymbol{\xi_g}, \boldsymbol{x_i}) + W_{yy}(\boldsymbol{\xi_g}, \boldsymbol{x_i}) \boldsymbol{P}(\boldsymbol{\xi_g}, \boldsymbol{x_i})) \boldsymbol{U}_g \qquad (\mathbf{5.41})$$

$$\sum_{g=1}^{N_g}(W(\boldsymbol{\xi_g},\boldsymbol{x_i})\,u_{xy}(\boldsymbol{x_i})+W_y(\boldsymbol{\xi_g},\boldsymbol{x_i})u_x(\boldsymbol{x_i})+W_x(\boldsymbol{\xi_g},\boldsymbol{x_i})u_y(\boldsymbol{x_i})$$

$$+W_{xy}(\boldsymbol{\xi_g},\boldsymbol{x_i})u(\boldsymbol{\xi_g}))$$

$$=\sum_{g=1}^{N_g}(W(\boldsymbol{\xi_g},\boldsymbol{x_i})\,\boldsymbol{P}_{xy}(\boldsymbol{\xi_g},\boldsymbol{x_i})+W_y(\boldsymbol{\xi_g},\boldsymbol{x_i})\boldsymbol{P}_x(\boldsymbol{\xi_g},\boldsymbol{x_i})$$

$$+W_x(\boldsymbol{\xi_g},\boldsymbol{x_i})\boldsymbol{P}_y(\boldsymbol{\xi_g},\boldsymbol{x_i})+W_{xy}(\boldsymbol{\xi_g},\boldsymbol{x_i})\boldsymbol{P}(\boldsymbol{\xi_g},\boldsymbol{x_i}))\boldsymbol{U}_g \qquad (\mathbf{5.42})$$

$$\boldsymbol{P}(x,y)=[1,(x-x_i)^1,(y-y_i)^1,(x-x_i)^2,(y-y_i)^2\,,(x-x_i)^1(y-y_i)^1]$$

$$\boldsymbol{U}_i=\left[U_g(0,0),U_g(1,0),U_g(0,1),U_g(2,0),U_g(0,2),U_g(1,1)\right]^T \qquad (\mathbf{5.43})$$

$$\sum_{g=1}^{N_g}W(\boldsymbol{\xi_g},\boldsymbol{x_i})\,v(\boldsymbol{x_i})=\sum_{g=1}^{N_g}W(\boldsymbol{\xi_g},\boldsymbol{x_i})\,\boldsymbol{P}(\boldsymbol{\xi_g},\boldsymbol{x_i})\boldsymbol{V}_g \qquad (\mathbf{5.44})$$

$$\sum_{g=1}^{N_g}(W(\boldsymbol{\xi_g},\boldsymbol{x_i})\,v_x(\boldsymbol{x_i})+W_x(\boldsymbol{\xi_g},\boldsymbol{x_i})v(\boldsymbol{x_i}))$$

$$=\sum_{g=1}^{N_g}(W(\boldsymbol{\xi_g},\boldsymbol{x_i})\,\boldsymbol{P}_x(\boldsymbol{\xi_g},\boldsymbol{x_i})+W_x(\boldsymbol{\xi_g},\boldsymbol{x_i})\boldsymbol{P}(\boldsymbol{\xi_g},\boldsymbol{x_i}))\boldsymbol{V}_g \qquad (\mathbf{5.45})$$

$$\sum_{g=1}^{N_g}(W(\boldsymbol{\xi_g},\boldsymbol{x_i})\,v_y(\boldsymbol{x_i})+W_y(\boldsymbol{\xi_g},\boldsymbol{x_i})v(\boldsymbol{x_i}))$$

$$=\sum_{g=1}^{N_g}(W(\boldsymbol{\xi_g},\boldsymbol{x_i})\,\boldsymbol{P}_y(\boldsymbol{\xi_g},\boldsymbol{x_i})+W_y(\boldsymbol{\xi_g},\boldsymbol{x_i})\boldsymbol{P}(\boldsymbol{\xi_g},\boldsymbol{x_i}))\boldsymbol{V}_g \qquad (\mathbf{5.46})$$

$$\sum_{g=1}^{N_g}(W(\boldsymbol{\xi_g},\boldsymbol{x_i})\,v_{xx}(\boldsymbol{x_i})+2W_x(\boldsymbol{\xi_g},\boldsymbol{x_i})v_x(\boldsymbol{x_i})+W_{xx}(\boldsymbol{\xi_g},\boldsymbol{x_i})v(\boldsymbol{x_i}))$$

$$=\sum_{g=1}^{N_g}(W(\boldsymbol{\xi_g},\boldsymbol{x_i})\,\boldsymbol{P}_{xx}(\boldsymbol{\xi_g},\boldsymbol{x_i})+2W_x(\boldsymbol{\xi_g},\boldsymbol{x_i})\boldsymbol{P}_x(\boldsymbol{\xi_g},\boldsymbol{x_i})$$

$$+W_{xx}(\boldsymbol{\xi_g},\boldsymbol{x_i})\boldsymbol{P}(\boldsymbol{\xi_g},\boldsymbol{x_i}))\boldsymbol{V}_g \qquad (\mathbf{5.47})$$

$$\sum_{g=1}^{N_g}(W(\boldsymbol{\xi_g},\boldsymbol{x_i})\,v_{yy}(\boldsymbol{x_i})+2W_y(\boldsymbol{\xi_g},\boldsymbol{x_i})v_y(\boldsymbol{x_i})+W_{yy}(\boldsymbol{\xi_g},\boldsymbol{x_i})v(\boldsymbol{x_i}))$$

$$= \sum_{g=1}^{N_g} (W(\boldsymbol{\xi_g}, \boldsymbol{x_i})\, \boldsymbol{P}_{yy}(\boldsymbol{\xi_g}, \boldsymbol{x_i}) + 2W_y(\boldsymbol{\xi_g}, \boldsymbol{x_i}) \boldsymbol{P}_y(\boldsymbol{\xi_g}, \boldsymbol{x_i}) + W_{yy}(\boldsymbol{\xi_g}, \boldsymbol{x_i}) \boldsymbol{P}(\boldsymbol{\xi_g}, \boldsymbol{x_i})) \boldsymbol{V}_g \quad (\mathbf{5.48})$$

$$\sum_{g=1}^{N_g} (W(\boldsymbol{\xi_g}, \boldsymbol{x_i})\, v_{xy}(\boldsymbol{x_i}) + W_y(\boldsymbol{\xi_g}, \boldsymbol{x_i}) v_x(\boldsymbol{x_i}) + W_x(\boldsymbol{\xi_g}, \boldsymbol{x_i}) v_y(\boldsymbol{x_i}) + W_{xy}(\boldsymbol{\xi_g}, \boldsymbol{x_i}) v(\boldsymbol{\xi_g}))$$

$$= \sum_{g=1}^{N_g} (W(\boldsymbol{\xi_g}, \boldsymbol{x_i})\, \boldsymbol{P}_{xy}(\boldsymbol{\xi_g}, \boldsymbol{x_i}) + W_y(\boldsymbol{\xi_g}, \boldsymbol{x_i}) \boldsymbol{P}_x(\boldsymbol{\xi_g}, \boldsymbol{x_i}) + W_x(\boldsymbol{\xi_g}, \boldsymbol{x_i}) \boldsymbol{P}_y(\boldsymbol{\xi_g}, \boldsymbol{x_i}) + W_{xy}(\boldsymbol{\xi_g}, \boldsymbol{x_i}) \boldsymbol{P}(\boldsymbol{\xi_g}, \boldsymbol{x_i})) \boldsymbol{V}_g \quad (\mathbf{5.49})$$

$$\boldsymbol{P}(x, y) = [1, (x - x_i)^1, (y - y_i)^1, (x - x_i)^2, (y - y_i)^2\,, (x - x_i)^1 (y - y_i)^1]$$

$$\boldsymbol{V}_g = \left[V_g(0,0), V_g(1,0), V_g(0,1), V_g(2,0), V_g(0,2), V_g(1,1)\right]^T \quad (\mathbf{5.50})$$

From the governing Equation (5.19), we can obtain the following equation by using the formalism of DTM for all *M* particles

$$(k+1)(k+2)U(k+2,h) + \frac{1-\upsilon_0}{2}(h+1)(h+2)U(k,h+2) + \frac{1+\upsilon_0}{2}(k+1)(h+1)V(k+1,h+1) = 0$$

$$\frac{1+\upsilon_0}{2}(k+1)(h+1)U(k+1,h+1) + \frac{1-\upsilon_0}{2}(k+1)(k+2)V(k+2,h) + (h+1)(h+2)V(k,h+2) = 0 \quad (\mathbf{5.51})$$

which yield for k=0 and h=0 respectively

$$U(2,0) + \frac{1-\upsilon_0}{2}U(0,2) + \frac{1+\upsilon_0}{2}V(1,1) = 0$$

$$\frac{1+\upsilon_0}{2}U(1,1) + \frac{1-\upsilon_0}{2}V(2,0) + V(0,2) = 0 \quad (\mathbf{5.52})$$

From the natural boundary conditions given by Equation (5.20), we can obtain the following equation by using the formalism of DTM.

For nodes located on the bottom and top surfaces, we have

$$\begin{bmatrix} \frac{1-v_0}{2} n_y(h+1)U(k,h+1) + \frac{1-v_0}{2} n_y(k+1)V(k+1,h) \\ v_0 n_y(k+1)U(k+1,h) + n_y(h+1)V(k,h+1) \end{bmatrix} = \begin{bmatrix} 0 \\ 0 \end{bmatrix} \quad (\mathbf{5.53})$$

which yields for k=0 and h=0 and k=1 and h=0

$$\begin{bmatrix} U(0,1) + V(1,0) \\ v_0 U(1,0) + V(0,1) \end{bmatrix} = \begin{bmatrix} 0 \\ 0 \end{bmatrix}$$

$$\begin{bmatrix} U(1,1) + V(2,0) \\ 2v_0 U(2,0) + V(1,1) \end{bmatrix} = \begin{bmatrix} 0 \\ 0 \end{bmatrix} \quad (\mathbf{5.54})$$

For the nodes located on the right surface, we have

$$\frac{E_0}{1-v_0^2} \begin{bmatrix} n_x(k+1)U(k+1,h) + v_0 n_x(h+1)V(k,h+1) \\ \frac{1-v_0}{2} n_x(h+1)U(k,h+1) + \frac{1-v_0}{2} n_x(k+1)V(k+1,h) \end{bmatrix}$$

$$= \begin{bmatrix} \bar{t_x} \\ \bar{t_y} \end{bmatrix} \quad (\mathbf{5.55})$$

which yields for k=0 and h=0

$$\frac{E_0}{1-v_0^2} \begin{bmatrix} U(1,0) + v_0 V(0,1) \\ \frac{1-v_0}{2} U(0,1) + V(1,0) \end{bmatrix} = \begin{bmatrix} \bar{t_x} \\ \bar{t_y} \end{bmatrix} \quad (\mathbf{5.56})$$

For the nodes located on the left surface, we have

$$\begin{bmatrix} U(0,0 \\ V(0,0) \end{bmatrix} = \begin{bmatrix} \bar{u} \\ \bar{v} \end{bmatrix} \quad (\mathbf{5.77})$$

Following, above nodal equations are assembled to obtain the global equations; then, boundary conditions are imposed by using the direct method and the resulting equation system is solved for all *M* particles.

DTM Based Meshless Method III Formulation:

By neglecting the third and higher order terms in the DTM expansions, the formulation of the DTM based meshless method III for a 2D elasticity problem can be written as follows

$$\sum_{g=1}^{N_g} W(\boldsymbol{\xi_g}, \boldsymbol{x_i}) u(\boldsymbol{x_i}) = \sum_{g=1}^{N_g} W(\boldsymbol{\xi_g}, \boldsymbol{x_i}) \, \boldsymbol{P}(\boldsymbol{\xi_g}, \boldsymbol{x_i}) \boldsymbol{U}_g$$

$$\sum_{g=1}^{N_g} W_x(\boldsymbol{\xi_g}, \boldsymbol{x_i}) u(\boldsymbol{x_i}) = \sum_{g=1}^{N_g} W_x(\boldsymbol{\xi_g}, \boldsymbol{x_i})\, \boldsymbol{P}(\boldsymbol{\xi_g}, \boldsymbol{x_i}) \boldsymbol{U}_g$$

$$\sum_{g=1}^{N_g} W_y(\boldsymbol{\xi_g}, \boldsymbol{x_i}) u(\boldsymbol{x_i}) = \sum_{g=1}^{N_g} W_y(\boldsymbol{\xi_g}, \boldsymbol{x_i})\, \boldsymbol{P}(\boldsymbol{\xi_g}, \boldsymbol{x_i}) \boldsymbol{U}_g$$

$$\sum_{g=1}^{N_g} W_{xx}(\boldsymbol{\xi_g}, \boldsymbol{x_i}) u(\boldsymbol{x_i}) = \sum_{g=1}^{N_g} W_{xx}(\boldsymbol{\xi_g}, \boldsymbol{x_i})\, \boldsymbol{P}(\boldsymbol{\xi_g}, \boldsymbol{x_i}) \boldsymbol{U}_g$$

$$\sum_{g=1}^{N_g} W_{yy}(\boldsymbol{\xi_g}, \boldsymbol{x_i}) u(\boldsymbol{x_i}) = \sum_{g=1}^{N_g} W_{yy}(\boldsymbol{\xi_g}, \boldsymbol{x_i})\, \boldsymbol{P}(\boldsymbol{\xi_g}, \boldsymbol{x_i}) \boldsymbol{U}_g$$

$$\sum_{g=1}^{N_g} W_{xy}(\boldsymbol{\xi_g}, \boldsymbol{x_i}) u(\boldsymbol{x_i}) = \sum_{g=1}^{N_g} W_{xy}(\boldsymbol{\xi_g}, \boldsymbol{x_i})\, \boldsymbol{P}(\boldsymbol{\xi_g}, \boldsymbol{x_i}) \boldsymbol{U}_g \qquad (\mathbf{5.58})$$

where

$$\boldsymbol{P}(x, y) = [1, (x - x_i)^1, (y - y_i)^1, (x - x_i)^2, (y - y_i)^2\,, (x - x_i)^1 (y - y_i)^1]$$

$$\boldsymbol{U}_i = \left[U_g(0,0), U_g(1,0), U_g(0,1), U_g(2,0), U_g(0,2), U_g(1,1)\right]^T \qquad (\mathbf{5.59})$$

$$\sum_{g=1}^{N_g} W(\boldsymbol{\xi_g}, \boldsymbol{x_i}) v(\boldsymbol{x_i}) = \sum_{g=1}^{N_g} W(\boldsymbol{\xi_g}, \boldsymbol{x_i})\, \boldsymbol{P}(\boldsymbol{\xi_g}, \boldsymbol{x_i}) \boldsymbol{V}_g$$

$$\sum_{g=1}^{N_g} W_x(\boldsymbol{\xi_g}, \boldsymbol{x_i}) v(\boldsymbol{x_i}) = \sum_{g=1}^{N_g} W_x(\boldsymbol{\xi_g}, \boldsymbol{x_i})\, \boldsymbol{P}(\boldsymbol{\xi_g}, \boldsymbol{x_i}) \boldsymbol{V}_g$$

$$\sum_{g=1}^{N_g} W_y(\boldsymbol{\xi_g}, \boldsymbol{x_i}) v(\boldsymbol{x_i}) = \sum_{g=1}^{N_g} W_y(\boldsymbol{\xi_g}, \boldsymbol{x_i})\, \boldsymbol{P}(\boldsymbol{\xi_g}, \boldsymbol{x_i}) \boldsymbol{V}_g$$

$$\sum_{g=1}^{N_g} W_{xx}(\boldsymbol{\xi_g}, \boldsymbol{x_i}) v(\boldsymbol{x_i}) = \sum_{g=1}^{N_g} W_{xx}(\boldsymbol{\xi_g}, \boldsymbol{x_i})\, \boldsymbol{P}(\boldsymbol{\xi_g}, \boldsymbol{x_i}) \boldsymbol{V}_g$$

$$\sum_{g=1}^{N_g} W_{yy}(\boldsymbol{\xi_g}, \boldsymbol{x_i}) v(\boldsymbol{x_i}) = \sum_{g=1}^{N_g} W_{yy}(\boldsymbol{\xi_g}, \boldsymbol{x_i})\, \boldsymbol{P}(\boldsymbol{\xi_g}, \boldsymbol{x_i}) \boldsymbol{V}_g$$

$$\sum_{g=1}^{N_g} W_{xy}(\boldsymbol{\xi_g}, \boldsymbol{x_i}) v(\boldsymbol{x_i}) = \sum_{g=1}^{N_g} W_{xy}(\boldsymbol{\xi_g}, \boldsymbol{x_i})\, \boldsymbol{P}(\boldsymbol{\xi_g}, \boldsymbol{x_i}) \boldsymbol{V}_g \qquad (\mathbf{5.60})$$

where

$$\boldsymbol{P}(x, y) = [1, (x - x_i)^1, (y - y_i)^1, (x - x_i)^2, (y - y_i)^2, (x - x_i)^1 (y - y_i)^1]$$

$$\boldsymbol{V}_g = \left[V_g(0,0), V_g(1,0), V_g(0,1), V_g(2,0), V_g(0,2), V_g(1,1)\right]^T \qquad (\mathbf{5.61})$$

The same equations obtained and given in the presentation of 2D formulations of DTM based meshless method II, essential boundary conditions and natural boundary conditions are also used for 2D formulations of DTM based meshless method III.

In Figures 5.13 to 5.15, variation of the displacement v on the bottom surface of the plate is shown for uniform particle placements of 16x4, 31x7 and 61x13.

It is observed in Figures 5.13 to 5.15 that accuracy of the DTM based meshless method II and III are better than that of the SSPH method and all methods show convergence as the number of nodes is increased.

The DTM based meshless method I is used to solve this problem but it did not yield satisfactory results; thus, only for 64 nodes the solution of the DTM based meshless method I is presented in Figure 5.13.

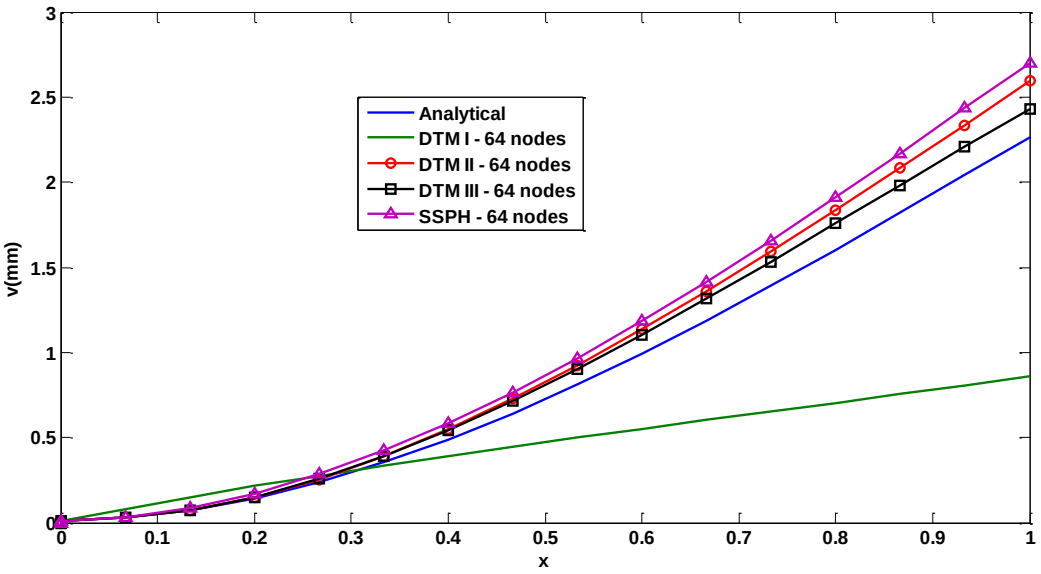

Figure 5. 13 : Comparison of the displacement *v* along the top surface for 64 nodes.

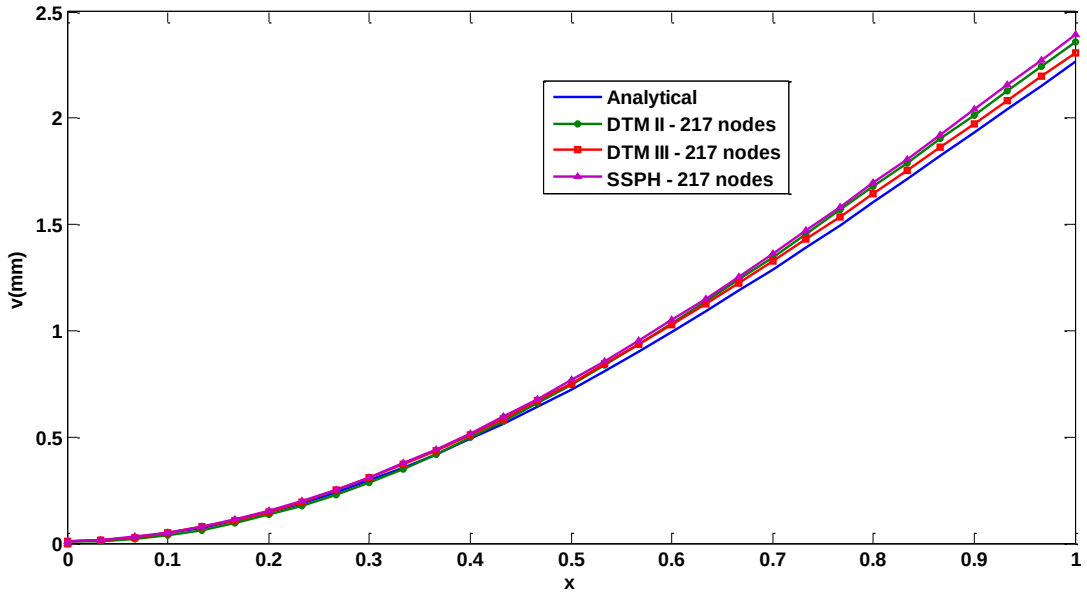

Figure 5. 14 : Comparison of the displacement *v* along the top surface for 217 nodes

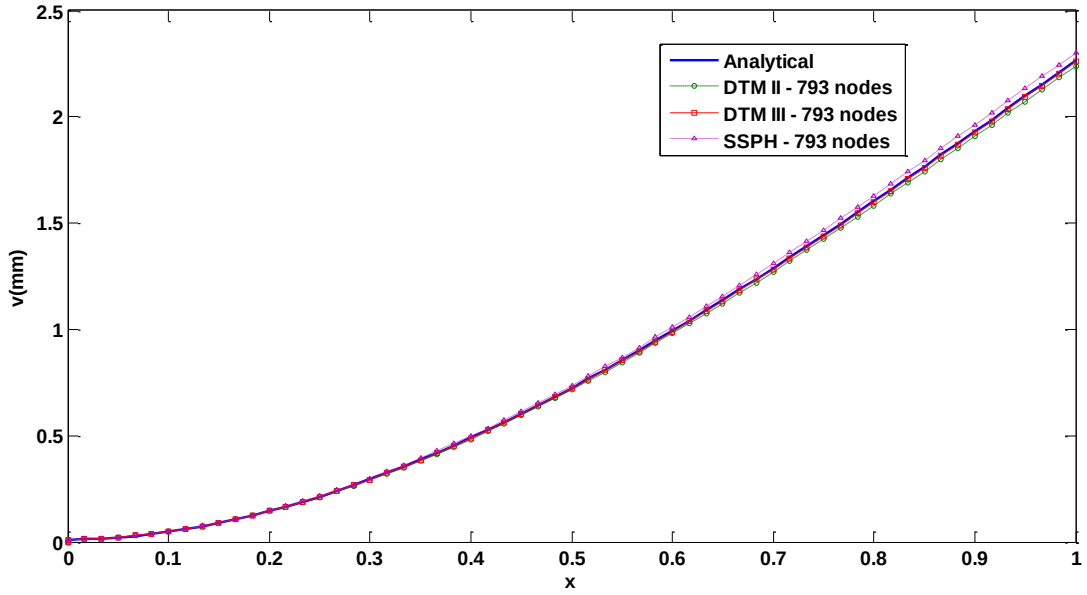

Figure 5. 15 : Comparison of the displacement *v* along the top surface for 793 nodes

In Table 5.7, L_2 error norms for different number of particles are given. It is clear that the DTM based meshless method III always give the lowest value comparing to the DTM based meshless method II and SSPH method.

For 61x13 uniform particle distribution, the displacement computed by using the DTM based meshless method is virtually indistinguishable from the analytical solution. However, the DTM based meshless method II gives slightly better results than the results obtained by the SSPH method.

Table 5.7 : Effect of number of particles on global L_2 error norm.

Node Distribution	DTM Based Meshless Method II	DTM Based Meshless Method III	SSPH
16x4	12.07	9.16	20.91
31x7	4.40	2.59	13.17
61x13	1.30	0.31	1.64

In Figure 5.16 to 5.18, the dimensionless stress $\sigma_{xx}(L_2/F_0)$ along the top surface of the plate for the analytical, DTM based meshless methods II and III and SSPH method is presented by using 16x4, 31x7 and 61x13 node distribution.

These are also evidence of the DTM based meshless methods II and III always give less deviation than the SSPH method.

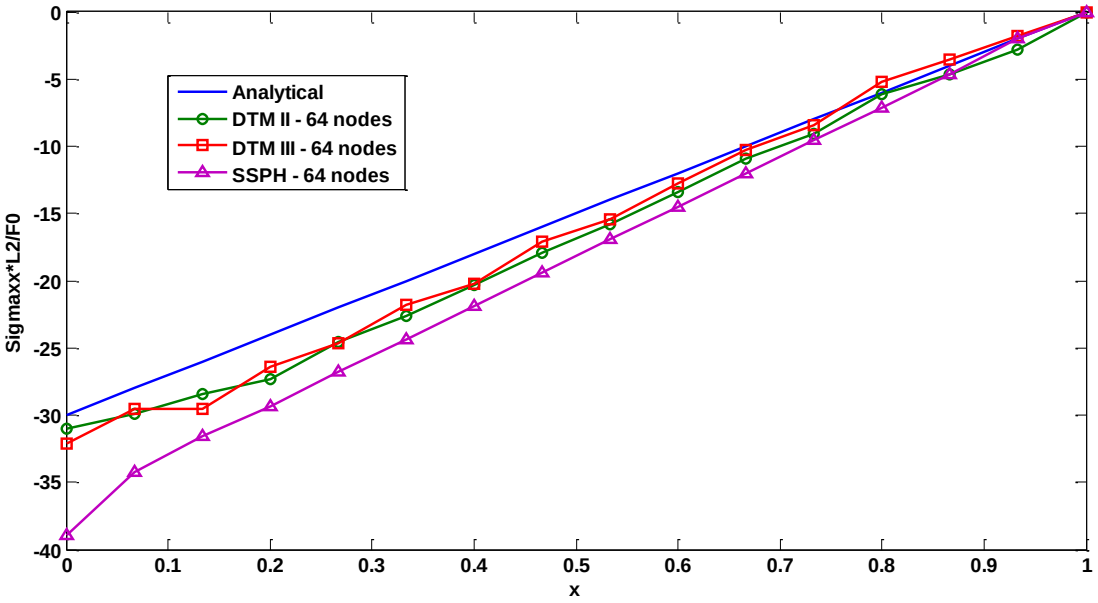

Figure 5. 16 : Comparison of the dimensionless stress $\sigma_{xx}(L_2/F_0)$ along the top surface of the plate for 64 nodes.

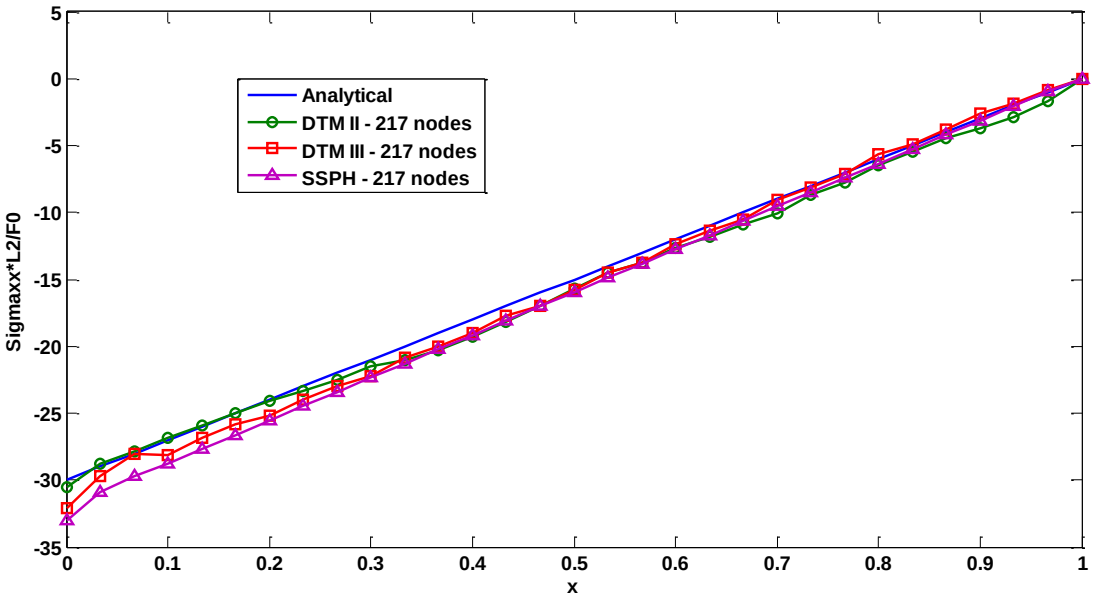

Figure 5. 17 : Comparison of the dimensionless stress $\sigma_{xx}(L_2/F_0)$ along the top surface of the plate for 217 nodes.

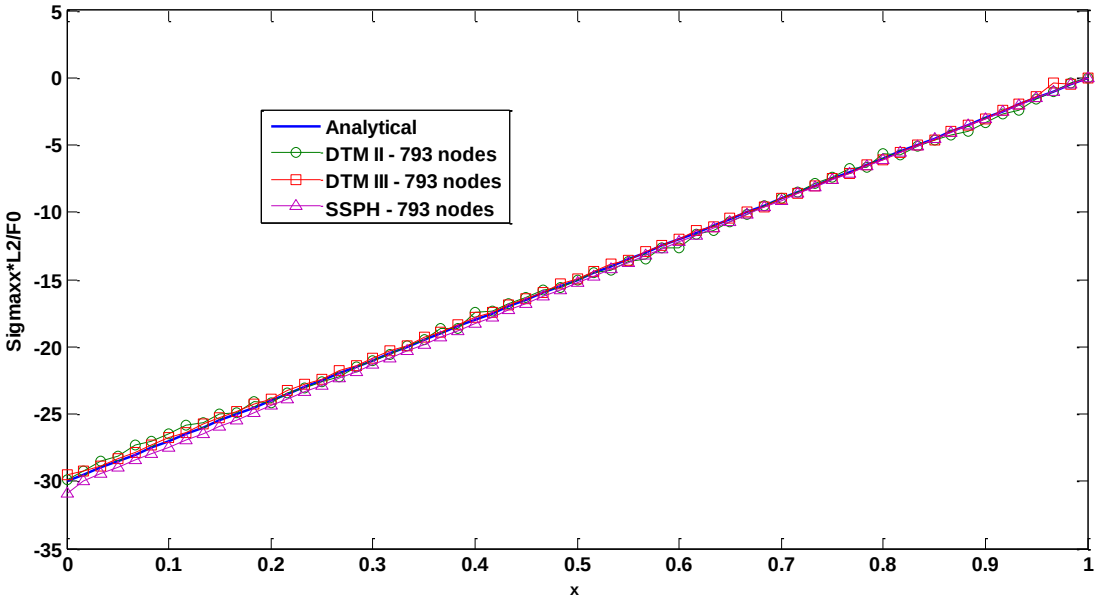

Figure 5. 18 : Comparison of the dimensionless stress $\sigma_{xx}(L_2/F_0)$ along the top surface of the plate for 793 nodes.

In Figure 5.16, It is observed that the DTM based meshless merhods II and III show better convergence than the SSPH method till the node distribution of 217 nodes. With the increasing number of nodes from that point, the convergence rate of the SSPH method is better than the other two methods.

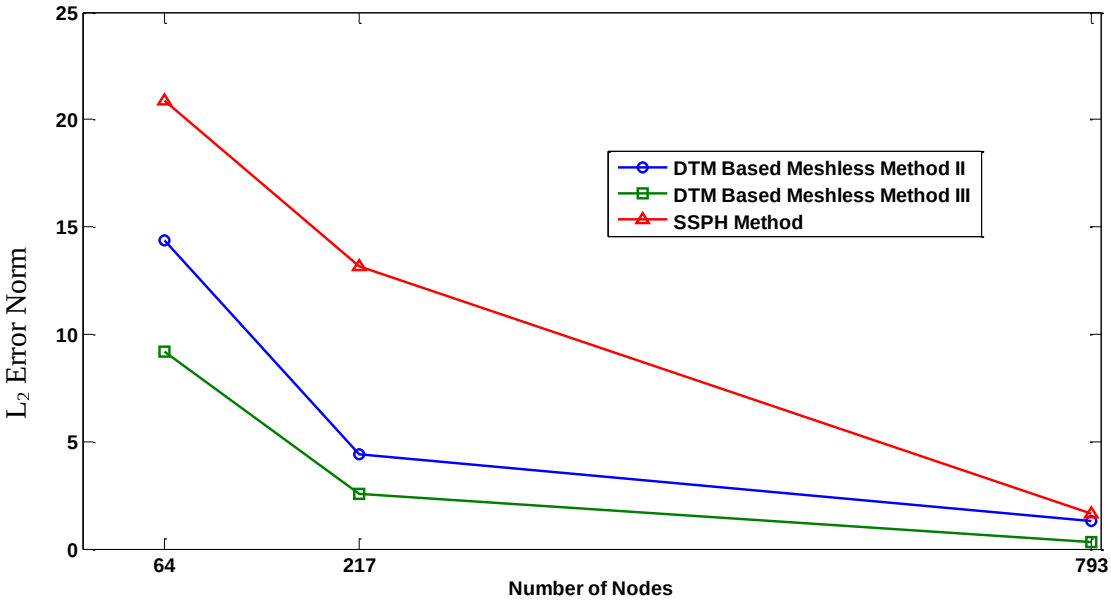

Figure 5. 19 : Comparison of the convergence rates of the studied methods.

CPU times required for the DTM based meshless methods II and III and SSPH method are given in Table 5.8 that are measured on a laptop having an Intel Core i7 CPU of 2.0 GHz by using the programs run on Matlab.

It is clear that CPU times required for the DTM based meshless methods II and III are much higher than those of the SSPH method provided that the same number of terms are employed in the associated TSEs for both methods. However, the codes developed for all methods can be optimized to decrease the CPU time required for the computations. Optimization of the codes to reduce the CPU times for the computations was not the focus of this thesis that will be pursued in future studies.

Table 5.8 : Comparison of the CPU time in seconds.

Node Distribution	DTM Based Meshless Method II	DTM Based Meshless Method III	SSPH
16x4	0.31	0.23	0.04
31x7	2.91	2.38	0.11
61x13	50.33	42.16	3.99

6. COMPARISON OF THE DTM BASED MESHLESS METHOD I AND THE SSPH METHOD BY USING COMPACTLY SUPPORTED RADIAL BASIS FUNCTIONS

By using compactly supported radial basis functions (CSRBFs), performance of the DTM based meshless method I is compared with the SSPH method. The basis functions are used to solve the numerical examples given in Section 5.2 and 5.3. Comparisons are made with the analytical solutions and results of the SSPH method. Total nine CSRBFs are examined to evaluate the accuracy of the DTM based meshless method I and SSPH method by considering various particle distributions and nonhomogeneous terms. It is observed that the use of CSRBFs yield better accuracy for both methods than revised super Gauss function, and both methods have the conventional convergence properties. The DTM based meshless method I yields smaller L_2 error norms than the SSPH method, especially in the existence of nonsmooth nonhomogeneous terms.

6.1 Compactly Supported Radial Basis Functions (CSRBF)

The nine CSRBFs listed in Table 6.1 are used as the kernel functions for the solutions of two problems given in Sections 5.2 and 5.3, where $r = |\boldsymbol{x} - \boldsymbol{\xi}|/h$ is the radius of the support domain, d is the shape parameter which is set to 2 for the DTM based meshless method I and 2.1 for the SSPH method (these values are selected since they yield the lowest L_2 error norms for each method), h is the smoothing length which is chosen to be equal to the minimum distance Δ between two adjacent particles. It is noteworthy that the first five CSRBFs in Table 1 are presented in Section and the last four CSRBFs in Table 1 are developed in this thesis. The revised Gauss compactly supported radial basis functions examined in this thesis are developed by performing some numerical analysis on a trial-and-error basis and as a result of comparative studies with the CSRBFs already presented in the literature.

Table 6.1 : Compactly supported radial basis functions.

No	Name	Expression
1	Wu-C2 [25]	$W(x,y)=\left(1-\frac{r}{d}\right)^5\left(8+40\frac{r}{d}+48\frac{r^2}{d^2}+25\frac{r^3}{d^3}+5\frac{r^4}{d^4}\right)$
2	Wu-C4 [25]	$W(x,y)=\left(1-\frac{r}{d}\right)^6\left(6+36\frac{r}{d}+82\frac{r^2}{d^2}+72\frac{r^3}{d^3}+30\frac{r^4}{d^4}+5\frac{r^5}{d^5}\right)$
3	Wendland-C2 [25]	$W(x,y)=\left(1-\frac{r}{d}\right)^4\left(1+4\frac{r}{d}\right)$
4	Wendland-C4 [25]	$W(x,y)=\left(1-\frac{r}{d}\right)^6\left(3+18\frac{r}{d}+35\frac{r^2}{d^2}\right)$
5	Wendland-C6 [25]	$W(x,y)=\left(1-\frac{r}{d}\right)^8\left(1+8\frac{r}{d}+25\frac{r^2}{d^2}+32\frac{r^3}{d^3}\right)$
6	Revised Gauss-I	$W(x,y)=\left(1-\frac{r^2}{d^2}\right)^4 e^{-\frac{r^2}{d^2}}$
7	Revised Gauss-II	$W(x,y)=\left(1-\frac{r^2}{d^2}\right)^6 e^{-\frac{r^2}{d^2}}$
8	Revised Gauss-III	$W(x,y)=\left(1-\frac{r^2}{d^2}\right)^8 e^{-\frac{r^2}{d^2}}$
9	Revised Gauss-IV	$W(x,y)=\left(1-\frac{r^2}{d^2}\right)^{10} e^{-\frac{r^2}{d^2}}$

6.2 Homogeneous Laplace Equation in 2D

By using the CSRBFs in Table 6.1, homogeneous Laplace equation in 2D is solved by using the DTM based meshless method I and SSPH method. When solving this problem, equally spaced 50, 171 and 629 particles are considered in the domain. The smoothing length h is equal to the minimum distance between two adjacent particles (i.e., $\mathbf{h} = \Delta$). Convergence and accuracy of the DTM based meshless method I and SSPH method are calculated by using the global L_2 error norm given in Equation (5.10).

Global L_2 error norms calculated by Equation **(5.10)** are given in Table 6.2 for the nine CSRBFs listed in Table 6.1 and revised super Gauss function of Equation **(5.9)** for DTM based meshless method I, II and III. It is clear that the L_2 error norms of the solutions of the DTM based meshless method I, II and III are lower than those of the SSPH method.

It is observed that the Wendland–C6 and Revised Gauss–III compactly supported radial basis functions yield relatively lower L_2 error norms for the DTM based meshless method I, II and III and SSPH method than the other kernel functions in Table 6.2. In addition, the DTM based meshless method I shows conventional convergence as the number of nodes is increased with all CSRBFs.

Table 6.2 : The global L_2 error norm for the DTM I and SSPH method.

CSRBF type		**DTM I**			**SSPH**		
		50 nodes	*171 nodes*	*629 nodes*	*50 nodes*	*171 nodes*	*629 nodes*
Wu-C2		1.5059	0.7936	0.4142	4.0096	2.1319	0.9894
Wu-C4		1.2487	0.6644	0.3440	3.1193	1.6470	0.7682
Wendland-C2		1.8227	0.9582	0.5036	4.8047	2.5661	1.1939
Wendland-C4		1.1709	0.6271	0.3239	2.6032	1.3696	0.6527
Wendland-C6		1.0537	0.5795	0.2997	1.4585	0.7659	0.3798
Revised Gauss-I		1.8522	0.9737	0.5120	5.3041	2.8393	1.2962
Revised Gauss-II		1.1921	0.6371	0.3293	2.8632	1.5096	0.7046
Revised Gauss-III		1.0548	0.5789	0.2992	1.5883	0.8324	0.4061
Revised Gauss-IV		1.0726	0.5948	0.3092	1.1051	0.6038	0.3102
RSGF	**DTM I**	3.7853	2.1886	1.2718	8.4205	4.3004	2.3956
	DTM II	3.2134	1.6750	0.9927			
	DTM III	3.7313	1.9813	1.0541			

Numerical solutions obtained by using 6 terms in the associated TSEs and node distributions of 50, 171 and 629 nodes are presented in Figures 6.1 to 6.6 for the Wendland-C6 and Revised Gauss-III compactly supported radial basis functions that yield more accurate results than the other CSRBFs.

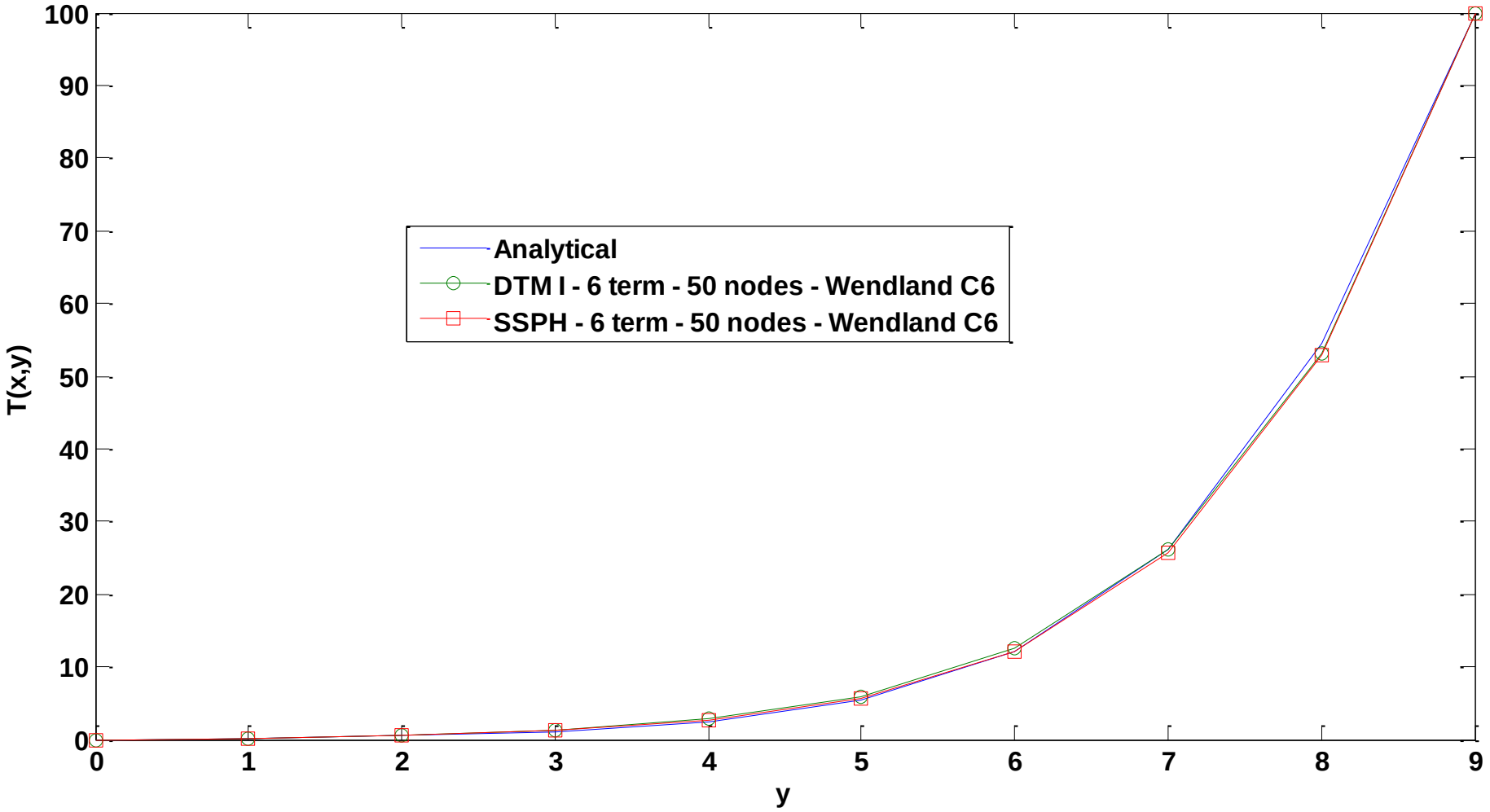

Figure 6.1 : Temperatures along the *y*-axis (*x*=2) computed by the DTM I, SSPH method and analytical solution - 50 Nodes (Wendland C6).

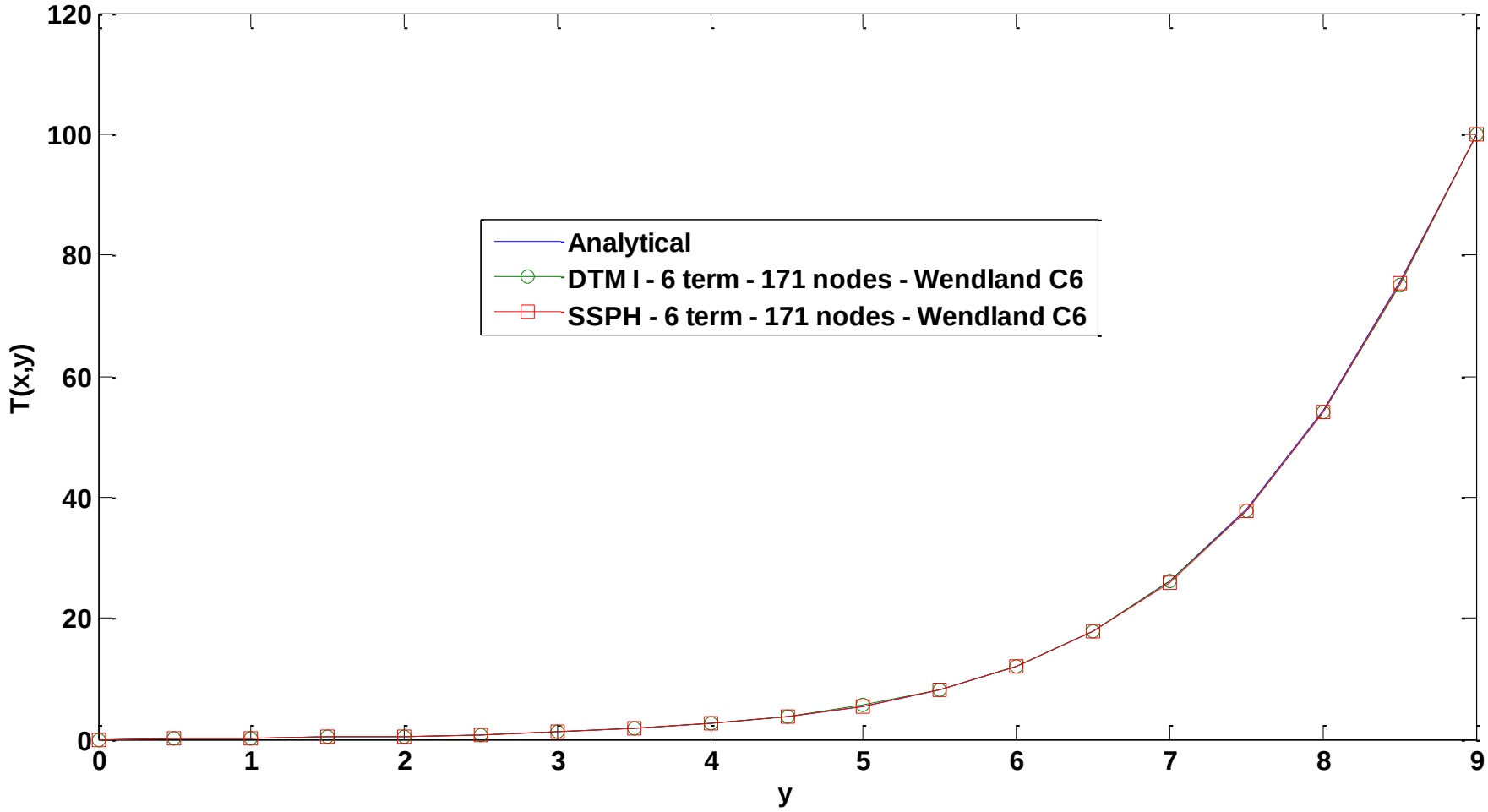

Figure 6.2 : Temperatures along the *y*-axis (*x*=2) computed by the DTM I, SSPH method and analytical solution - 171 nodes (Wendland C6).

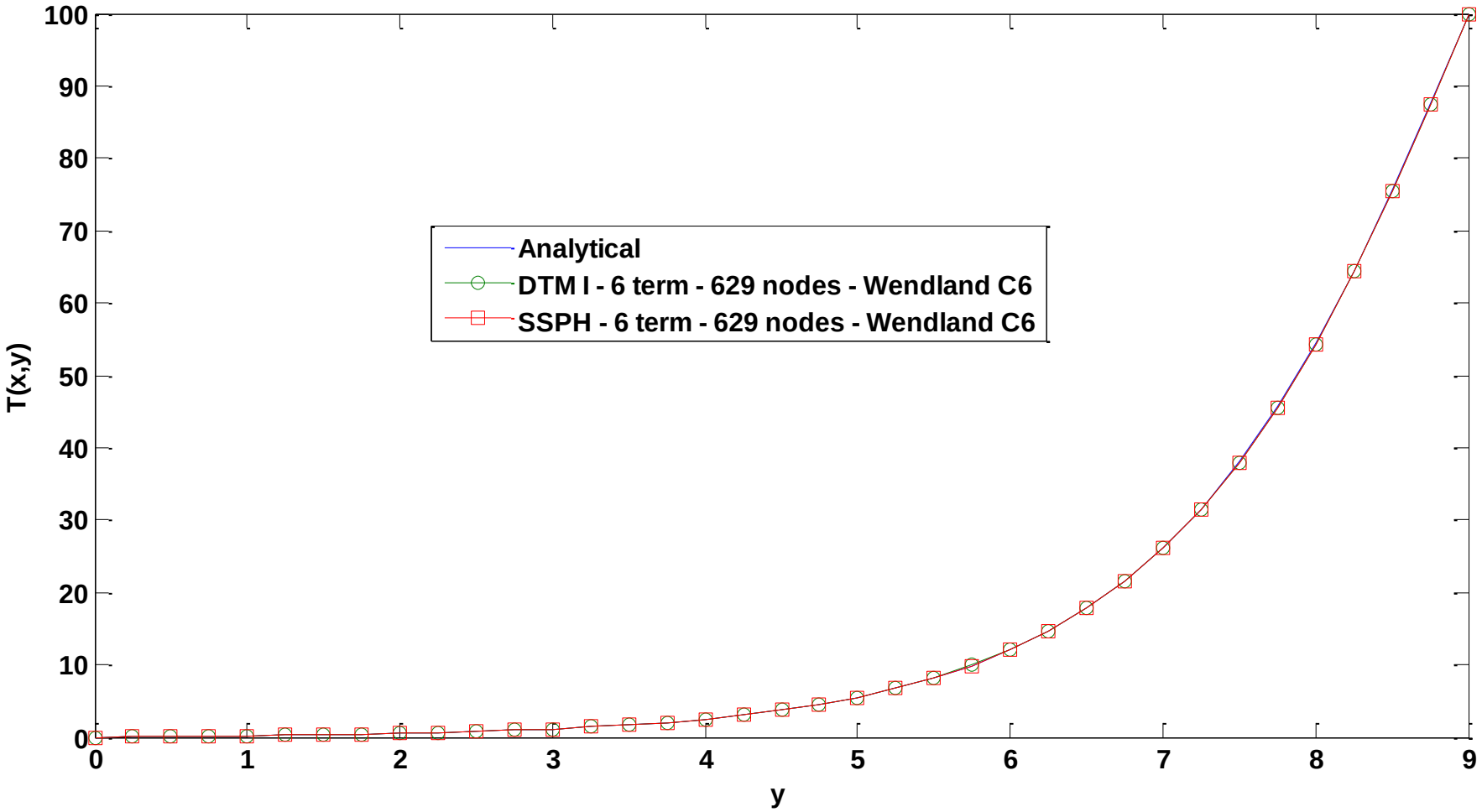

Figure 6.3 : Temperatures along the *y*-axis (*x*=2) computed by the DTM I, SSPH method and analytical solution - 629 nodes (Wendland C6).

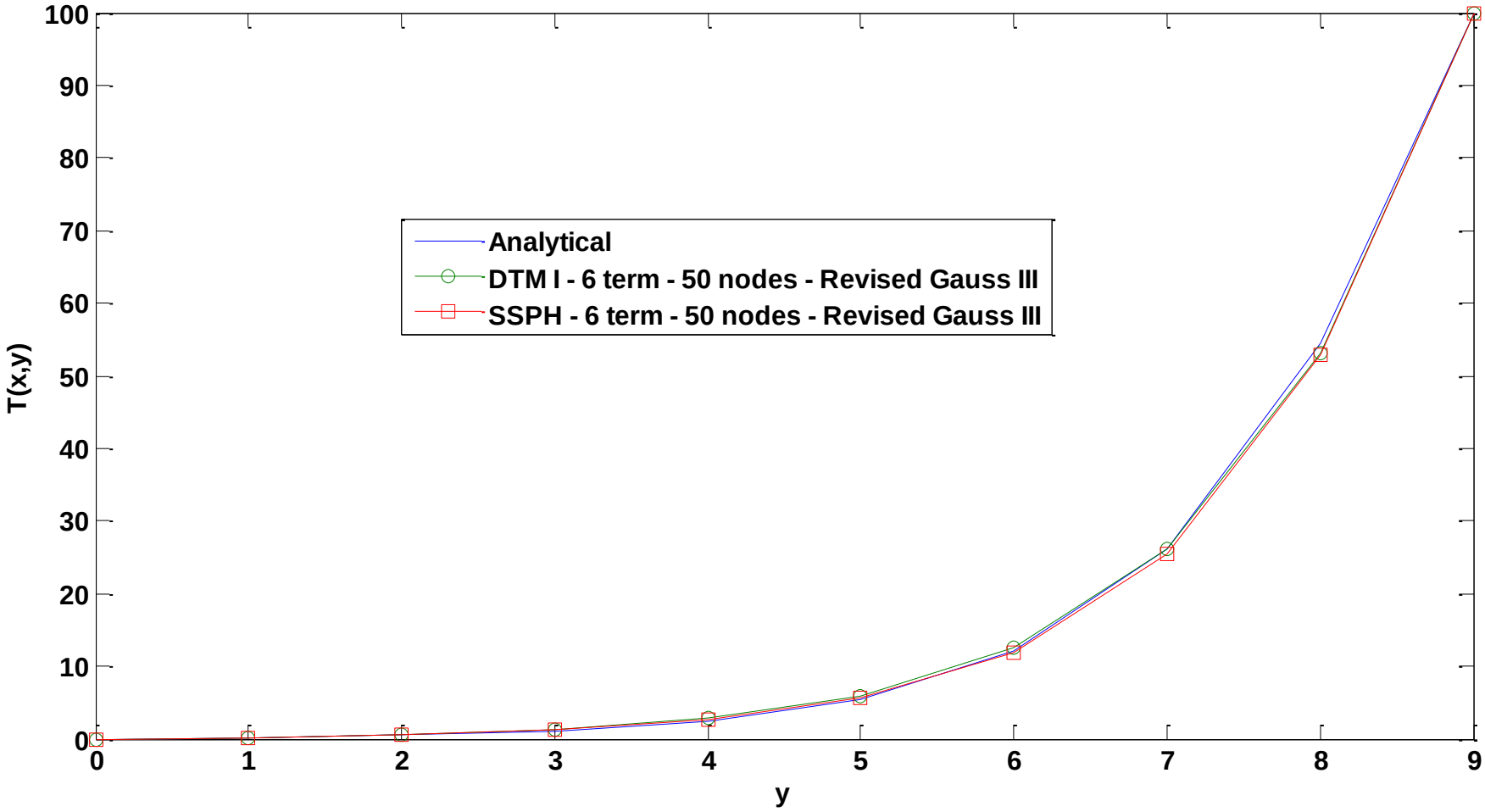

Figure 6.4 : Temperatures along the *y*-axis (*x*=2) computed by the DTM I, SSPH method and analytical solution - 50 Nodes (Revised Gauss III).

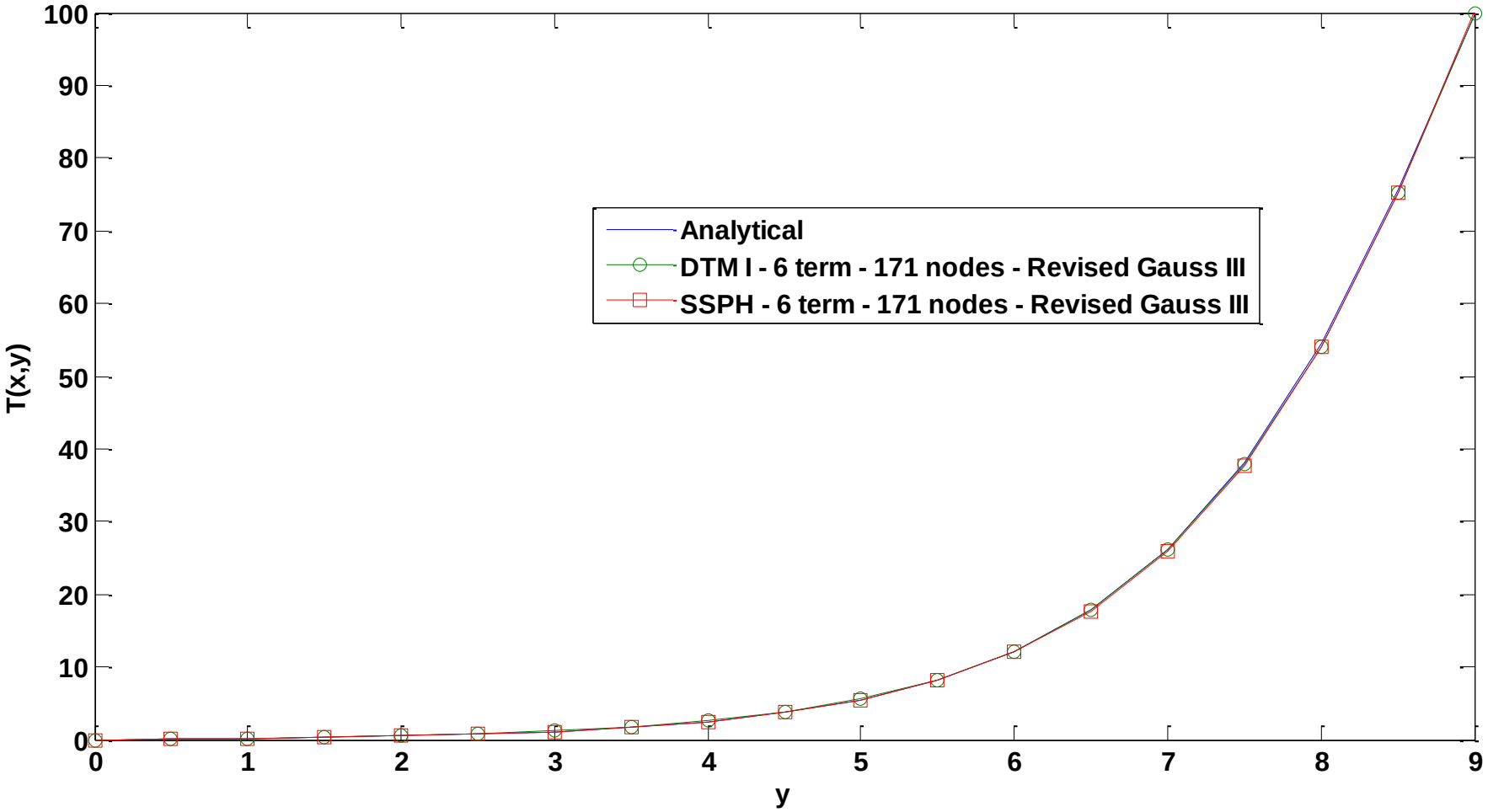

Figure 6.5 : Temperatures along the *y*-axis (*x*=2) computed by the DTM I, SSPH method and analytical solution - 171 nodes (Revised Gauss III).

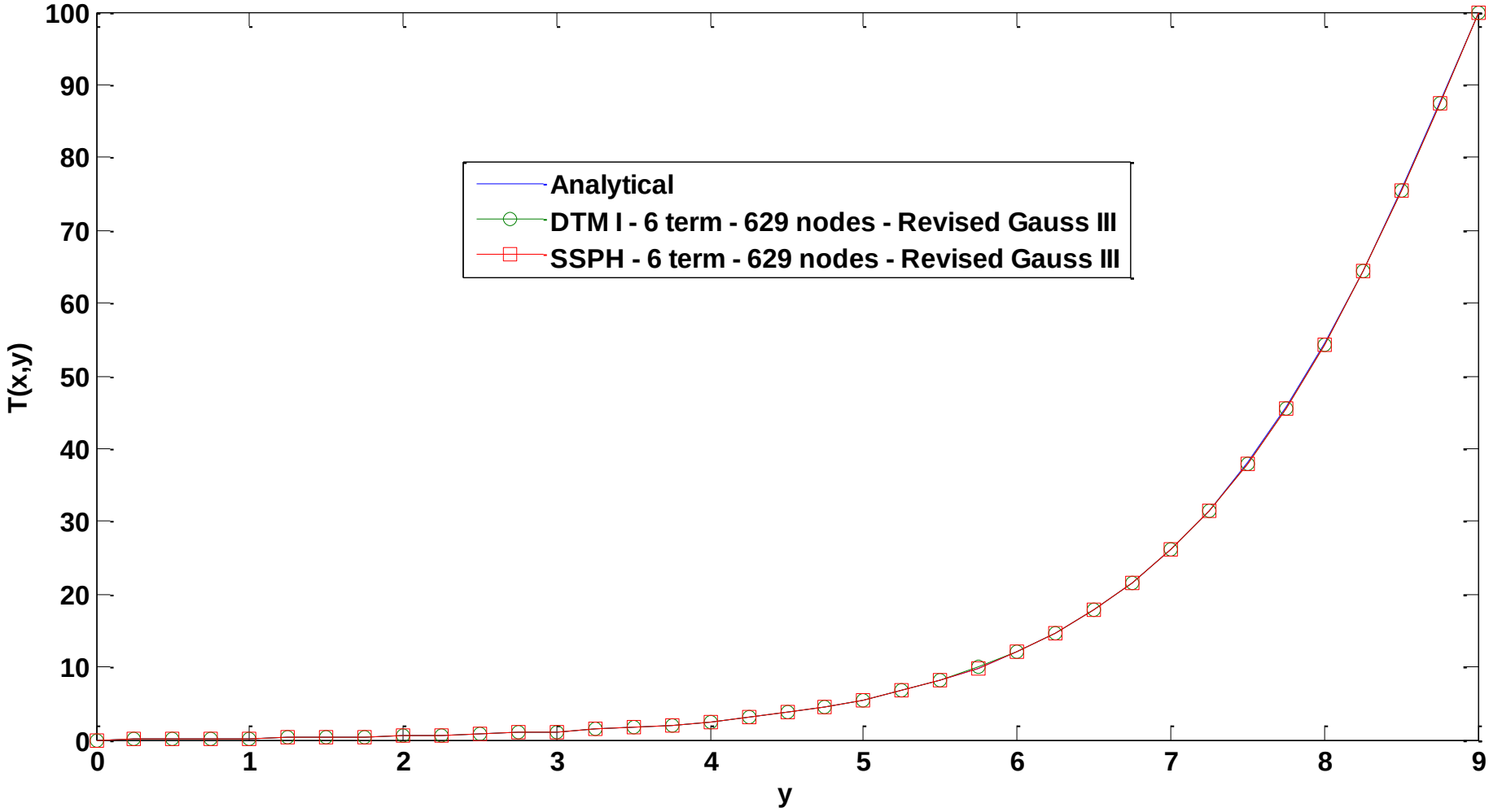

Figure 6.6 : Temperatures along the *y*-axis (*x*=2) computed by the DTM I, SSPH method and analytical solution - 629 nodes (Revised Gauss III).

It is observed in Figures 6.1 to 6.6 that accuracy of the DTM based meshless method I is better than that of the SSPH method. In comparison with the numerical results in Section 5.2 and 5.3 in which the revised super Gauss function is employed, the CSRBFs listed in Table 6.1 yield better accuracy for both the DTM based meshless method I and SSPH method.

6.3 Nonhomogeneous Laplace Equation in 2D

By using the CSRBFs in Table 6.1, nonhomogeneous Laplace equation in 2D is solved by using the DTM based meshless method I and SSPH method. The solution of this problem is obtained by using the same node distributions, kernel function and kernel function parameters employed in Section 6.2. Convergence and accuracy properties of the DTM based meshless method I and SSPH method are examined by using the global L_2 error norm given in Equation (5.10).

Global L_2 error norms calculated by Equation (5.10) are given in Table 6.3 for the nine CSRBFs listed in Table 6.1 and RSGF of Equation (5.9) for three different implementations of the DTM based meshless methods. It is clear that the L_2 error norms of the solutions of the DTM based meshless methods are lower than those of the SSPH method.

It is observed that the revised Gauss–IV compactly supported radial basis function gives the lowest L_2 error norms among the kernel functions in Table 6.1. In addition, the DTM based meshless method I shows conventional convergence as the number of nodes is increased with all CSRBFs.

Numerical solutions obtained by using 6 terms in the associated TSEs and node distributions of 50, 171 and 629 nodes are presented in Figures 6.7 to 6.9 which are obtained by using the revised Gauss-IV radial basis function that yield ther most accurate results among the other kernel functions.

It is observed in Figures 6.7 to 6.9 that the L_2 error norms of the DTM based meshless method I with the variation of the radius of the support domain (where $h=\Delta$) are much lower than those the SSPH method. The SSPH method does not provide solution if the shape parameter d is set to 2; however, the DTM based meshless method I gives a solution even if the shape parameter is set to 2.

Table 6.3 : The global L_2 error norm for the DTM I and SSPH method.

CSRBF type		DTM I			SSPH		
		50 nodes	*171 nodes*	*629 nodes*	*50 nodes*	*171 nodes*	*629 nodes*
Wu-C2		11.567	3.0664	0.7962	18.778	4.9771	1.2725
Wu-C4		10.488	2.7777	0.7211	16.419	4.3276	1.1218
Wendland-C2		12.657	3.3547	0.8709	20.794	5.4094	1.3977
Wendland-C4		10.063	2.6631	0.6912	14.987	3.9624	1.0279
Wendland-C6		8.719	2.2972	0.5956	11.384	3.0187	0.7838
Revised Gauss-I		12.752	3.3798	0.8774	22.000	5.6989	1.4711
Revised Gauss-II		10.188	2.6969	0.7000	15.715	4.1489	1.0759
Revised Gauss-III		8.8227	2.3254	0.6029	11.860	3.1456	0.8168
Revised Gauss-IV		8.1606	2.1434	0.5553	9.7571	2.5806	0.6697
RSGF	**DTM I**	21.310	8.1489	3.4977	38.133	10.0635	2.6664
	DTM II	19.453	5.3845	1.5820			
	DTM III	19.326	5.6586	1.4217			

Effects of the smoothing length parameter on accuracy are presented in Figures 6.10 to 6.12 in which it is observed that accuracy of the DTM based meshless method I is better than that of the SSPH method. Numerical results imply that the L_2 error norms of numerical solutions increase as the smoothing length parameter increases for both methods. In comparison with the numerical results in Section 5.2 and 5.3 obtained by using the revised super Gauss function as the kernel function, the CSRBFs listed in Table 6.1 yield better accuracy for both the DTM based meshless method I and SSPH method.

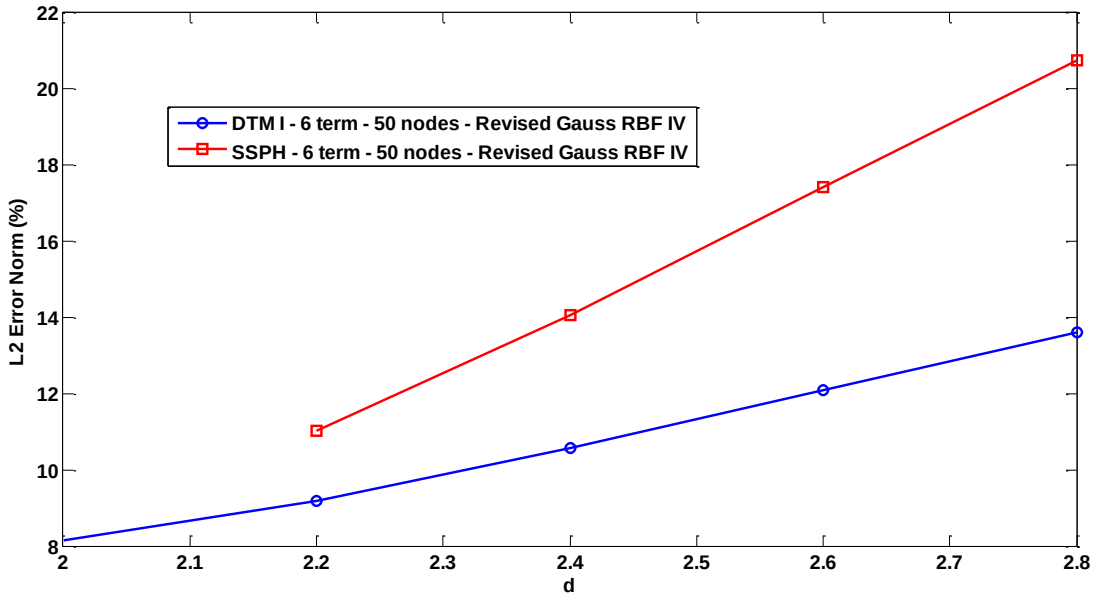

Figure 6.7 : The global L_2 error norms of the DTM I and SSPH method as the radius of the support domain (h=Δ) varies - 50 nodes.

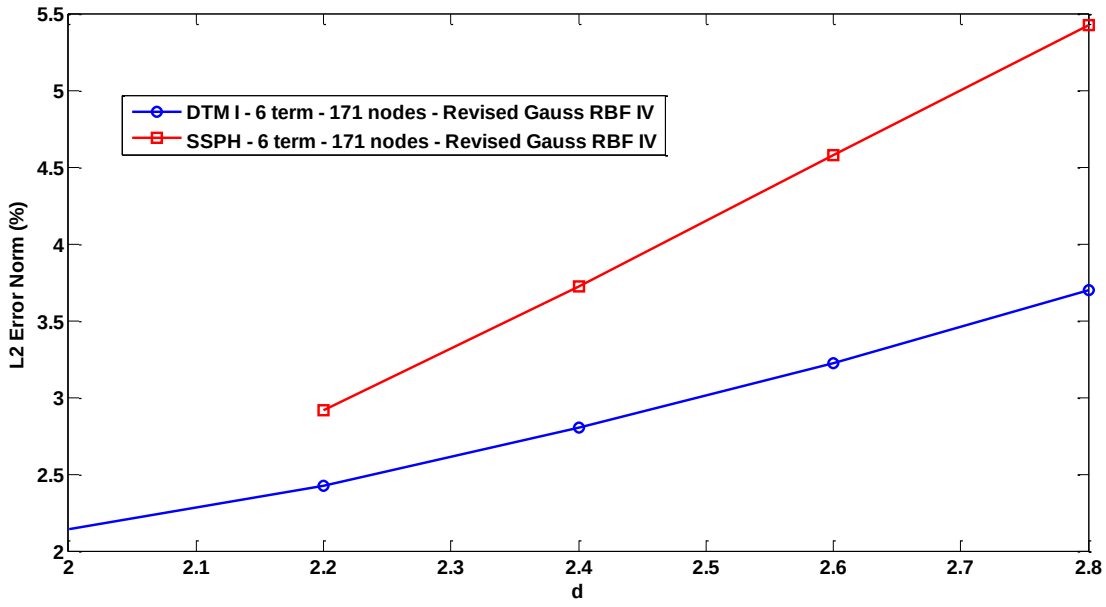

Figure 6.8 : The global L_2 error norms of the DTM I and SSPH method as the radius of the support domain (h=Δ) varies - 171 nodes.

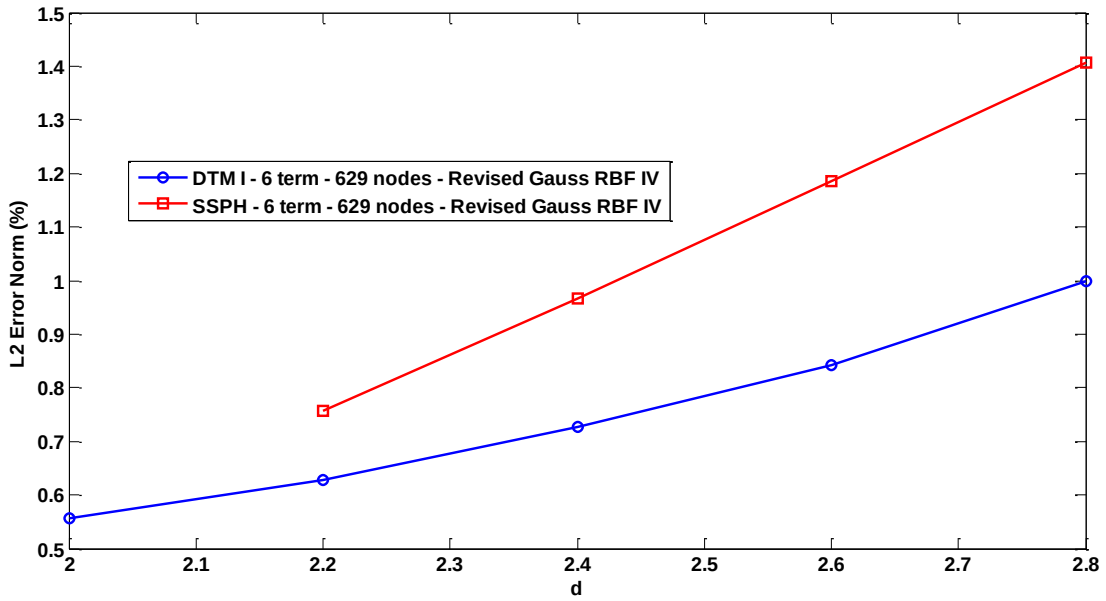

Figure 6.9 : The global L_2 error norms of the DTM I and SSPH method as the radius of the support domain ($h=\Delta$) varies - 629 nodes.

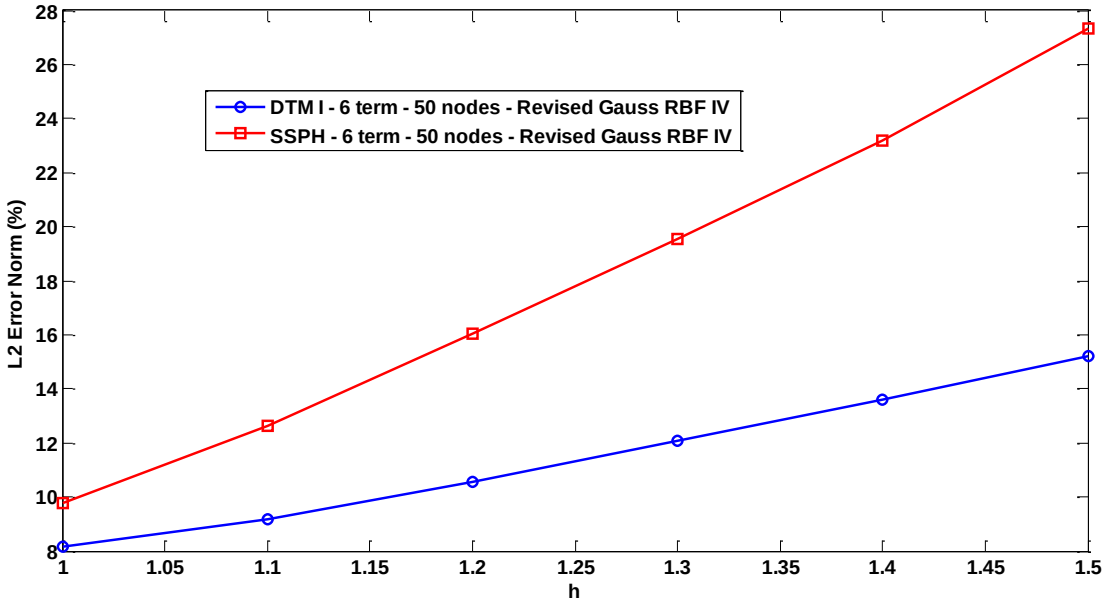

Figure 6.10 : The global L_2 error norms of the DTM I and SSPH method as the smoothing lenght varies - 50 nodes.

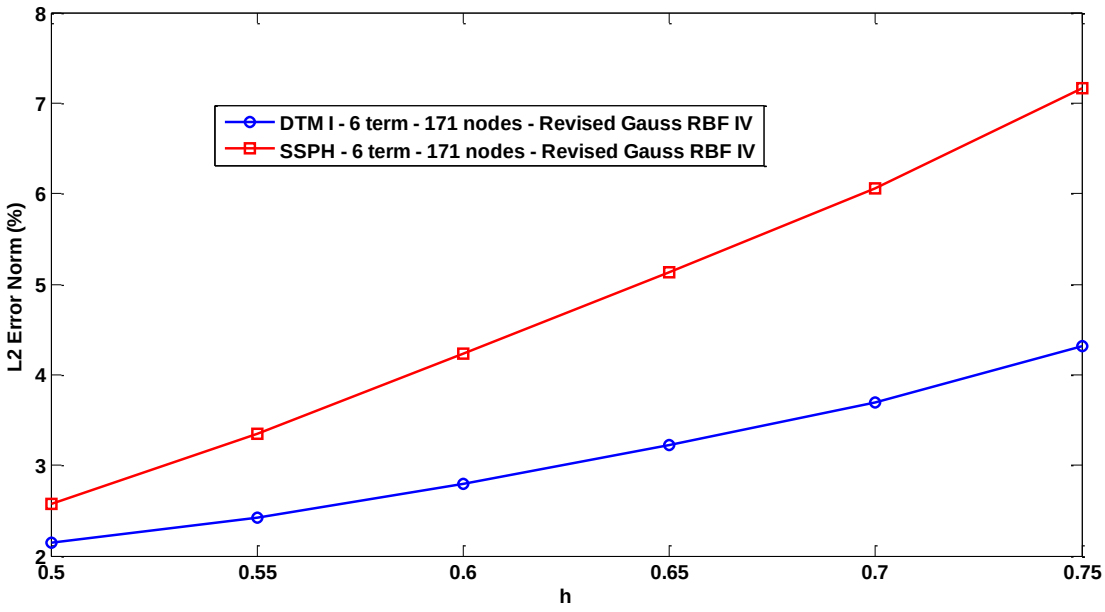

Figure 6.11 : The global L_2 error norms of the DTM I and SSPH method as the smoothing lenght varies - 171 nodes.

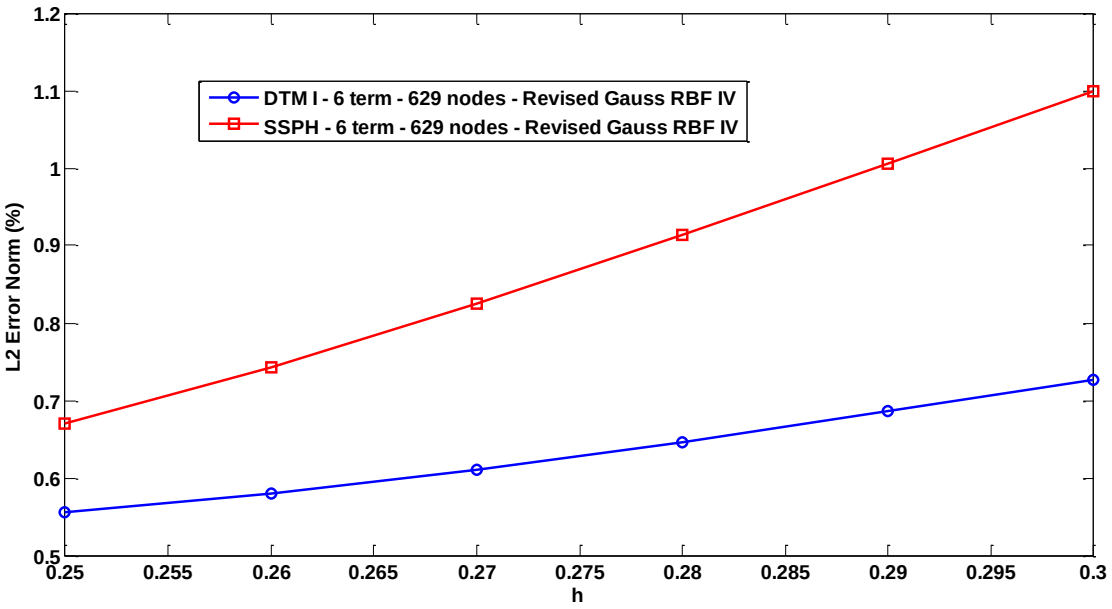

Figure 6.12 : The global L_2 error norms of the DTM I and SSPH method as the smoothing lenght varies - 629 nodes.

7. CONCLUSIONS AND RECOMMENDATIONS

Three new meshless approaches based on the Taylor series expansion and utilizing the formalism of the Differential Transform Method (DTM) called the DTM based meshless methods were developed.

The DTM based meshless methods and SSPH method were used to solve 1D nonhomogeneous boundary value problem, 2D homogeneous Laplace equation, 2D nonhomogeneous Laplace equation and plane stress deformations of a plate in 2D. Numerical solution obtained by each method is compared with the analytical solution for each problem studied.

The 1D nonhomogeneous boundary value problem was solved by the DTM based meshless methods I, II and III and SSPH method for the particle distributions of 5, 20 and 100 equally spaced particles in the problem domain. The global L_2 error norms of the solutions were calculated where different numbers of particles and terms in expansions were considered. It is clear that, even with the same number of terms, solutions of the DTM based meshless methods II and III agree very well with the analytical solution but those obtained by using the SSPH method and DTM based meshless method I differ noticeably from the analytical solution especially for 5 nodes and 5 terms in the TSEs. The DTM based meshless methods II and III agree very well with the analytical solution. The SSPH method cannot provide solution by using 5 nodes in the problem domain when it uses 6 terms in TSE.

The Laplace equation in 2D was also solved by using the DTM based meshless methods I, II and III and SSPH method for equally spaced 50, 171 and 629 particles. It is observed that accuracy of the DTM based meshless methods is better than that of SSPH method and all studied methods show convergence as the number of nodes is increased. It is clear that the L_2 error norms of the results of the DTM based meshless methods are much lower than those of the SSPH method provided that the same number of terms in the associated expansions are employed for both methods. By using the same number of terms, the DTM based meshless method II always gives the lowest global L_2 error norm when comparing with the other methods. The SSPH

method always gives the highest L_2 error norms for different number of nodes in the problem domain. Numerical results also show that lower L_2 error norms can be obtained for all methods as the number of particles distributed in the problem domain is increased. The DTM based meshlesh methods are also compared with the FEM in terms of global L_2 error norms. It is found that DTM based meshless methods always gave the lowest global L_2 error norms.

Moreover, the nonhomogeneous Laplace equation in 2D was solved by using the DTM based meshless methods I, II and III and SSPH method for equally spaced 50, 171 and 629 particles. It is found that accuracy of the DTM based meshless methods II and III are better than that of the DTM based meshless method I and SSPH method as the smoothing length parameter varies provided that the same number of terms are employed in the associated TSEs for both methods. Numerical results imply that the global L_2 error norm of numerical solutions increase as smoothing length parameter increases for all methods. It is observed that the SSPH method is stable for $h=1.8\Delta$ and node distribution of 171 nodes; however, the DTM based meshless methods are stable even for $h=2\Delta$. It is also observed that the SSPH method is stable for $h=2\Delta$ and node distribution of 629 nodes; however, the DTM based meshless methods II and III are stable even for $h=2.2\Delta$. Except for 629 nodes, the SSPH method always gives the highest global L_2 error norm; however, for 629 nodes the DTM based meshless method I gives the highest global L_2 error norm.

The plane stress deformations of a plate in 2D was solved by using the DTM based meshless methods II and III and SSPH method for equally spaced 64,217 and 793 particles. It is observed that accuracy of the DTM based meshless methods II and III are better than that of the SSPH method and both methods show convergence as the number of nodes is increased. The DTM based meshless method I is also used to solve the same problem but it did not yield satisfactory results; thus, only for 64 nodes, the solution is obtained by DTM based meshless method I. It is clear that DTM based meshless method III always give the lowest value comparing to the DTM based meshless method II and the SSPH method. For the 61x13 uniform node distribution, the displacement computed by using DTM based meshless methods is virtually indistinguishable from the analytical solution. However, the DTM based meshless method II gives slightly better results than the results obtained by the SSPH method. The dimensionless stress $\sigma_{xx}(L_2/F_0)$ along the top surface of the plate

obtained by the analytical solution, DTM based meshless methods II and III and SSPH method is presented by using 16x4, 31x7 and 61x13 node distribution. These are also the evidence of that the DTM based meshless methods II and III always give less deviation than the SSPH method. It is clear that CPU times required for the DTM based meshless methods II and III are much higher than those of the SSPH method provided that the same number of terms are employed in the associated TSEs for both methods. However, the codes developed for all methods can be optimized to decrease the CPU time required for the computations. Optimization of the codes to reduce the CPU times for the computations was not the focus of this thesis that will be pursued in future studies.

By using compactly supported radial basis functions (CSRBFs), performance of the DTM based meshless method I was compared with the SSPH method for the homogeneous and nonhomogeneous Laplace equations given in Chapter 5. Comparisons were made with the analytical solutions and results of the SSPH method. Total nine CSRBFs were examined to evaluate the accuracy of the DTM based meshless method I and SSPH method by considering various particle distributions and nonhomogeneous terms.

It is observed that the use of CSRBFs yield better accuracy for both methods than revised super Gauss function, and both methods have the conventional convergence properties. The DTM based meshless method I yields smaller L_2 error norms than the SSPH method, especially in the existence of nonsmooth nonhomogeneous terms.

It is observed that the Wendland–C6 and Revised Gauss–III compactly supported radial basis functions yield relatively lower L_2 error norms for the DTM based meshless method I, II and III and SSPH method than the other kernel functions in Table 6.2 for the homogeneous Laplace equation,. In addition, the DTM based meshless method I shows conventional convergence as the number of nodes is increased with all CSRBFs.

Nonhomogeneous Laplace equation in 2D was solved by using the DTM based meshless method I and SSPH method. The solution of this problem was obtained by using the same node distributions, kernel function and kernel function parameters employed in Section 6.2.

It is clear that the L_2 error norms of the solutions of the DTM based meshless methods are lower than those of the SSPH method.

It is observed that the revised Gauss–IV compactly supported radial basis function gives the lowest L_2 error norms among the kernel functions in Table 6.1. In addition, the DTM based meshless method I shows conventional convergence as the number of nodes is increased with all CSRBFs.

It is observed that the L_2 error norms of the DTM based meshless method I with the variation of the radius of the support domain (where $h=\Delta$) are much lower than those the SSPH method. The SSPH method does not provide solution if the shape parameter d is set to 2; however, the DTM based meshless method I gives a solution even if the shape parameter is set to 2.

It is observed that accuracy of the DTM based meshless method I is better than that of the SSPH method with then varying of the smoothing lenght. Numerical results imply that the L_2 error norms of numerical solutions increase as the smoothing length parameter increases for both methods. In comparison with the numerical results in Section 5.2 and 5.3 obtained by using the revised super Gauss function as the kernel function, the CSRBFs listed in Table 6.1 yield better accuracy for both the DTM based meshless method I and SSPH method.

For future studies, the following works can be recommended;

1. CPU time for DTM based meshless methods can be improved.
2. DTM based meshless methods can be implemented by using weak form formulation.
3. DTM based meshless methods can be used to solve dynamic and transient engineering problems.
4. DTM based meshless methods can be improved by developing a different weight function of which is much more suitable than the revised super Gauss function.
5. DTM based meshless methods can be used to solve nonlinear engineering problems.

REFERENCES

[1] **Porfiri, M.** (2006). Analysis by meshless local Petrov-Galerkin method of material discontinuities, pull-in instability in MEMS, vibrations of cracked beams, and finite deformations of rubberlike materials, *PhD Thesis,* Virginia State University, Virginia.

[2] **Yang, Q.** (2011). SPH simulation of fluid-structure interaction problems with application to hovercraft, PhD Thesis, Virginia State University, Virginia.

[3] **Chiu, Y.K.** (2011). A conservative meshless framework for conservation laws with applications in computational fluid dynamics, PhD Thesis, Stanford University, California.

[4] **Lucy, L.B.** (1977). A numerical approach to the testing of the fission hypothesis. *Astronomical Journal, 82,* 1013-1024.

[5] **Gingold, R.A., Monaghan, J.J.** (1977). Smooth particle hydrodynamics: theory and applications to non spherical stars. *Monthly Notices of the Royal Astronomical Society, 181,* 375-389.

[6] **Nayroles, B., Touzot, G., Villon, P.** (1992). Generalizing the finite element method:diffuse approximation and diffuse elements. *Computational Mechanics, 10,* 307-318.

[7] **Liu, W.K., Adee, J., Jun, S.** (1993). Reproducing kernel particle methods for elastic and plastic problerms. *Advanced Computational Methods for Material Modelling, **180**,* 175-190.

[8] **Belytschko, T., Lu, Y.Y., Gu, L.** (1994). Element free Galerkin methods. *International Journal for Numerical Methods in Engineering, 37,* 229-256.

[9] **Duarte, C.A., Oden, J.T.** (1996). An hp adaptive method using clouds. *Computer Methods in Applied Mechanics and Engineering, 139,* 237-262.

[10] **Onate, E., Idelsohn S., Zienkiewicz O.Z., Taylor R.L.** (1996). A finite point method in computational mechanics. Application to convective and transport flow. *International Journal for Numerical Methods in Engineering, 39,* 3839-3867.

[11] **Mukherjee, Y.X., Mukherjee, S.** (1997). A Boundary node method for potential problems. *International Journal for Numerical Methods in Engineering, 40,* 797-815.

[12] **Atluri, S.N., Zhu T.** (1998). A new meshless local Petrov-Galerkin (MLPG) approach in computational mechanics. *Computational Mechanics, 22,* 117-127.

[13] **Liu, G.R.** (1999). A point assembly method for stress analysis for solid. *Impact Response of Materials & Structures, V. P. W. Shim et al. eds,* 475-480.

[14] **Chen J.K., Beraun J.E., Jin C.J.** (1999). An improvement for tensile instability in smoothed particle hydrodynamics. *Computational Mechanics, 23,* 279-287.

[15] **Liu, G.R., Gu, Y.T.** (2000). Coupling element free Galerkin method with boundary point interpolation method. *Advances in Computational Engineering & Sciences,* 1427-1432.

[16] **De S., Bathe K.J.** (2000). The method of finite spheres. *Computational Mechanics, 25,* 329-345.

[17] **Aluru. N.R.** (2000). A point collocation method based on reproducing kernel approximations. *International Journal for Numerical Methods in Engineering, 47,* 1083-1121.

[18] **Li, G., Aluru. N.R.** (2002). Boundary cloud method: a combined scattered point/boundary integral approach for boundary-only analysis. *Computer Methods in Applied Mechanics and Engineering, 191,* 37-70.

[19] **Batra R.C., Zhang G.M.** (2004). Modified smoothed particle hydrodynamics method and its application to transient problems. *Computational Mechanics, 34,* 137-146.

[20] **Batra R.C., Zhang G.M.** (2008). SSPH basis functions for meshless methods, and comparison of solutions with strong and weak formulations. *Computational Mechanics, 41,* 527-545.

[21] **Zhang G.M., Batra R.C.** (2009). Symmetric smoothed particle hydrodynamics method and its application to elastic problems. *Computational Mechanics, 43,* 321-340.

[22] **Tsai C.L., Guan, Y.L., Batra R.C., Ohanehi, D.C., Dillard, J.G., Nicoli, E., Dillard, D.A.** (2013). Comparison of the performance of SSPH and MLS basis functions for two-dimensional linear elastostatics problems including quasistatic crack propagation. *Computational Mechanics, 51,* 19-34.

[23] **Karamanli A., Mugan A.** (2012). Solutions of two-dimensional heat transfer problems by using symmetric smoothed particle hydrodynamics method. *Journal of Applied and Computational Mathematics, 1,* 1-6.

[24] **Liu, G.R.** (2003). *Mesh Free Methods, Moving Beyond Finite Element Method.* CRC Press, Washington.

[25] **Liu, G.R.** (2003). *An Introduction* to *Meshfree Methods and Their Programming.* Springer, Dordrecht.

[26] **Libersky L.D., Petschek A.G.** (1991). *Smoothed Particle Hydrodynamics with Strength of Materials*. in H. Trease, J. Fritts and W. Crowley eds.,Proceedings of The Next Free Lagrange Conference, Springer-Verlag, NY,395,248-257.

[27] **Monaghan, J.J.** (1994). Simulating free surface flows with SPF. *Journal of Computational Physics, 110,* 399-406.

[28] **Liu, M.B., Liu, G.R., Lam, K.Y.** (2003). Meshfree particle simulation of the explosion process for high explosive in shaped charge. *Shock Waves, 12,* 509-520.

[29] **Liu, M.B., Liu, G.R., Lam, K.Y.** (2003). Computer simulation of the high explosive explosion using smoothed particle hydrodynamics methodology. *Computer&Fluids, 32,* 305-322.

[30] **Liu, M.B., Liu, G.R., Lam, K.Y.** (2003). A one dimensional meshfree particle formulation for simulating shock waves. *Shock Waves, 32,* 305-322.

[31] **Liu, M.B., Liu, G.R., Zong, Z., Lam, K.Y.** (2003). Smoothed particle hydrodynamics for numerical simulation of underwater explosions. *Computational Mechanics, 30,* 106-118.

[32] **Randles, P.W., Carney, T.C., Libersky, L.D., Renick, J.R., Petcheck, A.G.** (1995). Calculation of oblique impact and fracture of tungsten cubes using smoothed particle hydrodynamics. *International Journal of Impact Engineering, 17,* 661-672.

[33] **Johnson, G.R.** (1996). Normalized smoothing functions for SPH impact computations. *International Journal for Numerical Methods in Engineering, 39,* 2725-2741.

[34] **Libersky L.D., Petschek A.G.** (1991). Smooth particle hydrodynamics with strength of materials. Advances in the Free Lagrange Method, *Lecturer Notes in Physics, 395,* 248-257.

[35] **Benz, W., Asphaug, E.** (1995). Simulations of brittle solids using smoothed particle hydrodynamics. *Computer Physics Communications, 87,* 253-265.

[36] **Randles, P.W., Libersky, L.D.** (1996). Smoothed particle hydrodynamics some recent improvements and applications. *Computer Methods in Applied Mechanics and Engineering, 139,* 375-408.

[37] **Bonet, J., Kulasegaram, S.** (2000). Correction and stabilization of smooth particle hydrodynamics methods with applications in metal forming simulations. *International Journal for Numerical Methods in Engineering, 47,* 1189-1214.

[38] **Gray, J.P., Monaghan, J.J., Swift, R.P.** (2001). SPH elastic dynamics. *Computer Methods in Applied Mechanics and Engineering, 190,* 6641-6662.

[39] **Liu, W.K., Jun, S., Adee, J., Belytschko, T.** (1995). Reproducing kernel particle methods for structural dynamics. *International Journal for Numerical Methods in Engineering, 38,* 1655-1679.

[40] **Liu, W.K., Jun, S., Zhang, Y.F.** (1995). Reproducing kernel particle methods. *International Journal for Numerical Methods in Engineering, 38,* 1655-1679.

[41] **You, Y., Chen, J.S., Lu, H.** (2003). Filters, reproducing kernel, an adaptive meshfree method. *Computational Mechanics, 31,* 316-326.

[42] **Chen, J.S., Pan, C., Wu, C.T., Liu, W.K.** (1996). Reproducing kernel particle methods for large deformation analysis of nonlinear structures. *Computer Methods in Applied Mechanics and Engineering, 139,* 195-227.

[43] **Liu, W.K., Chen, Y., Chang, C.T., Belytschko, T.** (1996). Advances in multiple scale kernel particle methods. *Computational Mechanics, 18,* 73-111.

[44] **Chen, J.S., Yoon, S., Wang, H.P., Liu, W.K.** (2000). An inproved reproducing kernel particle method for nearly incompressible finite elasticity. *Computer Methods in Applied Mechanics and Engineering, 181,* 117-145.

[45] **Chen, J.S., Pan, C., Wu, C.T.** (1997). Large deformation analysis of rubber based on a Reproducing Kernel Particle Method. *Computational Mechanics, 19,* 211-227.

[46] **Chen, J.S., Han, W., Yang, Y., Meng, X.** (2003). A reproducing kernel method with nodal interpolation property. *International Journal for Numerical Methods in Engineering, 56,* 935-960.

[47] **Liu, W.K., Jun, S., Sihling, D.T., Chen, Y., Hao, W.** (1997). Multiresolution reproducing kernel particle method for computational fluid dynamics. *International Journal for Numerical Methods in Fluids, 24,* 1391-1415.

[48] **Chen, J.S., Wang, D.,** (2006). A constrained reproducing kernel particle formulation for shear deformable shell in Cartesian coordinates. *International Journal for Numerical Methods in Engineering, 68,* 151-172.

[49] **Chen, J.S., Hu, W., Hu, H.Y.** (2008). Reproducing kernel enhanced radial basis collocation method. *International Journal for Numerical Methods in Engineering, 75,* 600-627.

[50] **Lee, C.K., Shuai, Y.Y.** (2008). An automatic adaptive refinement procedure for the reproducing kernel particle method. Part i. *Computational Mechanics, 40,* 399-413.

[51] **Belytschko, T., Gu, L.**, **Lu, Y.Y.** (1994). Fracture and crack growth by element free Galerkin methods. *Modelling and Simulation in Material Science and Engineering, 2,* 519-534.

[52] **Belytschko, T., Lu, Y.Y., Gu, L.** (1995). Crack propagation by element free Galerkin methods. *Engineering Fracture Mechanics, 51,* 295-315.

[53] **Belytschko, T., Lu, Y.Y., Gu, L.** (1995). Element free Galerkin methods for static and dynamic fracture. *International Journal for Numerical Methods in Engineering, 32,* 2547-2570.

[54] **Lancaster, P., Salkauskas, K.** (1981). Surfaces generated by moving least squares methods. *Computational Mathematics, 37,* 141-158.

[55] **Fleming, M., Chu, Y.A., Moran, B., Belytschko, T.** (1997). Enriched element free Galerkin methods for crack tip fields. *International Journal for Numerical Methods in Engineering, 40,* 1483-1504.

[56] **Xu, Y., Saigal, S.** (1998). An element free Galerkin formulation for stable crack growth in an elastic solid. *Computer Methods in Applied Mechanics and Engineering, 154,* 331-343.

[57] **Tabbara, M.R., Stone, C.M.** (1998). A computational method for quasi-static fracture. *Computational Mechanics, 22,* 203-210.

[58] **Fleming, M.** (1997). The element free Galerkin method for fatigue and quasi-static fracture, *PhD Thesis,* Northwestern University, IL.

[59] **Ventura, G., Belytschko, T.** (2001). Level set crack propagation modelling in the element free Galerkin Method, *2nd European Conference on Computational mechanics,* 204-228, Poland.

[60] **Li, S., Simonsen, C.B.** (2007). Meshfree simulations of ductile crack propagations. *International Journal for Computational Methods in Engineering Science and Mechanics, 154,* 331-343.

[61] **Shepard, D.** (1968). A two dimensional function for irregularly spaced data. *ACM National Conference,* 527-524.

[62] **Liu, W.K., Jun, S., Zhang Y.F.** (1995). Reproducing kernel particle methods. *International Journal for Numerical Methods in Engineering, 20,* 1081-1106.

[63] **Lu, Y.Y., Belytschko, T., Gu, L.** (1994). A new implementation of the element free Galerkin method. *Computer Methods in Applied Mechanics and Engineering, 113,* 397-414.

[64] **Chen, J.S., Hu, W, Paso, M.** (2007). Orbital HP-Clouds for solving Schrodinger equation in quantum mechanics. *Computer Methods in Applied Mechanics and Engineering, 196,* 3693-3705.

[65] **Garcia, O., Fancello, E.A., De Barcellos C.S.** (1995). Hp-Clouds in Mindlin's thick plate model. *International Journal for Numerical Methods in Engineering, 47,* 1381-1400.

[66] **Zuppa, C.** (2005). Jackson type inequalities for hp clouds and error estimates. *Computer Methods in Applied Mechanics and Engineering, 194,* 1875-1887.

[67] **Onate, E., Idelshon, S., Zienkiewicz O.Z., Taylor R.L., Sacco, C.** (1996). A stabilized finite point method for analysis of fluid mechanics problems. *Computer Methods in Applied Mechanics and Engineering, 139,* 315-346.

[68] **Onate, E., Sacco, C., Idelshon, S.** (2000). A finite point method for incompressible flow problems. *Computing and Visualization in Science, 3,* 67-75.

[69] **Löhner, R., Sacco, C., Onate, E., Idelshon, S.** (2002). A finite point method for compressible flow. *International Journal for Numerical Methods in Engineering, 47,* 1381-1400.

[70] **Onate, E., Perazzo, F., Miquel, J.** (2001). A finite point method for elasticity problems. *International Centre for Numerical Methods in Engineering, 79,* 2151-2163.

[71] **Boroomand, B., Tabatabaei, A.A., Onate, E.** (2005). Simple modifications for stabilization of the finite point method. *International Journal for Numerical Methods in Engineering, 63,* 351-379.

[72] **Kothnur, V.S., Mukherjee, Y.X., Mukherjee, S.** (1999). Two-dimensional linear elasticity by the boundary node method. *International Journal of Solids and Structures, 36,* 1129-1147.

[73] **Chati, M.K., Mukherjee, S., Mukherjee, Y.X.** (1999). The boundary node method for three dimensional linear elasticity. *International Journal for Numerical Methods in Engineering, 46,* 1163-1184.

[74] **Tan, G., Cen, S., Wang, H., Yao, Z.** (2005). Applications of boundary node method to simulation of piezoelectric composites. *18th International Conference on Structural Mechanics in Reactor Technology,* China.

[75] **Mukherjee, Y.X., Mukherjee, S.** (1998). The boundary node method for potential problems. *International Journal for Numerical Methods in Engineering, 40,* 797-815.

[76] **Mukherjee, Y.X., Mukherjee, S.** (2000). The boundary node method for three dimensional problems in potential. *International Journal for Numerical Methods in Engineering, 47,* 1523-1547.

[77] **Han, Z.D., Atluri, S.N.** (2004). Meshless local Petrov-Galerkin (MLPG) approach for 3-dimensional elasto-dynamics. *International Journal for Numerical Methods in Engineering, 1,* 129-140.

[78] **Tabbara, M.R., Stone, C.M.** (2001). A meshless local Petrov Galerkin (MLPG) method for free and forced vibration analysis of solids. *Computational Mechanics, 27,* 188-198.

[79] **Long, S., Atluri, S.N.** (2002). A meshless local Petrov-Galerkin (MLPG) method for solving a bending problem of a thin plate. *Computer Modelling in Engineering & Sciences, 1,* 129-140.

[80] **Qian, L.F., Batra, R.C., Chen, L.M.** (2004). Analysis of cylindrical bending thermoelastic deformations of functionally graded plates by a meshless local Petrov Galerkin method. *Computational Mechanics, 33,* 263-273.

[81] **Batra, R.C., Ching, H.K.** (2002). Analysis of elastodynamics deformations near a crack/notch tip by a meshless local Petrov Galerkin (MLPG) method. *Computer Modelling in Engineering & Sciences, 3,* 717-730.

[82] **Batra, R.C., Porfiri, M.** (2008). Analysis of rubber-like materials using meshless local Petrov Galerkin (MLPG) method. *Communications in Numerical Methods in Engineering, 24,* 1781-1804.

[83] **Gilhooley, D.F., Batra, R.C., Xiao, J.R., McCharty, M.A., Gillespie, J.W.** (2007). Analysis of thick functionally graded plates by using higher-order shear and normal deformable plate theory and MLPG method with radial basis functions. *Composite Structures, 80,* 539-552.

[84] **Atluri, S.N., Cho, J.Y., Kim, H.G.** (1999). Analysis of thin beams, using the meshless local Petrov Galerkin method, with generalized moving least squares interpolation. *Computational Mechanics, 24,* 334-347.

[85] **Li, Q., Shen, S., Atluri, S.N.** (2003). Application of meshless local Petrov-Galerkin (MLPG) to problems with singularities, and material discontinuities, in 3-D. *Computer Modelling in Engineering & Sciences, 4,* 571-585.

[86] **Han, Z.D., Rajendran, A.M., Atluri, S.N.** (2005). Meshless local Petrov-Galerkin (MLPG) approaches for solving nonlinear problems with large deformations and rotations. *Computer Modelling in Engineering & Sciences, 10,* 1-12.

[87] **Sladek, J., Sladek, V., Atluri, S.N.** (2004). Meshless local Petrov-Galerkin method in anisotropic elasticity. *Computer Modelling in Engineering & Sciences, 6,* 477-489.

[88] **Sladek, J., Sladek, V., Tan, C.L., Atluri, S.N.** (2008). Analysis of transient heat conduction in 3D anisotropic functionally graded solids by the MLPG method. *Computer Modelling in Engineering & Sciences, 32,* 161-174.

[89] **Sladek, J., Sladek, V., Atluri, S.N.** (2004). Meshless local Petrov-Galerkin method for heat conduction problem in an anisotropic medium. *Computer Modelling in Engineering & Sciences, 6,* 309-318.

[90] **Liu, G.R., Gu Y.T.** (1999). A point interpolation method. *Proceedings of 4th Asia-Pacific Conference on Computational Mechanics,* 1009-1014, Singapore.

[91] **Gu, Y.T., Liu, G.R.** (2001). Using radial basis function in a boundary type meshless method, boundary point interpolation method (BPIM). *Inter. Conf. On Sci. & Engr. Comput.*, Beijing.

[92] **Liu, G.R., Yan L., Wang, J.G., Gu, Y.T.** (2002). Point interpolation method based on local residula formulation using radial basis functions. *Structural Engineering and Mechanics, 6,* 713-732.

[93] **Liu, G.R., Dai, K.Y., Lim, K.M., Gu, Y.T.** (2003), A radial point interpolation method for simulation of two-dimensional piezoelectric structures, *Smart Materials and Structures, 12,* 171-180.

[94] **Liu, G.R., Gu, Y.T.** (2001). A local radial point interpolation method (LRPIM) for free vibration analyses of 2-D solids. *Journal of Sound and Vibration, 246,* 29-46.

[95] **Liew, K.W., Chen, X.L.** (2004). Mesh-free radial point interpolation method for the buckling analysis of Mindlin plates subjected to in-plane point loads. *International Journal for Numerical Methods in Engineering, 60,* 1861-1877.

[96] **Kaufmann, T., Yu, Y., Engström, C., Chen, Z., Fumeaux, C.** (2012). Recent developments of the meshless radial point interpolation method for

time-domain elelctromagnetics. *International Journal for Numerical Modelling, 25,* 468-489.

[97] **Wendland, H.** (1995). Piecewise polynomial, positive definite and compactly supported radial basis functions of minimal degree. *Advances in Computational Mathematics, 4,* 389-396.

[98] **Wendland, H.** (1998). Error estimates for interpolation by compactly supported radial basis functions of minimal degree. *Journal of Approximation Theory, 93,* 258-396.

[99] **Wu, Z.** (1995). Compactly supported positive definite radial functions. *Advances in Computational Mathematics, 4,* 283-292.

[100] **Chen, J.K., Beraun, J.E., Carney, T.C.** (1999). A corrective smoothed particle method for boundary value problems in heat conduction. *International Journal for Numerical Methods in Engineering, 46,* 231-252.

[101] **Chen, J.K., Beraun, J.E., Jih, C.J.** (2001). A corrective smoothed particle method for transient elastoplastic dynamics. *Computational Mechanics, 27,* 177-187.

[102] **Gu, Y.T., Liu, G.R.** (2002). A boundary point interpolation method for stress analysis of solids. *Computational Mechanics, 28,* 47-54.

[103] **Gu, Y.T., Liu, G.R.** (2001). A boundary point interpolation method (BPIM) using radial function basis. *Conference on Computational Fluid and Solid Mechanics, MIT,* 1590-1592.

[104] **Gu, Y.T., Liu, G.R.** (2002). A boundary radial point interpolation method (BRPIM) for structural analyses. *Structural Engineering and Mechanics, 15,* 535-550.

[105] **Zhang, G.M., Batra, R.C.** (2007). Wave propagation in functionally graded materials by modified smoothed particle hydrodynamics (MSPH) method. *Journal of Computational Physics, 222,* 374-390.

[106] **Batra, R.C., Zhang, G.M.** (2007). Search algorithm, and simulation of elastodynamic crack propagation by modified smoothed particle hydrodynamics (MSPH) method. *Computational Mechanics, 40,* 531-546.

[107] **Batra, R.C., Zhang, G.M.** (2004). Analysis of adiabatic shear bands in elasto-thermo-viscoplastic materials by modified smoothed-particle hydrodynamics (MSPH) method. *Journal of Computational Physics, 201,* 172-190.

[108] **Batra, R.C., Zhang, G.M.** (2008). Modified Smoothed Particle Hydrodynamics (MSPH) basis functions for meshless methods, and

their application to axisymmetric Taylor impact test. *Journal of Computational Physics, 227,* 1962-1981.

[109] **Karamanli A., Mugan A.** (2013). Strong form meshless implementation of Taylor series method. *Applied Mathematics and Computations, 219,* 9069-9080.

[110] **Zhou, J.K.** (1986). Differential transform and its applications for electrical circuits. *Huazhong University Press,* China.

[111] **Chen, C.L., Lin, S.H., Chen, C.K.** (1996) Application of taylor transformation to nonlinear predictive control problem. *Applied Mathematical Modelling, 20,* 699-710.

[112] **Chiou, J.S., Tzeng, J.R.** (1996) Application of the taylor transform to non-linear vibration problems. *Journal of Vibration and Acoustics ,118,* 83-87.

[113] **Jang, M.J., Chen, C.L.** (1997) Analysis of the response of a strongly non-linear damped system using a differential transformation technique. *Applied Mathematics and Computations, 88,* 137-151.

[114] **Chen, C.L., Liu, Y.C.** (1998) Differential transformation technique for steady nonlinear heat conduction problems. *Applied Mathematics and Computations, 95,* 155-164.

[115] **Yu, L.T., Chen, C.K.** (1998) The solution of the Blasius equation by the differential transformation method. *Applied Mathematical Modelling, 28,* 101-111.

[116] **Yu, L.T., Chen. C.K.** (1998) Application of Taylor transformation to optimize rectangular fins with variable thermal parameters. *Applied Mathematical Modelling, 22,* 11-21.

[117] **Kuo, B.L.** (2003) Application of the differential transformation method to the solutions of Falkner-Skan wedge flow. *Acta Mechanica, 164,* 161-174.

[118] **Kuo, B.L.** (2004) Thermal boundary–layer problems in a semi–infinite plate by the differential transformation method. *Applied Mathematics and Computations, 150,* 303-320.

[119] **Chen, C.K., Chen, S.S.** (2004) Application of the differential transformation method to a nonlinear conservative system. *Applied Mathematics and Computations, 154,* 431-441.

[120] **Chen, C.K., Ho, S.H.** Solving partial differential equations by twodimensional differential transform. *Applied Mathematics and Computations, 106,* 171-179.

[121] **Ayaz, F.** (2004) Application of differential transform method to differential algebraic equations. *Applied Mathematics and Computations, 152,* 649-657.

[122] **Jang, M.J., Chen, C.K., Liu, Y.C.** (2001) Two-dimensional differential transform for partial differential equations. *Applied Mathematics and Computations, 121,* 261-270.

[123] **Liu, H., Song, Y.** (2007) Differential transform method applied to high index differential–algebraic equations. *Applied Mathematics and Computations, 184,* 748-753.

[124] **Ayaz, F.** (2004) Solutions of the system of differential equations by differential transform method. *Applied Mathematics and Computations, 147,* 547-567.

[125] **Yalcin, H.S., Arikoglu, A., Ozkol, I**. (2009) Free vibration analysis of circular plates by differential transform method. *Applied Mathematics and Computations, 212,* 377-386.

[126] **Arikoglu, A., Ozkol, I**. (2006) Solution of differential-difference equations by using differential transform method. *Applied Mathematics and Computations, 181,* 153-162.

[127] **Arikoglu, A., Ozkol. I.** (2006) Solution of difference equations by using differential transform method. *Applied Mathematics and Computations, 174,* 1216-1228.

[128] **Arikoglu, A., Ozkol, I.** (2005) Solution of boundary value problems for integro differential equations by using differential transform method. *Applied Mathematics and Computations, 168,* 1145-1158.

[129] **Bervillier, C.** (2012) Status of the differential transformation method. *Applied Mathematics and Computations, 218,* 10158-10170.

CURRICULUM VITAE

Name Surname: Armağan Fatih Karamanlı

Place and Date of Birth: Istanbul, 28.05.1977

Address: Bahçelievler Mah. Kerim Tekin Sok. No:4/23 Bahçelievler İST

E-Mail: armagan_k@yahoo.com

B.Sc.: Mechanical Engineering (ITU)

M.Sc.: Managerial Engineering (ITU)

Professional Experience and Rewards:

2012- : Joint Quality Manager, Erna Maş Makina Ticaret ve Sanayi A.Ş.

2008-2012: Specialist, Otokar Otomotiv ve Savunma Sanayi A.Ş.

2004-2008 : Specialist, Uzel Makina ve Ticaret Sanayi A.Ş.

List of Publications and Patents:

Karamanli A., Mugan A. (2013). Strong form meshless implementation of Taylor series method. *Applied Mathematics and Computations, **219**,* 9069-9080.

Karamanli A., Mugan A. (2012). Solutions of two-dimensional heat transfer problems by using symmetric smoothed particle hydrodynamics method. *Journal of Applied and Computational Mathematics, **1**,* 1-6.